# Validation of a Dynamic Simulation of a Five Degree of Freedom Point Contact Joint

by

Amanda Knutson

A thesis submitted to the Department of Mechanical

and Materials Engineering in conformity with the

requirements for the degree of Master of Science (Engineering)

Queen's University

Kingston, Ontario, Canada

October 2007

# Abstract

Amanda Knutson: Validation of a Dynamic Simulation of a Five Degree of Freedom Point Contact Joint. M.Sc. thesis, Queen's University at Kingston, October, 2007.

A new special case computer simulation to model the non-linear, three dimensional dynamic equations of motion of a five degree of freedom point contact joint has been developed and the functionality has been validated with data collected from a physical model.

A system physically realistic to model was designed with sphere in sphere contact. A small outboard body articulates within a larger inboard spherical cut out body and springs help provide stability to the system by attaching the outboard body to the ground. The outboard body can move relative to the inboard body in both a rolling and sliding manner.

The dynamic equations of motion were determined using Kane's formulation and a numerical solution was attained through the implementation of a fourth-fifth order, variable time step, Runge-Kutta integrator.

The positions of four markers, located on the outboard body of the system, were predicted in ground fixed coordinates by the solution routine. A physical model of the system was constructed and position locations of four markers located on the outboard body were captured by an Optotrak 3020 motion tracking system.

Both static and dynamic experimental trials were performed and compared to the simulation. For one test case, the experimental data frequency of oscillation was found to be $\omega_e = 2.33\ Hz$ and the simulation frequency was found to be $\omega_s = 2.37\ Hz$. Several sources for the discrepancies include viscous damping, a possible additional forcing function caused by lead wire sway, and neglecting the mass of the system's springs. Coulomb damping was included in the simulation.

Indexing terms: point contact joint, kinematics, dynamics, biomechanics

# Acknowledgments

The success of this project would not have been possible without the guidance and support of my research supervisor, Dr. R.J. Anderson. Thank you for all your help and encouragement.

In addition, I would like to express my great thanks to the HMRC staff for providing the Optotrak camera system used for the experimental portion of this work. Dr. K. Deluzio and Ms. L. Ploeg were excellent resources, and without their assistance the experimental phase would not have been as successful. Thank you also to Caleb Werner for his help with the Optotrak system and data collection process.

The technical support from the technical staff in the Department of Mechanical Engineering Machine Shop and Tech Shop was greatly appreciated. Also, thank you to Brett Jan and Chris Clark for their assistance and advise in regards to my physical model.

Thank you Mom and Dad, and Ally for all of your support throughout the years. Without you, this project would not have been possible. Finally, a big thank you to all of my friends, family and colleagues for lending an ear at those critical points in this research when it seemed as though there was no end in sight. Thank you for reminding me that not all problems are located in the math!

Financial assistance for the author was provided through a scholarship from the Natural Sciences and Engineering Research Council of Canada, a Queen's University Graduate Award, and a teaching assistantship and research assistantship in the Department of Mechanical and Materials Engineering.

This work is dedicated to my grandpa, Kenneth Knutson, who helped to start my engineering career!

# Contents

# List of Tables

# List of Figures

# Notation

*Subscripts:*

| | |
|---|---|
| $i$ | index |
| $B_i$ | pertaining to body $i$ |
| $cs$ | pertaining to a coordinate system |
| $G$ | center of mass of a body |
| 0 | pertaining to the ground fixed coordinate system |
| 1 | pertaining to the first coordinate system |
| 2 | pertaining to the second coordinate system |
| 3 | pertaining to the third coordinate system |
| 4 | pertaining to the fourth coordinate system |
| 5 | pertaining to the fifth coordinate system |
| $E$ | pertaining to spring E |
| $F$ | pertaining to spring F |
| $G$ | pertaining to spring G |
| $H$ | pertaining to spring H |
| $I$ | pertaining to spring I |
| $J$ | pertaining to spring J |
| $e$ | elastic potential |
| $g$ | gravitational potential |

*Overscripts:*

| | |
|---|---|
| $\vec{}$ | vector |

| | |
|---|---|
| $\dot{}$ | first time derivative |
| $\ddot{}$ | second time derivative |

*Variables:*

| | |
|---|---|
| $x$ | configuration coordinate, generalized speed |
| $g$ | acceleration due to gravity |
| $I_{ii}$ | mass moment of inertia |
| $I_{ij}$ | product of inertia |
| $L$ | length |
| $m$ | mass |
| $\delta$ | change in length |
| $\zeta$ | damping ratio |
| $\omega_n$ | natural frequency |
| $\omega_d$ | damped frequency |
| $T$ | kinetic energy |
| $U$ | potential energy |

*Vectors:*

| | |
|---|---|
| $\vec{P}$ | position vector |
| $\vec{V}$ | velocity vector |
| $\vec{A}$ | acceleration vector |
| $\vec{\omega}$ | angular velocity vector |
| $\vec{\alpha}$ | angular acceleration vector |
| $\vec{F}$ | force vector |
| $\vec{M}_i$ | external moment about $i$ |
| $\vec{D}ir$ | unit direction vector |
| $\vec{R}1$ | inboard radius vector |
| $\vec{R}2$ | outboard radius vector |
| $\vec{B}$ | center of mass to outboard center of rotation vector |

| | |
|---|---|
| $\vec{D}$ | body fixed spring attachment point vector |
| $\vec{Q}$ | Generalized Active Force vector |
| $\vec{Q}^*$ | Generalized Inertial Force vector |

*Matrices:*

| | |
|---|---|
| $[m]$ | mass matrix |
| $[I_i]$ | inertia matrix about the center of mass |
| $[R]$ | rotation matrix |
| $[T]$ | transformation matrix |
| $[QQ]$ | matrix of terms dependent on the derivative of generalized speeds |

# Chapter 1

# Introduction

## 1.1 Motivation

In the human body, the knee is one of the most complicated and intricate joints. At first glance, it appears to be a simple pin joint with one degree of freedom, similar to a hinge on a door, allowing flexion and extension about a fixed axis. Upon closer examination, the knee is found to be much more complicated, involving multiple joints, multiple points of contact, and multiple degrees of freedom. An extensive system of ligaments, tendons and muscles keep the various bony structures in place and articulating in an appropriate fashion. Knee injuries and ailments are quite common, and occasionally in some individuals the joint, either in part or as a whole, must be replaced with a prosthetic. This process is known as knee arthroplasty [29]. In order to assist the evaluation of prosthesis functionality, various mathematical models have been developed to represent the motion of the joint. Due to the complexity of the joint, developing an accurate mathematical model to represent the dynamic equations of motion has proven to be quite difficult. Although great efforts have been made in developing three dimensional knee models, most researchers seem to be satisfied to use commercial software packages to simulate system dynamics. Unfortunately, the joint libraries in these software packages do not include joints which can appropriately represent the complex contact and articulation found in the biomechanical application of the knee joint. Spatial point or line contact joints are known as higher

paired joints. Commonly, software packages will attempt to represent these higher paired joints by combining a series of lower paired joints which already exist within the joint library. These joints may transform a body from one point to another in three dimensional space; however, the path that the body follows to get there is not true to the articulation surface. Alternatively, researchers will use a maximal coordinate model, six degrees of freedom for each joint, and then attempt to reduce the model by introducing algebraic constraints which introduces a host of other problems including drift away from the contact surface. The underlying dynamics driving knee motion have been overlooked and as a result currently available simulations may not be providing an accurate representation of the motion. In addition, systematic validation techniques for joint simulations also seem to be lacking. A brief overview of knee anatomy is given below and is followed by a discussion of current knee dynamics models and joint options.

## 1.2 Literature Review

### 1.2.1 Knee Anatomy

The knee is composed of two distinct joints: the tibiofemoral joint and the patellofemoral joint. The tibiofemoral joint involves the interaction of the distal femur and the proximal tibia, and is responsible for motion between the thigh and the calf [17]. The patellofemoral joint involves the interaction of the patella and femur, and the main function is to act as a pulley for the quadriceps muscles [17]. Since the tibiofemoral joint is key in describing the motion of the knee joint, it will be examined in detail below. The structure and function of the knee joint reflect how it is integral to both the stability and mobility of the human body [17].

The tibiofemoral joint is a double condyloid joint [17]. Three rotational degrees of freedom are required to fully describe the rotational motion of the joint. Flexion and extension occurs in the sagittal plane, internal and external rotation occurs in the transverse plane, and abduction and adduction occurs in the frontal plane [17]. In addition to rotational motion, sliding occurs within the tibiofemoral joint at the

articulation surface. Translational anteroposterior and medial/lateral displacements occur through normal knee motion to follow the articulation surfaces [17]. Thus, five degrees of freedom are required to represent the overall motion between the thigh and shank. In addition, one or two points of contact are possible for tibiofemoral joint, as one or both of the condyles may be in contact. Figure 1.1 shows the various planes of knee motion [29].

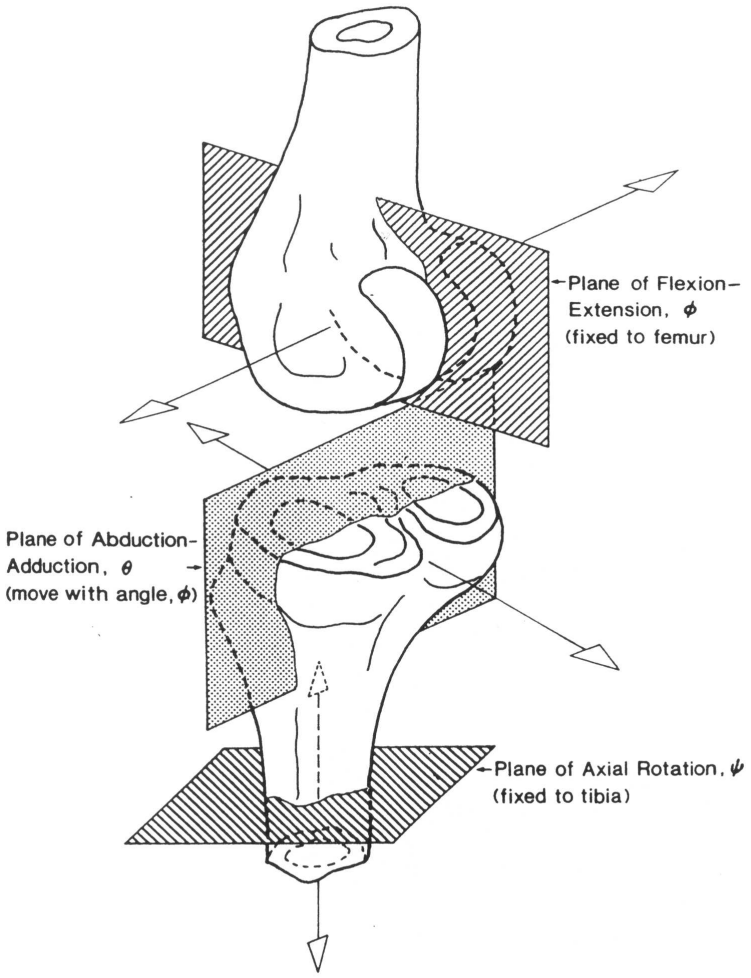


Figure 1.1: Planes of Knee Motion [29]

### 1.2.2 Total Knee Replacements

Total knee arthroplasty (TKA) is a surgical treatment for patients where disease, injury or congenital defects prevents normal knee function and unmanageable pain is present. The natural knee joint is removed and replaced by an artificial joint with the following components: femoral component, tibial plateau, tibial polyethylene insert and a patellar component [29]. Figure 1.2 shows the components in detail [30].

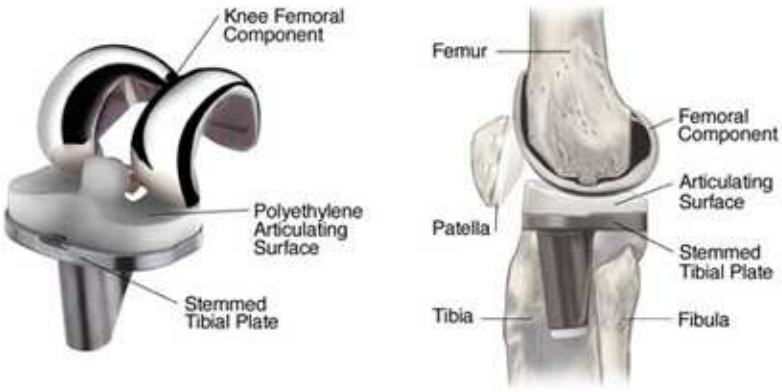


Figure 1.2: Artificial Knee by Zimmer [30]

Like many biomechanical devices, wear is a significant problem in the TKA and it can cause failure of the device [29]. The mechanisms and severity of wear are much different from those in the artificial hip joint and, as such, much research has been focused on studying the kinematics and dynamics of the knee, to help improve artificial knee designs and reduce wear. Three dimensional computer simulations for the time domain response of a knee joint subjected to time varying loads can greatly assist TKA designers, as they can test to see how their product performs before prototyping, and potentially optimize the articulation surfaces to minimize wear.

### 1.2.3 Dynamic Principles

In order to determine the time domain response of a system to varying forces, the equations of motion governing the systems dynamics must be derived. Generation of

the equations of motion can be performed by many different methods, three being: Newton-Euler, Lagrange, or Kane's Equations. These methods are briefly described below.

The Newton-Euler equations of motion are derived for a body in three dimensional space by applying two principles. Firstly, Newton's second law $F = ma$ is applied to sum the contributions of linear motion in each of three directions that define three dimensional space. Secondly, Euler's equations are used to sum the contributions of the angular motions about each of the three directions. This results in six equations of motion for the body. The equations are based on the acceleration, either linear or angular, of the configuration coordinates and therefore are found to be second order differential equations. In order to solve these complex non-linear differential equations, they must be 1) linearized or 2) coupled with algebraic constraint equations and solved numerically using a differential-algebraic equation (DAE) solver.

The Lagrangian method is based on energy principles and has two main advantages over the Newtonian approach. The kinematic analysis is less intense because the energy terms are based on velocity rather then acceleration and free body diagrams are not necessary as the forces of constraint are automatically eliminated in this method [2]. If it is desired to know the force of constraint, Lagrangian multipliers must be used to draw out this information. Second order, non-linear, differential equations are developed through this method and like the Newtonian method, a solution to a non-linear system can only be realized if the equations are linearized or solved numerically.

Kane's dynamic principle, developed in the 1980's, is a method based on linear and angular momentum. Generalized speeds are introduced as the state variables and as such, accelerations are first derivatives of the state variables. Unlike the previous two approaches, Kane's method results in a system of first order, ordinary, differential equations which can very easily be integrated using a numerical routine; therefore, this method is desirable for computer simulations. Although it is very efficient in terms of computational analysis, this method can be significantly more difficult to implement due to the fact that all physical meaning is lost. Also, since the method

is newer, it is less studied in comparison to the Newton or Lagrange approaches and there are fewer resources available. Finally, like the Lagrangian method, the forces of constraint are eliminated in this method. If contact information is required, an additional generalized speed that gives a partial velocity at the point of contact must be added to the system [15].

### 1.2.4 Mathematical Knee Models

Early research in the area of human mechanics was based on gathering information through experimental techniques. As computer systems advanced in the 1970's, mathematical models of joint motion and function began to evolve. A review of state of the art mathematical knee models, performed in 1988 by Hefzy [14], found that two branches of knee modeling existed: phenomenological models, and anatomical models.

#### Phenomenological Models

The first type, phenomenological models, treat the knee as either a simple hinge or a viscoelastic hinge joint. Simple hinge joints have been used mainly for predicting overall human gait motion and the viscoelastic hinge joints have been used in estimating response of the knee in dynamic loading while taking into account muscular and tendon forces [14]. While phenomenological models may be useful for making model estimations, they do not adequately represent the articulation found at the knee joint and as such will not be considered further.

#### Anatomical Models

Anatomical models make an attempt to represent the kinematics and kinetics of the knee in a way that takes into account the actual anatomy and degrees of freedom of the joint. Anatomical models can be divided into static and quasi-static models, and dynamic models.

Static and quasi-static models have been utilized to determine forces in the knee

under equilibrium conditions [14]. Several variations of these models have been introduced to determine the distributive forces in the muscles and ligaments and the contact forces between the bony structures under various joint loading conditions. One of the first comprehensive three dimensional quasi-static models was introduced by Wismans [28] in 1980. This model utilized polynomials to represent the curved articulation surfaces, and the femur and tibia were modeled as rigid bodies. The model did not take into consideration effects caused by the patellofemoral joint as only the tibiofemoral joint was examined. The effects of the menisci were ignored and the model was assumed to have two points of contact, one at each condyle. The effects of rigid versus deformable contact [5], as well as numerous ligament models [14] have been explored in detail in the static mode. Essinger, [9], was the first to develop a three dimensional, quasi-static model of the knee which included both the tibiofemoral and patellofemoral joints. In this model the femur, patella and patella tendon were assumed to be rigid bodies and the tibia was deformable [13]. The implicit finite element method has been employed extensively in this area of research [12]. Although the static and quasi-static models offer insight into the motion and forces experienced by the knee joint, a dynamic model is far more desirable in order to determine the time based response of the joint to varying applied loads.

Researchers have been trying to develop dynamic knee models since the early 1980's. Moeinzadeh noted that, in 1982, no biodynamical models were available for the knee [21]. He developed the first mathematical dynamic model of the tibiofemoral joint, by treating the femur and tibia as rigid bodies in a two dimensional analysis. The contact surface was estimated by a polynomial equation obtained from digitizing x-rays of human knee joints. The model was set to have three degrees of freedom, and one contact condition was described as an algebraic constraint. Ligaments were modeled as non-linear elastic springs. The non-linear equations of motion were developed using the Newton Euler approach. The equations were linearized and a numerical solution was realized through the Newton-Raphson iteration process.

The two dimensional model described above was followed up sometime later by Abdel-Rahman and Hefzy in 1997 [1], who created a three dimensional dynamic model. The

articulating surfaces were again represented by mathematical functions, and the joint ligaments were modeled as non-linear elastic springs. Rigid body motion was assumed. Six nonlinear equations of motion were generated and coupled with non-linear algebraic constraint equations and solved using a differential-algebraic equation solver [1] which incorporated the Newton-Raphson iteration method.

Caruntu and Hefzy further refined the model by including patellofemoral contact in 2004 [6]. They also allowed for deformable contact at the articulation surfaces. The preceding three dimensional models produced time domain solutions using a mathematical resolution technique. This method requires that the second order differential equations, generated through the Newton-Euler dynamic principle, be first cast as first order ordinary differential equations, by representing the second order terms as derivatives of the first order terms, and then combined with the algebraic constraint equations [6]. Next a backwards differentiation formula is used to approximate a solution for the first derivatives of the kinematic parameters. Finally a solution is predicted using the Newton Raphson iteration method.

Another method for predicting the time domain response to varying loads for a three dimensional knee model is to use an explicit finite element (FE) analysis. In this technique, a three dimensional finite element model is first produced and then the dynamic response of the model is predicted using an external dynamic simulation software package. A variety of three dimensional models have been produced, with most of the work concentrating on total knee replacement simulations, where a three dimensional computer model of the components exists and material properties are well defined.

Giddings, in 2001, developed a finite element model to examine the stresses and kinematics of a Scorpio total knee replacement [10]. The model was only given three degrees of freedom, flexion-extension rotation (one dof) and translational motion in the sagittal plane (two dof). The femoral component was modeled as a rigid body and the polyethylene tibial insert was modeled as a linear elastic deformable material. LS-DYNA3D (Livermore Technology Software Corporation), a commercial structural

dynamics package, was used to predict the time domain response of the model.

The same year, Godest also produced a finite element model to simulation the dynamic response of a PFC Sigma total knee replacement [11]. This model included five degrees of freedom, three rotational and two translational, which more closely represented the motions found in an actual knee. Similarly to Giddings model, the femoral component was modeled as a rigid body and the polyethylene tibial insert was modeled as a linear elastic deformable material. PAM-SAFE (ESI-Group), a dynamics package, was used to predict the systems dynamic response to time varying loads.

Halloran developed a finite element model for a total knee replacement, in 2004, which incorporated patellofemoral as well as tibiofemoral articulation. A rigid body analysis was performed for computational efficiency [12]. Unlike previous FE analyses which used commercial multibody dynamics packages, Halloran implemented a model of joint motion by writing a processing script to incorporate a three-cylindric model of joint motion, which was then interfaced with the output results database [12]. The three-cylindric joint is composed of three cylindrical joints in series - which together yield six degrees of freedom.

Piazza and Delp [25] used the multibody dynamics package, SD/FAST (Parametric Technology Corporation), to determine the response of a three dimensional knee model. The thigh was not constrained relative to the shank, and thus the model assumed six degrees of freedom at the tibiofemoral knee joint and used a rigid body contact model to limit the motion.

Bei and Fregly [4] have focused on trying to combine deformable contact with three dimensional dynamic analysis. The model created originally has six degrees of freedom at the knee joint, however three degrees of freedom are eliminated from the simulation by using fluoroscopically measured kinematics [3]. Pro/MECHANICA MOTION (Parametric Technology Corporation) was the multibody dynamics software package used; however, it was noted that the following other software packages are available:

Software for Interactive Musculoskeletal Modeling (SIMM) and the Dynamics Pipeline (Motion Analysis Corporation), Musculoskeletal Modeling in Simulink (MMS)(A.E. Mann Institute for Biomedical Engineering), ADAMS (MSC Software), Autolev (Online Dynamics), and DADS (LMS International).

Delp et al. investigated the creation of an open-source software system, OpenSim, developed to handle dynamic simulations of musculoskeletal structures [7]. It was noted that in addition to the multibody dynamics software packages listed above, Visual 3D and Anybody are also both used to produce biomechanical dynamic simulations.

It is important to understand the methods underlying these multibody dynamics packages and to explore the joint libraries to see what kind of options are available for connecting bodies. Several packages commonly used in dynamics simulations are examined below.

MSC-ADAMS:
ADAMS (Automatic Dynamic Analysis of Mechanical Systems) is a commercially available software package designed to determine the kinematics and kinetics of mechanical systems. Dynamic equations of motion are developed using the Newtonian approach. Algebraic constraint equations are applied to the governing systems of differential equations in order to restrict motion (degrees of freedom) [22].

LSDYNA-3D:
This package is used to provide dynamic analysis of finite element models. The Newton-Euler method is used to determine the dynamic equations of motion for the model and constraint equations are defined to limit motion. Only the following six joints are defined in the joint library: spherical, revolute, cylindrical, planar, translational and universal. These are all lower paired joints and none alone have more than four degrees of freedom [18].

SD/FAST:
This method is based on Kane's principles of dynamics, and solutions are determined by an implementation of a Runge-Kutta numerical integration routine. Upon close examination of the available joints in the SD/FAST users manual, it was determined that the six degree of freedom joint used to model knee motion is actually a composite joint. A ball and socket joint, with three rotational degrees of freedom, is added to three unidirectional slider joints. Unobstructed, this free joint will describe motion of a body from one configuration to another in three dimensional space; however, the translation will be restricted to be along a defined set of axes. Thus, following a curved surface using this joint is impossible.

Pro/MECHANICA MOTION:
This package is very similar to SD/Fast. It solves a system of rigid bodies connected by either rigid or flexible joints. The systems dynamic equations of motion are developed using Kane's method and the system is solved using a fourth order, variable time step, Runge-Kutta integrator [8].

SIMM and the Dynamics Pipeline:
SIMM is one of the most popular biomechanical simulation software packages. It is specifically designed to deal with living organisms and, unlike many modeling packages, it has the ability to incorporate the use of biomaterials such as bones, muscles, ligaments, and tendons [23]. The dynamics equations of motion of systems modeled in SIMM are determine by the Dynamics Pipeline, which incorporates muscle force. The Dynamics Pipeline uses SD/FAST to predict the dynamic response of a model so the issues discussed above in regards to SD/FAST are also relevant here [25].

### 1.2.5 Higher Paired Joints

Kempson [16] noted that the development of spatial higher pair (point contact) joints has been limited due to the complex nature of these systems and he provided a thorough review of the previous literature in his work[16]. Several authors have made

contributions to this field and there are a limited number of models available [16], including work by Balling, Shabana, Pfister, Tasora, and Kim. It is important to note that experimental validation has not been performed for any computer simulations available at this point in time. Kempson developed a general multibody dynamics formulation for the computer simulation of a higher paired joint. Attempts were made to test the validity of the formulation by implementing a special case, sphere on sphere articulation model, and comparing the results to those based on hand derived analytical test cases. No experimental validation was attempted for his work.

## 1.3 Research Outline

The first goal of this research project was to develop a computer simulation to predict the three dimensional dynamic equations of motion, through the implementation of Kane's equations, for a five degree of freedom point contact joint. The joint had to be one for which a physical model could be constructed. The method used to form the equations of motion was based on the general case research completed by Kempson. Developing a special case joint that can be physically modeled involves assigning new configuration coordinates and generalized speeds and the joint requires additional forces to provide system stability. Also, the effects of friction had to be considered.

In order to ensure the functionality of the three dimensional simulation, a simpler two dimensional case was first modeled. The two dimensional case included rolling and sliding motion of a planar point contact joint, involving two rotational degrees of freedom. The Kane's simulation was compared to a Lagrangian model derived for the same system to check on its accuracy. In addition, the total energy of the conservative system was calculated and verified not to change as a further check on accuracy.

Once the two dimensional model was validated, the method was expanded to the three dimensional case. The three dimensional simulation had five rotational degrees of freedom.

The second goal of this research was to validate the three dimensional computer simulation with data collected from a physical system. This was a very important

step in the progression of developing a point contact joint simulation, as currently no experimental validations are known to exist for spatial higher pairs. A physical model of the system was constructed and analysis of the motions of the joint was performed. The results from the experimental model were compared to the results predicted by the computer simulation in both static and dynamic cases. Friction in the system was addressed and, where possible, appropriately modeled in the simulation, as the experimental set up had sources of friction that could not be eliminated.

# Chapter 2

# Computer Simulation

The goal for the computer simulation phase of this project was to develop a new special case code for a three dimensional dynamic model of a five degree of freedom point contact joint. It was desired to represent the fully non linear equations of motion in the solution and for the model to be valid for large angles. The output from the computer simulation was eventually compared to experimental data obtained through testing a physical model of the same system, see Chapter 3.

## 2.1 General Description

Several changes were made to the five degree of freedom, point contact, sphere on sphere system, shown below in Figure 2.1, first modeled by Kempson [16].

The system he modelled was found to be unrealistic to physically model so the articulation surface was changed to sphere in sphere contact. Kempson's model was found to have several locations where singularities occurred with the new articulation surface. New configuration coordinates and generalized speeds were introduced in order to generate a computer simulation with as few singularities as possible. Springs were also added to the system to provide stability and to introduce the idea of having external forces other than gravity acting on the outboard body.

The configuration of the system used here is shown in Figure 2.2.

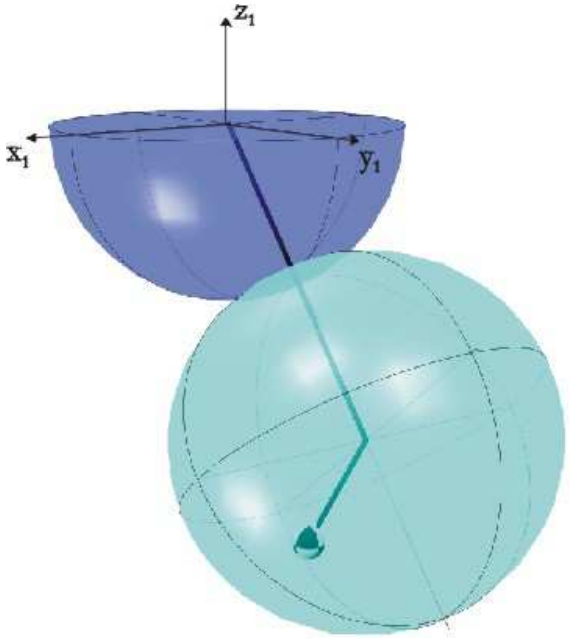


Figure 2.1: Five Degree of Freedom System Modeled by Kempson [16]

The smaller outboard body articulates within the larger spherical cutout in both a rolling (rotational) and sliding (translational) manner. This contact surface greatly simplifies the computer simulation model. There are three degrees of freedom associated with rotational motion as the outboard body can roll in any direction. Since the outboard body must follow the spherical articulation surface, there are only two degrees of freedom associated with translational motion - for example, the x and y positions in three space can be selected but the z position will always be a function of these two coordinates.

Utilizing the method for model formulation outlined by Kempson, a new special case code was developed to model the modified system [16]. The non linear equations of motion were generated numerically using Kane's approach to modeling system dynamics. A variable time step Runge-Kutta solution method was employed.

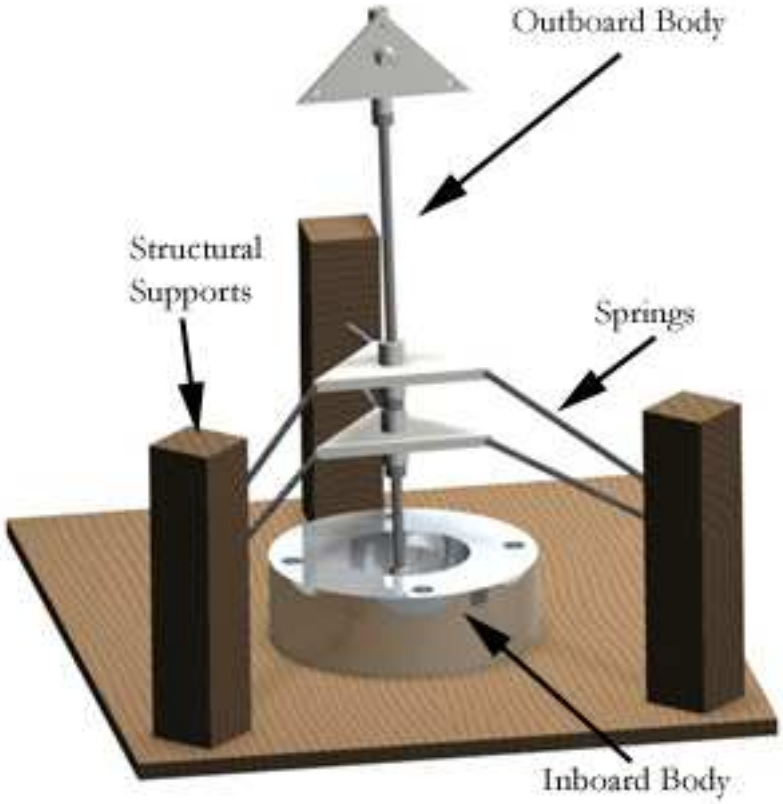


Figure 2.2: Depiction of Three Dimensional Model

## 2.2 Dynamic Formulation: Method of Generating the Equations of Motion

In this section, the formation of Kane's equations was explored and a method for application was formed. Several key features of Kane's method such as generalized speeds and partial velocities are explained in detail. Kane's approach to deriving the equations of motion for a system was employed in the computer simulation because unlike the Newtonian and Lagrangian methods, first order differential equations are generated, thus simplifying the numerical solution routine. Kane's method is based on the principles of linear and angular momentum [15]. The method partitions the general formulas for the time rate of change of linear and angular momentum into portions in the directions of a set of specified generalized speeds.

### 2.2.1 Coordinate Systems

It is important to assign coordinate systems to any dynamic model. This process is highly dependent on the system being analyzed and it is not uncommon to have several different coordinate systems to represent each of the bodies present. It is critical to note whether ground fixed or body fixed coordinate systems have been applied and if body fixed coordinates are being used, the angular velocity and angular acceleration of the coordinate system must be determined.

### 2.2.2 Configuration Coordinates and Generalized Speeds

Before beginning the analysis, configuration coordinates and generalized speeds are assigned to the system. Instead of basing the analysis on the configuration coordinates, as in the Newtonian or Lagrangian approach, Kane's method is based on the generalized speeds of the system. The generalized speeds, denoted $u_i$, can be selected in any manner, but they must be independent of one another so that changes to one speed will not affect any other speed. The number of generalized speeds is dependent on the number of degrees of freedom of the system, with one generalized speed being required for each degree of freedom.

### 2.2.3 Kinematics

As in any dynamic analysis, the kinematics of the system must be determined before Kane's equations can be applied. Starting with position vectors, the absolute velocity and absolute acceleration vectors of the center of mass of each body in the system can be determined by taking derivatives with respect to time as follows. First the position of the center of mass of body B, denoted $\vec{P}_{G_B}$ is found relative to a fixed point. The absolute velocity of the center of mass of body B is found by differentiating the position vector as follows,

$$\vec{V}_{G_B} = \frac{d}{dt}\vec{P}_{G_B} \tag{2.1}$$

$$\vec{V}_{G_B} = \dot{\vec{P}}_{G_B} + \vec{\omega}_{CS} \times \vec{P}_{G_B} \tag{2.2}$$

where $\vec{\omega}_{CS}$ represents the angular velocity of the coordinate system and $\dot{\vec{P}}_{G_B}$ is the rate of change of magnitude of the position vector with respect to time. When differentiating any vector, there are two components: the change in magnitude of the vector and the change in direction of the vector associated with the coordinate system. This process is repeated to find the absolute acceleration of the center of mass of body B.

$$\vec{A}_{G_B} = \frac{d}{dt}\vec{V}_{G_B} \tag{2.3}$$

$$\vec{A}_{G_B} = \dot{\vec{V}}_{G_B} + \vec{\omega}_{CS} \times \vec{V}_{G_B} \tag{2.4}$$

The absolute angular velocity of body B can be represented by $\vec{\omega}_B$. The angular acceleration is then found by differentiating the angular velocity vector with respect to time.

$$\vec{\alpha}_B = \frac{d}{dt}\vec{\omega}_B \tag{2.5}$$

$$\vec{\alpha}_B = \dot{\vec{\omega}}_B + \vec{\omega}_{CS} \times \vec{\omega}_B \tag{2.6}$$

where $\dot{\vec{\omega}}_B$ represents the rate of change of magnitude of the angular velocity with respect to time.

### 2.2.4 Principles of Linear and Angular Momentum

Kane's equations rely on the principles of linear and angular momentum. The equation for the rate of change of linear momentum, for any body, B, in a system, is given by [19],

$$\sum \vec{F} = \frac{d}{dt}\left\{[m]\,\vec{V}_{G_B}\right\} \tag{2.7}$$

where $\sum \vec{F}$ is the sum of all the forces on body B, $[m]$ is the mass matrix of the body, and $\vec{V}_{G_B}$ is the absolute velocity of the center of mass of body B.

The equation for the rate of change of angular momentum, for any body, B, in a system, is give by [19],

$$\sum \vec{M}_{G_B} = \frac{d}{dt} \{[I]\, \vec{\omega}_B\} \tag{2.8}$$

where $\sum \vec{M}_{G_B}$ is the sum of all the moments on body B about the center of mass, G, of the body, $[I]$ is the inertia tensor, and $\vec{\omega}_B$ is the angular velocity of body B.

The inertial tensor for any three dimensional body is given by,

$$[I] = \begin{bmatrix} I_{xx} & -I_{xy} & -I_{xz} \\ -I_{yx} & I_{yy} & -I_{yz} \\ -I_{zx} & -I_{zy} & I_{zz} \end{bmatrix} \tag{2.9}$$

where $I_{xx}$, $I_{yy}$, and $I_{zz}$ represent the mass moment of inertia of body B about the center of mass, G, and the remaining terms are products of inertia.

These equations are rearranged so that all terms appear on the left hand side of the equation.

$$\sum \vec{F} - \frac{d}{dt} \left\{ [m]\, \vec{V}_{G_B} \right\} = \{0\} \tag{2.10}$$

$$\sum \vec{M}_{G_B} - \frac{d}{dt} \{[I]\, \vec{\omega}_B\} = \{0\} \tag{2.11}$$

The above equations are expanded.

$$\sum \vec{F} - [\dot{m}]\vec{V}_{G_B} - [m]\, \frac{d}{dt}\vec{V}_{G_B} = \{0\} \tag{2.12}$$

$$\sum \vec{M}_{G_B} - [\dot{I}]\vec{\omega}_B - [I]\, \frac{d}{dt}\vec{\omega}_B = \{0\} \tag{2.13}$$

### 2.2.5 Partial Velocity and Partial Angular Velocity Vectors

In order to apply Kane's Equations, the next quantity that needs to be calculated is the partial velocity vector with respect to each generalized speed, $u_i$. This partial velocity vector, represented by $\frac{\partial \vec{V}_{G_B}}{\partial u_i}$, determines what portion of the time rate of change of linear momentum should be aligned in the $u_i$ direction.

Similarly, the partial angular velocity vector with respect to each generalized speed, $u_i$, needs to be determined and this quantity indicates what portion of the time rate of change of angular momentum should be aligned in the $u_i$ direction. This partial angular velocity vector is denoted $\frac{\partial \vec{\omega}_B}{\partial u_i}$.

### 2.2.6 Constructing Kane's Equations

The partial velocity vectors and the momentum (equations 2.10 and 2.11) can now be combined to form Kane's equations of motion. The dot product of the partial velocity vector and the time rate of change of linear momentum (equation 2.10) and the dot product of the partial angular velocity and the time rate of change of angular momentum (equation 2.11) are found for each generalized speed, $u_i$, for each body in the system. For body B, the equations are derived below.

$$\frac{\partial \vec{V}_{G_B}}{\partial u_i} \cdot \sum \vec{F}_B + \frac{\partial \vec{V}_{G_B}}{\partial u_i} \cdot \left\{ -[\dot{m}]\vec{V}_{G_B} - [m]\,\frac{d}{dt}\vec{V}_{G_B} \right\} = \{0\} \tag{2.14}$$

$$\frac{\partial \vec{\omega}_B}{\partial u_i} \cdot \sum \vec{M}_{G_B} + \frac{\partial \vec{\omega}_B}{\partial u_i} \cdot \left\{ -[\dot{I}]\vec{\omega}_B - [I]\,\frac{d}{dt}\vec{\omega}_B \right\} = \{0\} \tag{2.15}$$

These two equations for body B can now be added together to create one equation for each generalized speed, $u_i$.

$$\begin{aligned} \frac{\partial \vec{V}_{G_B}}{\partial u_i} \cdot \sum \vec{F}_B + \frac{\partial \vec{\omega}_B}{\partial u_i} \cdot \sum \vec{M}_{G_B} + \frac{\partial \vec{V}_{G_B}}{\partial u_i} \cdot \left\{ -[\dot{m}]\vec{V}_{G_B} - [m]\,\frac{d}{dt}\vec{V}_{G_B} \right\} \\ + \frac{\partial \vec{\omega}_B}{\partial u_i} \cdot \left\{ -[\dot{I}]\vec{\omega}_B - [I]\,\frac{d}{dt}\vec{\omega}_B \right\} = \{0\} \end{aligned} \tag{2.16}$$

Kane divides the above equation into two sections, generalized inertial forces and generalized active forces. Generalized inertial forces, denoted $\vec{Q}^*$, sum the contribution

of those quantities which depend on the time rate of change of momentum, and the generalized active forces, denoted $\vec{Q}$, sum the contributions of external loads. For body B, the generalized inertial force is found to be,

$$\vec{Q}^*_{B_i} = \frac{\partial \vec{V}_{G_B}}{\partial u_i} \cdot \left\{ -[\dot{m}]\vec{V}_{G_B} - [m]\,\frac{d}{dt}\vec{V}_{G_B} \right\} + \frac{\partial \vec{\omega}_B}{\partial u_i} \cdot \left\{ -[\dot{I}]\vec{\omega}_B - [I]\,\frac{d}{dt}\vec{\omega}_B \right\} \tag{2.17}$$

Similarly, the generalized active force for body B is given by the following,

$$\vec{Q}_{B_i} = \frac{\partial \vec{V}_{G_B}}{\partial u_i} \cdot \sum \vec{F}_B + \frac{\partial \vec{\omega}_B}{\partial u_i} \cdot \sum \vec{M}_{G_B} \tag{2.18}$$

Most systems do not have a single body so in order to apply Kane's method to a multibody system the contributions from each body must be added together to obtain a single equation for each generalized speed. For any generalized speed, $u_i$, Kane's formulation is represented by the following,

$$\sum_{B=1}^{N} \vec{Q}^*_{B_i} + \sum_{B=1}^{N} \vec{Q}_{B_i} = \{0\} \tag{2.19}$$

where N represents the number of bodies in the system.

## 2.3 Planar Example

In order to formulate the complex three dimensional model, it was decided that it would be beneficial to first model a simpler two dimensional joint of the same configuration; rolling and sliding on a circular surface. The two dimensional model was formulated using Kane's equations and it was compared to a Lagrangian formulation for the same joint. The two models are explained in detail below and a comparison of the results follows.

### 2.3.1 Two Dimensional Case Modeled with Kane's Equations

The two dimensional case modeled is depicted below in Figure 2.3. Each of the model parameters shown in Figure 2.3 is described in detail in Table 2.1 below.

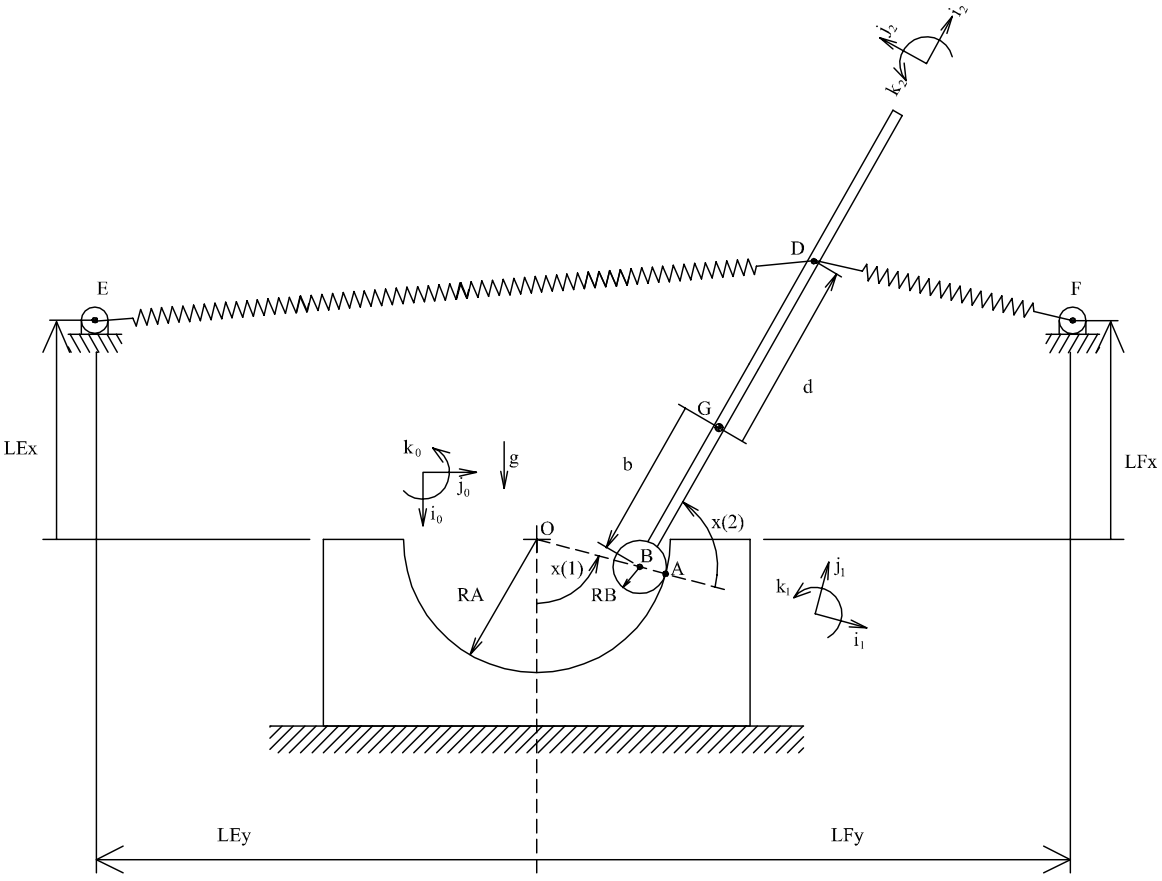


Figure 2.3: Depiction of Two Dimensional Model

### Coordinate Systems

Three coordinate systems were assigned to the model as depicted above - a ground fixed coordinate system located at the center of the circular cut out $(\hat{i}_0, \hat{j}_0, \hat{k}_0)$, an intermediate coordinate system, aligned with the radial line intersecting the point of contact, $(\hat{i_1}, \hat{j_1}, \hat{k_1})$, and a body fixed coordinate system in the outboard body $(\hat{i_2}, \hat{j_2}, \hat{k_2})$.

### Configuration Coordinates and Generalized Speeds

The first step in developing the equations of motion for the system was to determine which configuration coordinates and generalized speeds to use. Since the two dimensional system depicted above has two degrees of freedom (the outboard body can slide

| Variable Name | Definition |
|---|---|
| $RA$ | radius of the fixed sphere |
| $RB$ | radius of the moving sphere |
| $O$ | center of the fixed sphere (a fixed point in space) |
| $B$ | center of the moving sphere |
| $A$ | contact point between the fixed and moving spheres |
| $G$ | center of mass of the moving body |
| $E$ | ground fixed spring attachment point for spring E |
| $F$ | ground fixed spring attachment point for spring F |
| $b$ | distance from the center of the moving sphere to the center of mass of the moving body |
| $d$ | distance from the center of mass moving sphere to the body fixed spring attachment location |
| $\vec{LE}$ | vector from the center of the fixed sphere to the ground fixed spring E attachment location |
| $\vec{LF}$ | vector from the center of the fixed sphere to the ground fixed spring F attachment location |
| $g$ | gravitational acceleration |

Table 2.1: Model Parameters.

along the circular contact surface or it can rotate about the z axis), two generalized speeds were required to generate the model. The configuration coordinates were selected to represent rotations from the ground fixed coordinate system to the body fixed coordinate system. The first configuration coordinate, $x(1)$, represents the positive (counter-clockwise) rotation about the $z_0$ axis which transforms from coordinate system $(\hat{i_0}, \hat{j_0}, \hat{k_0})$ to coordinate system $(\hat{i_1}, \hat{j_1}, \hat{k_1})$. The second configuration coordinate, $x(2)$, represents the positive (counter-clockwise) rotation about the $z_1$ axis which transforms from coordinate system $(\hat{i_1}, \hat{j_1}, \hat{k_1})$ to coordinate system $(\hat{i_2}, \hat{j_2}, \hat{k_2})$. The generalized speeds, $x(3)$ and $x(4)$, were selected to be the time derivatives of the configuration coordinates, $x(1)$ and $x(2)$, respectively.

$$\begin{aligned} x(3) &= \dot{x}(1) \\ x(4) &= \dot{x}(2) \end{aligned} \tag{2.20}$$

It is important to note that these generalized speeds are linearly independent and form an orthonormal basis [15].

### Transformation Matrices

As many models involve more than one coordinate system, transformation matrices must be constructed to easily facilitate transforming vectors from one coordinate system to another. In this model it is desired to be able to transform both from ground fixed to body fixed coordinates and from body fixed to ground fixed coordinates. The transformation from ground fixed coordinates to body fixed coordinates requires two rotations. The rotation from the ground fixed coordinate system, $(\hat{i_0}, \hat{j_0}, \hat{k_0})$, to the intermediate coordinate system, $(\hat{i_1}, \hat{j_1}, \hat{k_1})$, is represented by the first configuration coordinate, $x(1)$. The transformation matrix from coordinate system $(\hat{i_0}, \hat{j_0}, \hat{k_0})$ to coordinate system $(\hat{i_1}, \hat{j_1}, \hat{k_1})$ is shown below.

$$\left[R_{x(1)}\right] = \begin{bmatrix} \cos x(1) & -\sin x(1) & 0 \\ \sin x(1) & \cos x(1) & 0 \\ 0 & 0 & 1 \end{bmatrix} \tag{2.21}$$

The rotation from the intermediate coordinate system, $(\hat{i_1}, \hat{j_1}, \hat{k_1})$, to the body fixed coordinate system, $(\hat{i_2}, \hat{j_2}, \hat{k_2})$, is represented by the second configuration coordinate, $x(2)$. The transformation matrix from coordinate system $(\hat{i_1}, \hat{j_1}, \hat{k_1})$ to coordinate system $(\hat{i_2}, \hat{j_2}, \hat{k_2})$ is shown below.

$$\left[R_{x(2)}\right] = \begin{bmatrix} \cos x(2) & -\sin x(2) & 0 \\ \sin x(2) & \cos x(2) & 0 \\ 0 & 0 & 1 \end{bmatrix} \tag{2.22}$$

The transformation matrix from the ground fixed coordinate system to the body fixed coordinate system is given by the following,

$$[T] = \left[R_{x(1)}\right]\left[R_{x(2)}\right] \tag{2.23}$$

This simplifies to,

$$[T] = \begin{bmatrix} \cos\left(x(1)+x(2)\right) & -\sin\left(x(1)+x(2)\right) & 0 \\ \sin\left(x(1)+x(2)\right) & \cos\left(x(1)+x(2)\right) & 0 \\ 0 & 0 & 1 \end{bmatrix} \tag{2.24}$$

The transformation from body fixed coordinates to ground fixed coordinates also requires two rotations. The rotation from the body fixed coordinate system, $(\hat{i_2}, \hat{j_2}, \hat{k_2})$, to the intermediate coordinate system, $(\hat{i_1}, \hat{j_1}, \hat{k_1})$, is represented by a clockwise rotation of second configuration coordinate, $x(2)$. The transformation matrix from coordinate system $(\hat{i_2}, \hat{j_2}, \hat{k_2})$ to coordinate system $(\hat{i_1}, \hat{j_1}, \hat{k_1})$ is shown below.

$$\left[TR_{x(2)}\right] = \begin{bmatrix} \cos x(2) & \sin x(2) & 0 \\ -\sin x(2) & \cos x(2) & 0 \\ 0 & 0 & 1 \end{bmatrix} \tag{2.25}$$

The rotation from the intermediate coordinate system, $(\hat{i_1}, \hat{j_1}, \hat{k_1})$, to the ground fixed coordinate system, $(\hat{i_0}, \hat{j_0}, \hat{k_0})$, is represented by a clockwise rotation of the configuration coordinate, $x(1)$. The transformation matrix from coordinate system $(\hat{i_1}, \hat{j_1}, \hat{k_1})$ to coordinate system $(\hat{i_0}, \hat{j_0}, \hat{k_0})$ is shown below.

$$\left[TR_{x(1)}\right] = \begin{bmatrix} \cos x(1) & \sin x(1) & 0 \\ -\sin x(1) & \cos x(1) & 0 \\ 0 & 0 & 1 \end{bmatrix} \tag{2.26}$$

The transformation matrix from the body fixed coordinate system to the ground fixed coordinate system is given by the following,

$$[TT] = \left[TR_{x(2)}\right]\left[TR_{x(1)}\right] \tag{2.27}$$

This simplifies to,

$$[TT] = \begin{bmatrix} \cos(x(1)+x(2)) & \sin(x(1)+x(2)) & 0 \\ -\sin(x(1)+x(2)) & \cos(x(1)+x(2)) & 0 \\ 0 & 0 & 1 \end{bmatrix} \tag{2.28}$$

**Absolute Angular Velocity of Outboard Body**

The angular velocity of the outboard body is represented by the following equation.

$$\vec{\omega}_2 = \begin{Bmatrix} 0 \\ 0 \\ x(3) \end{Bmatrix} + \begin{Bmatrix} 0 \\ 0 \\ x(4) \end{Bmatrix} \tag{2.29}$$

It is important to note that the angular velocity represented by equation 2.29 is in the body fixed coordinate system $(\hat{i_2}, \hat{j_2}, \hat{k_2})$. Thus, the angular velocity of the coordinate system, $\vec{\omega}_{CS}$, is equal to the angular velocity of the outboard body, $\vec{\omega}_2$.

**Angular Acceleration**

The angular acceleration of the outboard body is found by differentiating the angular velocity, equation 2.29, with respect to time.

$$\vec{\alpha}_2 = \frac{d}{dt}\vec{\omega}_2 \tag{2.30}$$

$$\vec{\alpha}_2 = \dot{\vec{\omega}}_2 + \vec{\omega}_{CS} \times \vec{\omega}_2 \tag{2.31}$$

Since the angular velocity of the coordinate system is equal to the angular velocity of the outboard body the second term of equation 2.31 is zero. The simplified equation for the angular acceleration is given by,

$$\vec{\alpha}_2 = \begin{Bmatrix} 0 \\ 0 \\ \dot{x}(3) \end{Bmatrix} + \begin{Bmatrix} 0 \\ 0 \\ \dot{x}(4) \end{Bmatrix} \tag{2.32}$$

**Position Vector**

It is necessary to determine the position vector in order to calculate the absolute velocity, partial velocities and absolute acceleration of the center of mass of the outboard body. Referring to Figure 2.3, the vector describing the position from the ground fixed origin, point O, to the center of mass of the outboard body, point G, is given by the following expression, see Figure 2.3.

$$\vec{P}_{G2} = \vec{R1}^{T} \begin{Bmatrix} \hat{i_0} \\ \hat{j_0} \\ \hat{k_0} \end{Bmatrix} - \vec{R2}^{T} \begin{Bmatrix} \hat{i_2} \\ \hat{j_2} \\ \hat{k_2} \end{Bmatrix} - \vec{B}^{T} \begin{Bmatrix} \hat{i_2} \\ \hat{j_2} \\ \hat{k_2} \end{Bmatrix} \tag{2.33}$$

where $\vec{R1}$ is the vector from point O to point A, $\vec{R2}$ is the vector from point B to point A, and $\vec{B}$ is the vector from point G to point B

Since the above expression uses multiple coordinate systems, the component written in the ground fixed system was transformed to the body fixed system by multiplying by the transformation matrix $[T]$ derived earlier in equation 2.24.

$$\vec{P}_{G2} = \vec{R1}^{T} [T] \begin{Bmatrix} \hat{i_2} \\ \hat{j_2} \\ \hat{k_2} \end{Bmatrix} - \vec{R2}^{T} \begin{Bmatrix} \hat{i_2} \\ \hat{j_2} \\ \hat{k_2} \end{Bmatrix} - \vec{B}^{T} \begin{Bmatrix} \hat{i_2} \\ \hat{j_2} \\ \hat{k_2} \end{Bmatrix} \tag{2.34}$$

The vector $\vec{R1}$ is defined in the ground fixed coordinate system to be,

$$\vec{R1} = \begin{Bmatrix} RA\cos x(1) \\ RA\sin x(1) \\ 0 \end{Bmatrix} \tag{2.35}$$

The vector $\vec{R2}$ is defined in the body fixed coordinate system to be,

$$\vec{R2} = \begin{Bmatrix} RB\cos x(2) \\ -RB\sin x(2) \\ 0 \end{Bmatrix} \tag{2.36}$$

The vector $\vec{B}$ is defined in the body fixed coordinate system to be,

$$\vec{B} = \left\{ \begin{array}{c} -b \\ 0 \\ 0 \end{array} \right\} \tag{2.37}$$

It should be noted that $\vec{B}$ remains constant in the body fixed coordinate system for any point in time, while $\vec{R}1$ and $\vec{R}2$ change as the angles $x(1)$ and $x(2)$ change.

### Absolute Velocity

The absolute velocity of the center of mass of the outboard body was found by differentiating the position vector with respect to time. In the body fixed coordinate system, the absolute velocity was found to be,

$$\vec{V}_{G2} = \frac{d\vec{P}_{G2}}{dt} \tag{2.38}$$

$$\vec{V}_{G2} = \dot{\vec{P}}_{G2} + \vec{\omega}_{CS} \times \vec{P}_{G2} \tag{2.39}$$

Since the velocity expression is formed in body fixed coordinates, the term $\vec{\omega}_{CS}$ can be replaced with the angular velocity of the outboard body, $\vec{\omega}_2$. Using the expression derived for $\vec{P}_{G2}$ in equation 2.34 the velocity vector is found to be,

$$\begin{aligned} \vec{V}_{G2} = \dot{\vec{R}}1^T [T] \left\{ \begin{array}{c} \hat{i_2} \\ \hat{j_2} \\ \hat{k_2} \end{array} \right\} + \vec{R}1^T [\dot{T}] \left\{ \begin{array}{c} \hat{i_2} \\ \hat{j_2} \\ \hat{k_2} \end{array} \right\} - \dot{\vec{R}}2^T \left\{ \begin{array}{c} \hat{i_2} \\ \hat{j_2} \\ \hat{k_2} \end{array} \right\} - \dot{\vec{B}}^T \left\{ \begin{array}{c} \hat{i_2} \\ \hat{j_2} \\ \hat{k_2} \end{array} \right\} \\ + \vec{\omega}_2 \times \left[ \vec{R}1^T [T] \left\{ \begin{array}{c} \hat{i_2} \\ \hat{j_2} \\ \hat{k_2} \end{array} \right\} - \vec{R}2^T \left\{ \begin{array}{c} \hat{i_2} \\ \hat{j_2} \\ \hat{k_2} \end{array} \right\} - \vec{B}^T \left\{ \begin{array}{c} \hat{i_2} \\ \hat{j_2} \\ \hat{k_2} \end{array} \right\} \right] \end{aligned} \tag{2.40}$$

It should be noted that since $\vec{B}$ is not time dependent the term $\dot{\vec{B}}$ goes to zero. Kempson [16] proved the following identity which also helps to further simplifies the expression above.

$$\vec{R1}^T[\dot{T}] + \vec{\omega}_2 \times \vec{R1}^T[T] = \{0\} \tag{2.41}$$

In simplified form, the absolute velocity of the center of mass of the outboard body is represented by,

$$\vec{V}_{G2} = \dot{\vec{R1}}^T[T] \begin{Bmatrix} \hat{i_2} \\ \hat{j_2} \\ \hat{k_2} \end{Bmatrix} - \dot{\vec{R2}}^T \begin{Bmatrix} \hat{i_2} \\ \hat{j_2} \\ \hat{k_2} \end{Bmatrix} + \vec{\omega}_2 \times \left[ -\vec{R2}^T \begin{Bmatrix} \hat{i_2} \\ \hat{j_2} \\ \hat{k_2} \end{Bmatrix} - \vec{B}^T \begin{Bmatrix} \hat{i_2} \\ \hat{j_2} \\ \hat{k_2} \end{Bmatrix} \right] \tag{2.42}$$

The vector $\dot{\vec{R1}}$ was found by differentiating $\vec{R1}$, given by equation 2.35, with respect to time.

$$\dot{\vec{R1}} = \begin{Bmatrix} -x(3)RA\sin x(1) \\ x(3)RA\cos x(1) \\ 0 \end{Bmatrix} \tag{2.43}$$

The vector $\dot{\vec{R2}}$ was found by differentiating $\vec{R2}$, given by equation 2.36, with respect to time.

$$\dot{\vec{R2}} = \begin{Bmatrix} -x(4)RB\sin x(2) \\ -x(4)RB\cos x(2) \\ 0 \end{Bmatrix} \tag{2.44}$$

**Absolute Acceleration**

The absolute acceleration vector of the center of mass of the outboard body, in body fixed coordinates, was determined by differentiating the velocity vector, equation 2.42, with respect to time.

$$\vec{A}_{G2} = \frac{d\vec{V}_{G2}}{dt} \tag{2.45}$$

$$\vec{A}_{G2} = \dot{\vec{V}}_{G2} + \vec{\omega}_{CS} \times \vec{V}_{G2} \tag{2.46}$$

Since the acceleration expression is formed in body fixed coordinates, the term $\vec{\omega}_{CS}$ can be replaced with the angular velocity of the outboard body, $\vec{\omega}_2$. Using the expression derived for $\vec{V}_{G2}$ in equation 2.42 the acceleration vector is found to be,

$$\begin{aligned}
\vec{A}_{G2} = {} & \ddot{\vec{R}}1^T\,[T] \begin{Bmatrix} \hat{i_2} \\ \hat{j_2} \\ \hat{k_2} \end{Bmatrix} + \dot{\vec{R}}1^T[\dot{T}] \begin{Bmatrix} \hat{i_2} \\ \hat{j_2} \\ \hat{k_2} \end{Bmatrix} - \ddot{\vec{R}}2^T \begin{Bmatrix} \hat{i_2} \\ \hat{j_2} \\ \hat{k_2} \end{Bmatrix} \\
& + \frac{d}{dt}(\vec{\omega}_2) \times \left[ -\vec{R}2^T \begin{Bmatrix} \hat{i_2} \\ \hat{j_2} \\ \hat{k_2} \end{Bmatrix} - \vec{B}^T \begin{Bmatrix} \hat{i_2} \\ \hat{j_2} \\ \hat{k_2} \end{Bmatrix} \right] \\
& + \vec{\omega}_2 \times \left[ -\dot{\vec{R}}2^T \begin{Bmatrix} \hat{i_2} \\ \hat{j_2} \\ \hat{k_2} \end{Bmatrix} - \dot{\vec{B}}^T \begin{Bmatrix} \hat{i_2} \\ \hat{j_2} \\ \hat{k_2} \end{Bmatrix} \right] \\
& + \vec{\omega}_2 \times \left[ \dot{\vec{R}}1^T\,[T] \begin{Bmatrix} \hat{i_2} \\ \hat{j_2} \\ \hat{k_2} \end{Bmatrix} - \dot{\vec{R}}2^T \begin{Bmatrix} \hat{i_2} \\ \hat{j_2} \\ \hat{k_2} \end{Bmatrix} \right] \\
& + \vec{\omega}_2 \times \left[ \vec{\omega}_2 \times \left[ -\vec{R}2^T \begin{Bmatrix} \hat{i_2} \\ \hat{j_2} \\ \hat{k_2} \end{Bmatrix} - \vec{B}^T \begin{Bmatrix} \hat{i_2} \\ \hat{j_2} \\ \hat{k_2} \end{Bmatrix} \right] \right]
\end{aligned} \tag{2.47}$$

Again, it is important to note that since $\vec{B}$ is not time dependent, the term $\dot{\vec{B}}$ goes to zero. The identity shown below, described by Equation 2.41, can also be applied to equation 2.47, as this identity is valid for any vector.

$$\dot{\vec{R}}1^T[\ddot{T}] + \vec{\omega}_2 \times \dot{\vec{R}}1^T\,[T] = \{0\} \tag{2.48}$$

The simplified equation for the absolute acceleration of the center of mass of the outboard body is found to be,

$$\vec{A}_{G2} = \ddot{\vec{R}}1^T\,[T]\begin{Bmatrix}\hat{i_2}\\ \hat{j_2}\\ \hat{k_2}\end{Bmatrix} - \ddot{\vec{R}}2^T\begin{Bmatrix}\hat{i_2}\\ \hat{j_2}\\ \hat{k_2}\end{Bmatrix} + \vec{\alpha}_2 \times \left[-\vec{R}2^T\begin{Bmatrix}\hat{i_2}\\ \hat{j_2}\\ \hat{k_2}\end{Bmatrix} - \vec{B}^T\begin{Bmatrix}\hat{i_2}\\ \hat{j_2}\\ \hat{k_2}\end{Bmatrix}\right] + 2\vec{\omega}_2 \times \left[-\dot{\vec{R}}2^T\begin{Bmatrix}\hat{i_2}\\ \hat{j_2}\\ \hat{k_2}\end{Bmatrix}\right] + \vec{\omega}_2 \times \left[\vec{\omega}_2 \times \left[-\vec{R}2^T\begin{Bmatrix}\hat{i_2}\\ \hat{j_2}\\ \hat{k_2}\end{Bmatrix} - \vec{B}^T\begin{Bmatrix}\hat{i_2}\\ \hat{j_2}\\ \hat{k_2}\end{Bmatrix}\right]\right] \tag{2.49}$$

The vector $\ddot{\vec{R}}1$ was found by differentiating $\dot{\vec{R}}1$, equation 2.43, with respect to time.

$$\ddot{\vec{R}}1 = \begin{Bmatrix} -\dot{x}(3)RA\sin x(1) - x(3)^2 RA\cos x(1) \\ \dot{x}(3)RA\cos x(1) - x(3)^2 RA\sin x(1) \\ 0 \end{Bmatrix} \tag{2.50}$$

The vector $\ddot{\vec{R}}2$ was found by differentiating $\dot{\vec{R}}2$, Equation 2.44, with respect to time.

$$\ddot{\vec{R}}2 = \begin{Bmatrix} -\dot{x}(4)RB\sin x(2) - x(4)^2 RB\cos x(2) \\ -\dot{x}(4)RB\cos x(2) + x(4)^2 RB\sin x(2) \\ 0 \end{Bmatrix} \tag{2.51}$$

In order to implement the numerical solution routine, it is critical to separate all terms in the equations of motion into a matrix of partial derivatives with respect to each $\dot{x}$ term and a vector of non $\dot{x}$ terms. At this point, the acceleration of the center of mass of the outboard body must be sectioned into $\dot{x}(3)$, $\dot{x}(4)$ and non $\dot{x}$ terms.

The first term appearing in equation 2.49, $\ddot{\vec{R}}1$, has both $\dot{x}(3)$ and non $\dot{x}$ terms so it must be split into two pieces. Taking the partial derivative of $\ddot{\vec{R}}1$ with respect to $\dot{x}(3)$ yields the following,

$$\ddot{\vec{R}}1_{\dot{x}(3)} = \left\{ \begin{array}{c} -RA\sin x(1) \\ RA\cos x(1) \\ 0 \end{array} \right\} \tag{2.52}$$

The vector of non $\dot{x}$ terms is given by,

$$\ddot{\vec{R}}1_{x} = \left\{ \begin{array}{c} -x(3)^2 RA\cos x(1) \\ -x(3)^2 RA\sin x(1) \\ 0 \end{array} \right\} \tag{2.53}$$

The term $\ddot{\vec{R}}1$ can now be written as a combination of equations 2.52 and 2.53 as follows,

$$\ddot{\vec{R}}1 = \ddot{\vec{R}}1_{\dot{x}(3)}\left[\dot{x}(3)\right] + \ddot{\vec{R}}1_{x} \tag{2.54}$$

The transformation matrix [T] does not have any $\dot{x}$ terms; therefore, it does not need to be sectioned.

The next term appearing in equation 2.49, $\ddot{\vec{R}}2$, has both $\dot{x}(4)$ and non $\dot{x}$ terms so it must be split into two pieces. Taking the partial derivative of $\ddot{\vec{R}}2$ with respect to $\dot{x}(4)$ yields the following,

$$\ddot{\vec{R}}2_{\dot{x}(4)} = \left\{ \begin{array}{c} -RB\sin x(2) \\ -RB\cos x(2) \\ 0 \end{array} \right\} \tag{2.55}$$

The vector of non $\dot{x}$ terms is given by,

$$\ddot{\vec{R}}2_{x} = \left\{ \begin{array}{c} -x(4)^2 RB\cos x(2) \\ x(4)^2 RB\sin x(2) \\ 0 \end{array} \right\} \tag{2.56}$$

The term $\ddot{\vec{R}}2$ can now be written as a combination of equations 2.55 and 2.56 as follows,

$$\ddot{\vec{R}}2 = \ddot{\vec{R}}2_{\dot{x}(4)}\left[\dot{x}(4)\right] + \ddot{\vec{R}}2_{x} \tag{2.57}$$

The term $\vec{\alpha}_2$, derived in equation 2.32, has $\dot{x}(3)$ and $\dot{x}(4)$ terms. Taking the partial derivative with respect to $\dot{x}(3)$ gives,

$$\vec{\alpha}_{2_{\dot{x}(3)}} = \left\{ \begin{array}{c} 0 \\ 0 \\ 1 \end{array} \right\} \tag{2.58}$$

Similarly, taking the partial derivative with respect to $\dot{x}(4)$ gives,

$$\vec{\alpha}_{2_{\dot{x}(4)}} = \left\{ \begin{array}{c} 0 \\ 0 \\ 1 \end{array} \right\} \tag{2.59}$$

The term $\vec{\alpha}_2$ can now be written as a combination of equations 2.58 and 2.59 as follows,

$$\vec{\alpha}_2 = \vec{\alpha}_{2_{\dot{x}(3)}}\left[\dot{x}(3)\right] + \vec{\alpha}_{2_{\dot{x}(4)}}\left[\dot{x}(4)\right] \tag{2.60}$$

The rest of the terms in equation 2.49 are non $\dot{x}$ dependent so they do not need to be sectioned. The absolute acceleration of the center of mass of the outboard body can now be written as,

$$\vec{A}_{G2} = \left( \ddot{\vec{R}}1^T_{\dot{x}(3)} [T] \begin{Bmatrix} \hat{i_2} \\ \hat{j_2} \\ \hat{k_2} \end{Bmatrix} + \vec{\alpha}_{2_{\dot{x}(3)}} \times \left[ -\vec{R}2^T \begin{Bmatrix} \hat{i_2} \\ \hat{j_2} \\ \hat{k_2} \end{Bmatrix} - \vec{B}^T \begin{Bmatrix} \hat{i_2} \\ \hat{j_2} \\ \hat{k_2} \end{Bmatrix} \right] \right) \dot{x}(3)$$
$$+ \left( -\ddot{\vec{R}}2^T_{\dot{x}(4)} \begin{Bmatrix} \hat{i_2} \\ \hat{j_2} \\ \hat{k_2} \end{Bmatrix} + \vec{\alpha}_{2_{\dot{x}(4)}} \times \left[ -\vec{R}2^T \begin{Bmatrix} \hat{i_2} \\ \hat{j_2} \\ \hat{k_2} \end{Bmatrix} - \vec{B}^T \begin{Bmatrix} \hat{i_2} \\ \hat{j_2} \\ \hat{k_2} \end{Bmatrix} \right] \right) \dot{x}(4)$$
$$+ \ddot{\vec{R}}1^T_x [T] \begin{Bmatrix} \hat{i_2} \\ \hat{j_2} \\ \hat{k_2} \end{Bmatrix} - \ddot{\vec{R}}2_x \begin{Bmatrix} \hat{i_2} \\ \hat{j_2} \\ \hat{k_2} \end{Bmatrix} + 2\vec{\omega}_2 \times \left[ -\dot{\vec{R}}2^T \begin{Bmatrix} \hat{i_2} \\ \hat{j_2} \\ \hat{k_2} \end{Bmatrix} \right]$$
$$+ \vec{\omega}_2 \times \left[ \vec{\omega}_2 \times \left[ -\vec{R}2^T \begin{Bmatrix} \hat{i_2} \\ \hat{j_2} \\ \hat{k_2} \end{Bmatrix} - \vec{B}^T \begin{Bmatrix} \hat{i_2} \\ \hat{j_2} \\ \hat{k_2} \end{Bmatrix} \right] \right] \quad (2.61)$$

To simplify equation 2.61, the group of terms dependent on $\dot{x}(3)$ are expressed as $\vec{A}_{G2_{\dot{x}(3)}}$, the group of terms dependent on $\dot{x}(4)$ are expressed as $\vec{A}_{G2_{\dot{x}(4)}}$, and the rest of the terms are expressed as $\vec{A}_{G2_x}$.

$$\vec{A}_{G2} = \vec{A}_{G2_{\dot{x}(3)}} [\dot{x}(3)] + \vec{A}_{G2_{\dot{x}(4)}} [\dot{x}(4)] + \vec{A}_{G2_x} \quad (2.62)$$

### Partial Angular Velocity

As noted in section 2.2, the partial derivative of the angular velocity with respect to each generalized speed is needed to form the equations of motion based on Kane's principles. In the planar case there are only two generalized speeds, $x(3)$ and $x(4)$, thus the two partial angular velocities are given below.

$$\frac{\partial \vec{\omega}_2}{\partial x(3)} = \begin{Bmatrix} 0 \\ 0 \\ 1 \end{Bmatrix} \quad (2.63)$$

$$\frac{\partial \vec{\omega}_2}{\partial x(4)} = \left\{ \begin{array}{c} 0 \\ 0 \\ 1 \end{array} \right\} \tag{2.64}$$

**Partial Absolute Velocity**

The partial absolute velocity with respect to each generalized speed is also required to form the equations of motion. The partial absolute velocity with respect to the first generalized speed is found by differentiating equation 2.42 with respect to $x(3)$. The transformation matrix [T], and the vectors $\vec{R2}$ and $\vec{B}$ do not depend on either of the generalized speeds so they remains as constants in the differentiation.

$$\frac{\partial \vec{V}_{G2}}{\partial x(3)} = \frac{\partial \dot{\vec{R}}1^T}{\partial x(3)} [T] \left\{ \begin{array}{c} \hat{i_2} \\ \hat{j_2} \\ \hat{k_2} \end{array} \right\} - \frac{\partial \dot{\vec{R2}}^T}{\partial x(3)} \left\{ \begin{array}{c} \hat{i_2} \\ \hat{j_2} \\ \hat{k_2} \end{array} \right\} + \frac{\partial \vec{\omega}_2}{\partial x(3)} \times \left[ -\vec{R2}^T \left\{ \begin{array}{c} \hat{i_2} \\ \hat{j_2} \\ \hat{k_2} \end{array} \right\} - \vec{B}^T \left\{ \begin{array}{c} \hat{i_2} \\ \hat{j_2} \\ \hat{k_2} \end{array} \right\} \right] \tag{2.65}$$

The vector $\dot{\vec{R2}}$, equation 2.44, does not contain any $x(3)$ terms so the partial derivative of $\dot{\vec{R2}}$ with respect to $x(3)$ is zero. This simplifies equation 2.65 to the following,

$$\frac{\partial \vec{V}_{G2}}{\partial x(3)} = \frac{\partial \dot{\vec{R}}1^T}{\partial x(3)} [T] \left\{ \begin{array}{c} \hat{i_2} \\ \hat{j_2} \\ \hat{k_2} \end{array} \right\} + \frac{\partial \vec{\omega}_2}{\partial x(3)} \times \left[ -\vec{R2}^T \left\{ \begin{array}{c} \hat{i_2} \\ \hat{j_2} \\ \hat{k_2} \end{array} \right\} - \vec{B}^T \left\{ \begin{array}{c} \hat{i_2} \\ \hat{j_2} \\ \hat{k_2} \end{array} \right\} \right] \tag{2.66}$$

By differentiating equation 2.43 with respect to generalized speed $x(3)$, the following expression was derived for $\frac{\partial \dot{\vec{R}}1}{\partial x(3)}$,

$$\frac{\partial \dot{\vec{R}}1}{\partial x(3)} = \left\{ \begin{array}{c} -RA \sin x(1) \\ RA \cos x(1) \\ 0 \end{array} \right\} \tag{2.67}$$

Similarly, the partial absolute velocity with respect to the second generalized speed is found by differentiating equation 2.42 with respect to $x(4)$. Again, the transformation matrix [T], and the vectors $\vec{R2}$ and $\vec{B}$ do not depend on either of the generalized speeds so they remain as a constant in the differentiation.

$$\frac{\partial \vec{V}_{G2}}{\partial x(4)} = \frac{\partial \dot{\vec{R1}}^T}{\partial x(4)} [T] \begin{Bmatrix} \hat{i_2} \\ \hat{j_2} \\ \hat{k_2} \end{Bmatrix} - \frac{\partial \dot{\vec{R2}}^T}{\partial x(4)} \begin{Bmatrix} \hat{i_2} \\ \hat{j_2} \\ \hat{k_2} \end{Bmatrix} + \frac{\partial \vec{\omega}_2}{\partial x(4)} \times \left[ -\vec{R2}^T \begin{Bmatrix} \hat{i_2} \\ \hat{j_2} \\ \hat{k_2} \end{Bmatrix} - \vec{B}^T \begin{Bmatrix} \hat{i_2} \\ \hat{j_2} \\ \hat{k_2} \end{Bmatrix} \right] \quad (2.68)$$

The vector $\dot{\vec{R1}}$, equation 2.43, does not contain any $x(4)$ terms so the partial derivative of $\dot{\vec{R2}}$ with respect to $x(4)$ is zero. This simplifies equation 2.68 to the following,

$$\frac{\partial \vec{V}_{G2}}{\partial x(4)} = -\frac{\partial \dot{\vec{R2}}^T}{\partial x(4)} \begin{Bmatrix} \hat{i_2} \\ \hat{j_2} \\ \hat{k_2} \end{Bmatrix} + \frac{\partial \vec{\omega}_2}{\partial x(4)} \times \left[ -\vec{R2}^T \begin{Bmatrix} \hat{i_2} \\ \hat{j_2} \\ \hat{k_2} \end{Bmatrix} - \vec{B}^T \begin{Bmatrix} \hat{i_2} \\ \hat{j_2} \\ \hat{k_2} \end{Bmatrix} \right] \quad (2.69)$$

By differentiating equation 2.44 with respect to generalized speed $x(4)$, the following expression was derived for $\frac{\partial \dot{\vec{R2}}}{\partial x(4)}$,

$$\frac{\partial \dot{\vec{R2}}}{\partial x(4)} = \begin{Bmatrix} -RB \sin x(2) \\ -RB \cos x(2) \\ 0 \end{Bmatrix} \quad (2.70)$$

**Generalized Inertial Forces**

The inertial terms of Kane's equations, represented in equation 2.17, can now be assembled for each generalized speed. It is important to note that the mass matrix $[m]$ and the inertia tensor $[I]$ are not changing with respect to time so the terms $[\dot{m}]$

and $[\dot{I}]$ of equation 2.17 are set to zero. For the generalized speed, $x(3)$, equation 2.17 becomes,

$$\vec{Q}^*_{x(3)} = \frac{\partial \vec{V}_{G_2}}{\partial x(3)} \cdot \left\{ - [m] \, \vec{A}_{G_2} \right\} + \frac{\partial \vec{\omega}_2}{\partial x(3)} \cdot \{ - [I] \, \vec{\alpha}_2 \} \tag{2.71}$$

Similarly, for generalized speed, $x(4)$, equation 2.17 becomes,

$$\vec{Q}^*_{x(4)} = \frac{\partial \vec{V}_{G_2}}{\partial x(4)} \cdot \left\{ - [m] \, \vec{A}_{G_2} \right\} + \frac{\partial \vec{\omega}_2}{\partial x(4)} \cdot \{ - [I] \, \vec{\alpha}_2 \} \tag{2.72}$$

These equations needs to be divided into a matrix of partial derivatives with respect to each $\dot{x}$ term and a vector of non $\dot{x}$ terms. Using equations 2.62 and 2.60, equation 2.71 can be sectioned into $\dot{x}(3)$, $\dot{x}(4)$, and non $\dot{x}$ components.

$$\begin{aligned} \vec{Q}^*_{x(3)} = & \left[ \frac{\partial \vec{V}_{G_2}}{\partial x(3)} \cdot \left\{ - [m] \, \vec{A}_{G_{2_{\dot{x}(3)}}} \right\} + \frac{\partial \vec{\omega}_2}{\partial x(3)} \cdot \left\{ - [I] \, \vec{\alpha}_{2_{(\dot{x})(3)}} \right\} \right] \dot{x}(3) \\ & + \left[ \frac{\partial \vec{V}_{G_2}}{\partial x(3)} \cdot \left\{ - [m] \, \vec{A}_{G_{2_{\dot{x}(4)}}} \right\} + \frac{\partial \vec{\omega}_2}{\partial x(3)} \cdot \left\{ - [I] \, \vec{\alpha}_{2_{(\dot{x})(4)}} \right\} \right] \dot{x}(4) \\ & + \frac{\partial \vec{V}_{G_2}}{\partial x(3)} \cdot \left\{ - [m] \, \vec{A}_{G_{2_x}} \right\} \end{aligned} \tag{2.73}$$

The group of terms dependent on $\dot{x}(3)$ can be represented by the following,

$$QQ^*_{11} = \frac{\partial \vec{V}_{G_2}}{\partial x(3)} \cdot \left\{ - [m] \, \vec{A}_{G_{2_{\dot{x}(3)}}} \right\} + \frac{\partial \vec{\omega}_2}{\partial x(3)} \cdot \left\{ - [I] \, \vec{\alpha}_{2_{(\dot{x})(3)}} \right\} \tag{2.74}$$

The group of terms dependent on $\dot{x}(4)$ can be represented by the following,

$$QQ^*_{12} = \frac{\partial \vec{V}_{G_2}}{\partial x(3)} \cdot \left\{ - [m] \, \vec{A}_{G_{2_{\dot{x}(4)}}} \right\} + \frac{\partial \vec{\omega}_2}{\partial x(3)} \cdot \left\{ - [I] \, \vec{\alpha}_{2_{(\dot{x})(4)}} \right\} \tag{2.75}$$

The group of non $\dot{x}$ dependent terms can be represented by the following,

$$Q^*_1 = \frac{\partial \vec{V}_{G_2}}{\partial x(3)} \cdot \left\{ - [m] \, \vec{A}_{G_{2_x}} \right\} \tag{2.76}$$

Using equations 2.61 and 2.60, equation 2.72 can be sectioned into $\dot{x}(3)$, $\dot{x}(4)$, and non $\dot{x}$ components.

$$\vec{Q}^*_{x(4)} = \left[\frac{\partial \vec{V}_{G_2}}{\partial x(4)} \cdot \left\{-\left[m\right]\vec{A}_{G_{2_{\dot{x}(3)}}}\right\} + \frac{\partial \vec{\omega}_2}{\partial x(4)} \cdot \left\{-\left[I\right]\vec{\alpha}_{2_{\dot{(x)}(3)}}\right\}\right]\dot{x}(3)$$
$$+ \left[\frac{\partial \vec{V}_{G_2}}{\partial x(4)} \cdot \left\{-\left[m\right]\vec{A}_{G_{2_{\dot{x}(4)}}}\right\} + \frac{\partial \vec{\omega}_2}{\partial x(4)} \cdot \left\{-\left[I\right]\vec{\alpha}_{2_{\dot{(x)}(4)}}\right\}\right]\dot{x}(4)$$
$$+ \frac{\partial \vec{V}_{G_2}}{\partial x(4)} \cdot \left\{-\left[m\right]\vec{A}_{G_{2_x}}\right\} \quad (2.77)$$

The group of terms dependent on $\dot{x}(3)$ can be represented by the following,

$$QQ^*_{21} = \frac{\partial \vec{V}_{G_2}}{\partial x(4)} \cdot \left\{-\left[m\right]\vec{A}_{G_{2_{\dot{x}(3)}}}\right\} + \frac{\partial \vec{\omega}_2}{\partial x(4)} \cdot \left\{-\left[I\right]\vec{\alpha}_{2_{\dot{(x)}(3)}}\right\} \quad (2.78)$$

The group of terms dependent on $\dot{x}(4)$ can be represented by the following,

$$QQ^*_{22} = \frac{\partial \vec{V}_{G_2}}{\partial x(4)} \cdot \left\{-\left[m\right]\vec{A}_{G_{2_{\dot{x}(4)}}}\right\} + \frac{\partial \vec{\omega}_2}{\partial x(4)} \cdot \left\{-\left[I\right]\vec{\alpha}_{2_{\dot{(x)}(4)}}\right\} \quad (2.79)$$

The group of non $\dot{x}$ dependent terms can be represented by the following,

$$Q^*_2 = \frac{\partial \vec{V}_{G_2}}{\partial x(4)} \cdot \left\{-\left[m\right]\vec{A}_{G_{2_x}}\right\} \quad (2.80)$$

The partial derivative matrix of $\dot{(x)}$ terms and vector of non $\dot{x}$ terms can now be assembled.

$$\left\{\begin{array}{c} Q^*_{x(3)} \\ Q^*_{x(4)} \end{array}\right\} = \left[\begin{array}{cc} QQ^*_{11} & QQ^*_{12} \\ QQ^*_{21} & QQ^*_{22} \end{array}\right]\left\{\begin{array}{c} \dot{x}(3) \\ \dot{x}(4) \end{array}\right\} + \left\{\begin{array}{c} Q^*_1 \\ Q^*_2 \end{array}\right\} \quad (2.81)$$

**Generalized Active Forces**

The following external forces are exerted on the outboard body of the system: the force due to gravity and the force of the system's springs. The external forces were first compiled in the ground fixed coordinate system and then transformed to the body fixed coordinate system using transformation matrix $[T]$. The force due to gravity, in ground fixed coordinates, is given by the following,

$$\vec{F}_{grav} = \left\{ \begin{array}{c} mg \\ 0 \\ 0 \end{array} \right\} \tag{2.82}$$

where $m$ is the mass of the outboard body, and $g$ is the acceleration due to gravity.

The force of the system's springs was more complex to calculate. The force in each of the springs was calculated separately in the ground fixed coordinate system and then transformed to the body fixed coordinate system. The ground fixed spring end locations ($\vec{LE}$ and $\vec{LF}$), and the body fixed spring end location ($\vec{D}$), as shown in figure 2.3, and the unstretched spring lengths ($ED$ and $FD$), and the spring constants ($K_E$ and $K_F$), were all input into the simulation as constants.

The first step in calculating a spring force is to determine the length of the spring. A position vector is defined from each of the ground fixed spring attachment points to the body fixed spring attachment point. For the spring on the left (spring E), see Figure 2.3, the position vector is described as follows,

$$\vec{P}_{ED} = -\vec{LE}^T \left\{ \begin{array}{c} \hat{i_0} \\ \hat{j_0} \\ \hat{k_0} \end{array} \right\} + \vec{R1}^T \left\{ \begin{array}{c} \hat{i_0} \\ \hat{j_0} \\ \hat{k_0} \end{array} \right\} - \vec{R2}^T \left\{ \begin{array}{c} \hat{i_2} \\ \hat{j_2} \\ \hat{k_2} \end{array} \right\} - \vec{B}^T \left\{ \begin{array}{c} \hat{i_2} \\ \hat{j_2} \\ \hat{k_2} \end{array} \right\} + \vec{D}^T \left\{ \begin{array}{c} \hat{i_2} \\ \hat{j_2} \\ \hat{k_2} \end{array} \right\} \tag{2.83}$$

It is required that all terms be in the ground fixed coordinate system, so the transformation matrix $[TT]$, Equation 2.28, was used to convert vectors from the body fixed coordinate system. After transformation, the position vector of equation 2.83 becomes,

$$\vec{P}_{ED} = -\vec{LE}^T \begin{Bmatrix} \hat{i_0} \\ \hat{j_0} \\ \hat{k_0} \end{Bmatrix} + \vec{R1}^T \begin{Bmatrix} \hat{i_0} \\ \hat{j_0} \\ \hat{k_0} \end{Bmatrix} - \vec{R2}^T [TT] \begin{Bmatrix} \hat{i_0} \\ \hat{j_0} \\ \hat{k_0} \end{Bmatrix} - \vec{B}^T [TT] \begin{Bmatrix} \hat{i_0} \\ \hat{j_0} \\ \hat{k_0} \end{Bmatrix} + \vec{D}^T [TT] \begin{Bmatrix} \hat{i_0} \\ \hat{j_0} \\ \hat{k_0} \end{Bmatrix} \quad (2.84)$$

The length of spring E can now be found by calculating the magnitude of the position vector $\vec{P}_{ED}$. This quantity is denoted $|\vec{P}_{ED}|$.

Similar expressions can be derived for the spring on the right (spring F).

$$\vec{P}_{FD} = -\vec{LF}^T \begin{Bmatrix} \hat{i_0} \\ \hat{j_0} \\ \hat{k_0} \end{Bmatrix} + \vec{R1}^T \begin{Bmatrix} \hat{i_0} \\ \hat{j_0} \\ \hat{k_0} \end{Bmatrix} - \vec{R2}^T \begin{Bmatrix} \hat{i_2} \\ \hat{j_2} \\ \hat{k_2} \end{Bmatrix} - \vec{B}^T \begin{Bmatrix} \hat{i_2} \\ \hat{j_2} \\ \hat{k_2} \end{Bmatrix} + \vec{D}^T \begin{Bmatrix} \hat{i_2} \\ \hat{j_2} \\ \hat{k_2} \end{Bmatrix} \quad (2.85)$$

$$\vec{P}_{FD} = -\vec{LF}^T \begin{Bmatrix} \hat{i_0} \\ \hat{j_0} \\ \hat{k_0} \end{Bmatrix} + \vec{R1}^T \begin{Bmatrix} \hat{i_0} \\ \hat{j_0} \\ \hat{k_0} \end{Bmatrix} - \vec{R2}^T [TT] \begin{Bmatrix} \hat{i_0} \\ \hat{j_0} \\ \hat{k_0} \end{Bmatrix} - \vec{B}^T [TT] \begin{Bmatrix} \hat{i_0} \\ \hat{j_0} \\ \hat{k_0} \end{Bmatrix} + \vec{D}^T [TT] \begin{Bmatrix} \hat{i_0} \\ \hat{j_0} \\ \hat{k_0} \end{Bmatrix} \quad (2.86)$$

The length of spring F can now be found by calculating the magnitude of the position vector $\vec{P}_{FD}$. This quantity is denoted $|\vec{P}_{FD}|$.

The next step is to calculate the total stretch from equilibrium for each spring. This is accomplished by subtracting the equilibrium spring length from the spring length as follows,

$$\delta_E = |\vec{P}_{ED}| - ED \tag{2.87}$$

$$\delta_F = |\vec{P}_{FD}| - FD \tag{2.88}$$

The spring force acts in the opposite direction of the spring length position vector. A unit vector in the direction of the applied force for spring E is given by,

$$\vec{D}ir_E = -\frac{\vec{P}_{ED}}{|\vec{P}_{ED}|} \tag{2.89}$$

Similarly, a unit vector in the direction of the applied force for spring F is given by,

$$\vec{D}ir_F = -\frac{\vec{P}_{FD}}{|\vec{P}_{FD}|} \tag{2.90}$$

The force in each spring can now be calculated.

$$\vec{F}_E = K_E\ \delta_E\ \vec{D}ir_E \tag{2.91}$$

$$\vec{F}_F = K_F\ \delta_F\ \vec{D}ir_F \tag{2.92}$$

The external forces are now transformed to the body fixed coordinate system by multiplying by the transformation matrix $[T]$, Equation 2.24, as follows,

$$\vec{F}_{grav_2} = \vec{F}^T_{grav}\,[T] \left\{ \begin{array}{c} \hat{i_2} \\ \hat{j_2} \\ \hat{k_2} \end{array} \right\} \tag{2.93}$$

$$\vec{F}_{E_2} = \vec{F}^T_{E}\,[T] \left\{ \begin{array}{c} \hat{i_2} \\ \hat{j_2} \\ \hat{k_2} \end{array} \right\} \tag{2.94}$$

$$\vec{F}_{F_2} = \vec{F}_F^T \, [T] \left\{ \begin{array}{c} \hat{i_2} \\ \hat{j_2} \\ \hat{k_2} \end{array} \right\} \tag{2.95}$$

The sum of the forces on the outboard body in the body fixed coordinate system is given by,

$$\sum \vec{F} = \vec{F}_{grav_2} + \vec{F}_{E_2} + \vec{F}_{F_2} \tag{2.96}$$

The sum of the moments on the outboard body, about the center of mass, G, is found by taking the cross product of the position from the center of mass to the point of force application and the applied force. Since the gravitation force acts at the center of mass, the resultant moment contribution from this force is zero. The springs forces are located at a distance $\vec{D}$ away from the center of mass, so the sum of the moments on the outboard body about the center of mass, G is given by,

$$\sum \vec{M}_{G_2} = \vec{D} \times \sum \left( \vec{F}_{E_2} + \vec{F}_{F_2} \right) \tag{2.97}$$

The generalized active forces can now be assembled using equation 2.18 for each generalized speed. For the generalized speed $x(3)$, the active force is found to be,

$$\vec{Q}_{x(3)} = \frac{\partial \vec{V}_{G_2}}{\partial x(3)} \cdot \sum \vec{F} + \frac{\partial \vec{\omega}_2}{\partial x(3)} \cdot \sum \vec{M}_{G_2} \tag{2.98}$$

Similarly, for the generalized speed $x(4)$, the active force is found to be,

$$\vec{Q}_{x(4)} = \frac{\partial \vec{V}_{G_2}}{\partial x(4)} \cdot \sum \vec{F} + \frac{\partial \vec{\omega}_2}{\partial x(4)} \cdot \sum \vec{M}_{G_2} \tag{2.99}$$

The generalized active forces can be represented by the following column vector,

$$\left\{ \begin{array}{c} Q_{x(3)} \\ Q_{x(4)} \end{array} \right\} = \left\{ \begin{array}{c} Q_1 \\ Q_2 \end{array} \right\} \tag{2.100}$$

**Assembling Kane's Equations**

Using the quantities derived in equation 2.81 and 2.100, Kane's equation's can be assembled as per equation 2.19.

$$\begin{bmatrix} QQ^*_{11} & QQ^*_{12} \\ QQ^*_{21} & QQ^*_{22} \end{bmatrix} \begin{Bmatrix} \dot{x}(3) \\ \dot{x}(4) \end{Bmatrix} + \begin{Bmatrix} Q^*_1 \\ Q^*_2 \end{Bmatrix} + \begin{Bmatrix} Q_1 \\ Q_2 \end{Bmatrix} = \begin{Bmatrix} 0 \\ 0 \end{Bmatrix} \tag{2.101}$$

The vector of first derivative of generalized speeds can be determined by grouping the non $\dot{x}$ terms on the right hand side of equation 2.101 and by multiplying both sides of the equation by the inverse of the $QQ$ matrix.

$$\begin{Bmatrix} \dot{x}(3) \\ \dot{x}(4) \end{Bmatrix} = [QQ]^{-1} \left\{ - \begin{Bmatrix} Q^*_1 \\ Q^*_2 \end{Bmatrix} - \begin{Bmatrix} Q_1 \\ Q_2 \end{Bmatrix} \right\} \tag{2.102}$$

### 2.3.2 Two Dimensional Case: Lagrangian Model

The system depicted in Figure 2.3 was also modeled using the Lagrangian approach to show that the formulation derived through Kane's method was correct. The derivation of the equations of motion is shown in detail in Appendix A.

Once the equations of motion were determined, a numerical solution over a period of time was produced by integrating the equations of motion using a fourth/fifth order, variable time step, Runge-Kutta integration routine.

### 2.3.3 Comparison of the Two Dimensional Models

In order to compare the two dimensional models produced using the equations of motion derived from Kane's method and the Lagrangian method, arbitrary system parameters were assigned to the models. Comparison plots of the two generalized coordinates, $x(1)$ and $x(2)$ are shown below. Figures 2.4 and 2.5 show results obtained with the initial conditions set to $x(1) = 20°$, $x(2) = 180°$, $x(3) = 0\ rad/s$, and $x(4) = 0\ rad/s$. Figures 2.6 and 2.7 show results obtained with $x(1) = 0°$, $x(2) = 150°$, $x(3) = 0\ rad/s$, and $x(4) = 0\ rad/s$.

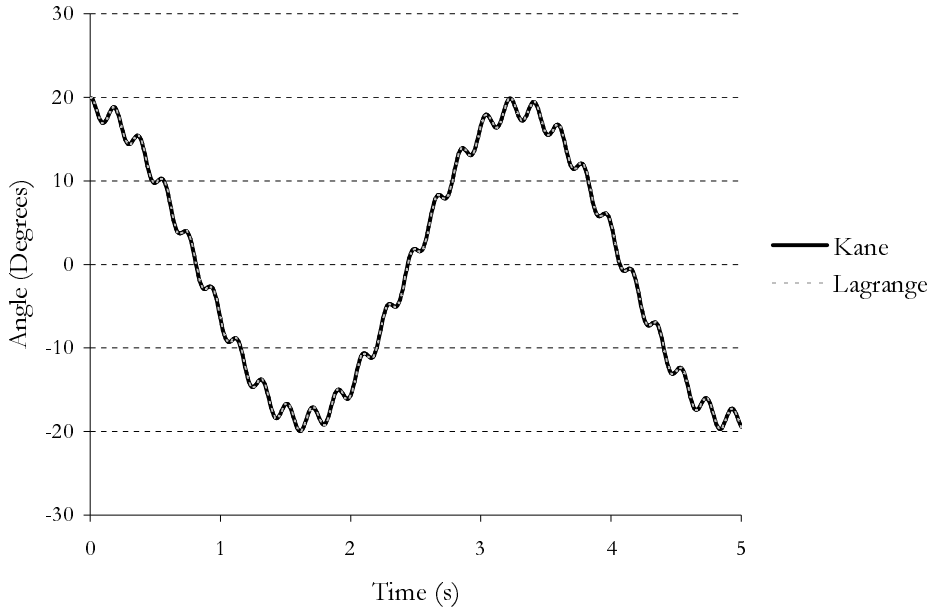


Figure 2.4: Comparison of Simulation Results for Case 1: x(1) versus Time

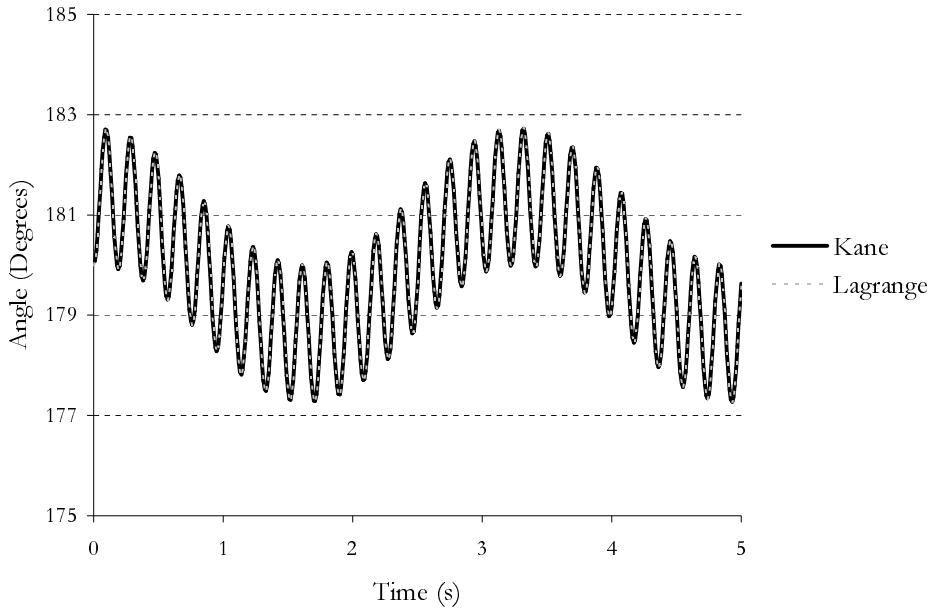


Figure 2.5: Comparison of Simulation Results for Case 1: x(2) versus Time

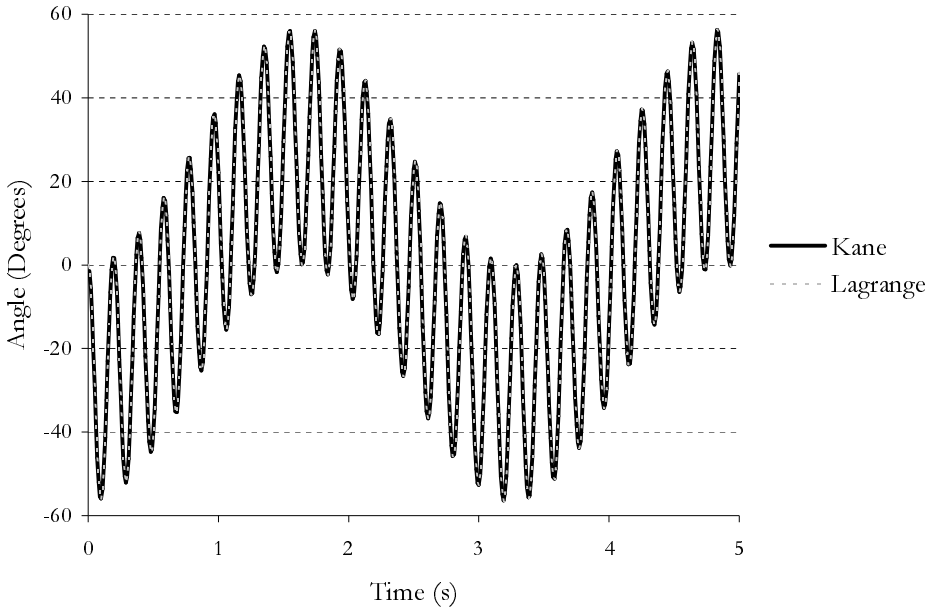


Figure 2.6: Comparison of Simulation Results for Case 2: x(1) versus Time

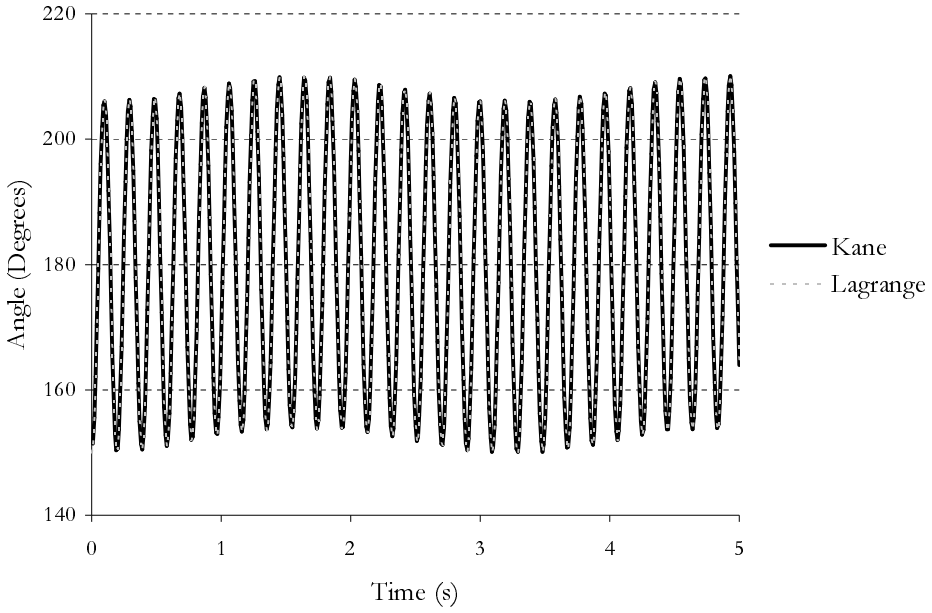


Figure 2.7: Comparison of Simulation Results for Case 2: x(2) versus Time

From the plots shown above, the methods were found to yield identical results to six significant figures. The total energy as a function of time was also found for each model by summing the contributions of the kinetic, gravitational potential, and elastic potential energy in the systems. Since the two dimensional system is an ideal model, it was expected that if the simulations were working properly, the total energy in the system would remain constant for all time. Both models were found to agree with this, adding further proof that the two dimensional Kane's model was predicting accurate system dynamics.

## 2.4 Three Dimensional Model

Once it was determined that the two dimensional model was functioning properly, Kane's method for deriving the equations of motion was extended to the three dimensional simulation. The model parameters match that of the two dimensional model with additional parameters defined to account for the third dimension and six springs. The set up of the model is described below and the development of the equations of motion is shown in detail in Appendix B.

### Coordinate Systems

Six coordinate systems were required to adequately represent all vectors in the three dimensional model. Similarly to the two dimensional model, a ground fixed coordinate system, $(\hat{i_0}, \hat{j_0}, \hat{k_0})$, was located at the center of spherical cut out. Four intermediate coordinate systems, $(\hat{i_1}, \hat{j_1}, \hat{k_1})$, $(\hat{i_2}, \hat{j_2}, \hat{k_2})$, $(\hat{i_3}, \hat{j_3}, \hat{k_3})$, and $(\hat{i_4}, \hat{j_4}, \hat{k_4})$, were assigned according to rotations prescribed by the configuration coordinates described below. A body fixed coordinate system, $(\hat{i_5}, \hat{j_5}, \hat{k_5})$, was assigned to the outboard body.

### Configuration Coordinates and Generalized Speeds

As in the two dimensional model, the configuration coordinates were selected to represent rotations from the ground fixed coordinate system to the body fixed coordinate system. The first configuration coordinate, $x(1)$, represents the positive

(counter-clockwise) rotation about the $z_0$ axis which transforms from coordinate system $(\hat{i_0}, \hat{j_0}, \hat{k_0})$ to coordinate system $(\hat{i_1}, \hat{j_1}, \hat{k_1})$. The second configuration coordinate, $x(2)$, represents the positive (counter-clockwise) rotation about the $\hat{j_1}$ axis which transforms from coordinate system $(\hat{i_1}, \hat{j_1}, \hat{k_1})$ to coordinate system $(\hat{i_2}, \hat{j_2}, \hat{k_2})$. These first two rotations identify the point of contact of the two articulating bodies. The next three rotations orient the outboard body in space. The third configuration coordinate, $x(3)$, represents the positive (counter-clockwise) rotation about the $z_2$ axis which transforms from coordinate system $(\hat{i_2}, \hat{j_2}, \hat{k_2})$ to coordinate system $(\hat{i_3}, \hat{j_3}, \hat{k_3})$. The fourth configuration coordinate, $x(4)$, represents the positive (counter-clockwise) rotation about the $\hat{j_3}$ axis which transforms from coordinate system $(\hat{i_3}, \hat{j_3}, \hat{k_3})$ to coordinate system $(\hat{i_4}, \hat{j_4}, \hat{k_4})$. The fifth configuration coordinate, $x(5)$, represents the positive (counter-clockwise) rotation about the $\hat{i_4}$ axis which transforms from coordinate system $(\hat{i_4}, \hat{j_4}, \hat{k_4})$ to the body fixed coordinate system $(\hat{i_5}, \hat{j_5}, \hat{k_5})$. Figure 2.8 shows the planar rotations to go from the ground fixed coordinate system to the body fixed coordinate system.

The generalized speeds, $x(6)$, $x(7)$, $x(8)$, $x(9)$, and $x(10)$, were selected to be the time derivatives of the configuration coordinates, $x(1)$, $x(2)$, $x(3)$, $x(4)$, $x(5)$, respectively.

$$\begin{aligned} x(6) &= \dot{x}(1) \\ x(7) &= \dot{x}(2) \\ x(8) &= \dot{x}(3) \\ x(9) &= \dot{x}(4) \\ x(10) &= \dot{x}(5) \end{aligned} \tag{2.103}$$

The remaining portion of the three dimensional model was derived as per the two dimensional model and a complete review is given in Appendix B.

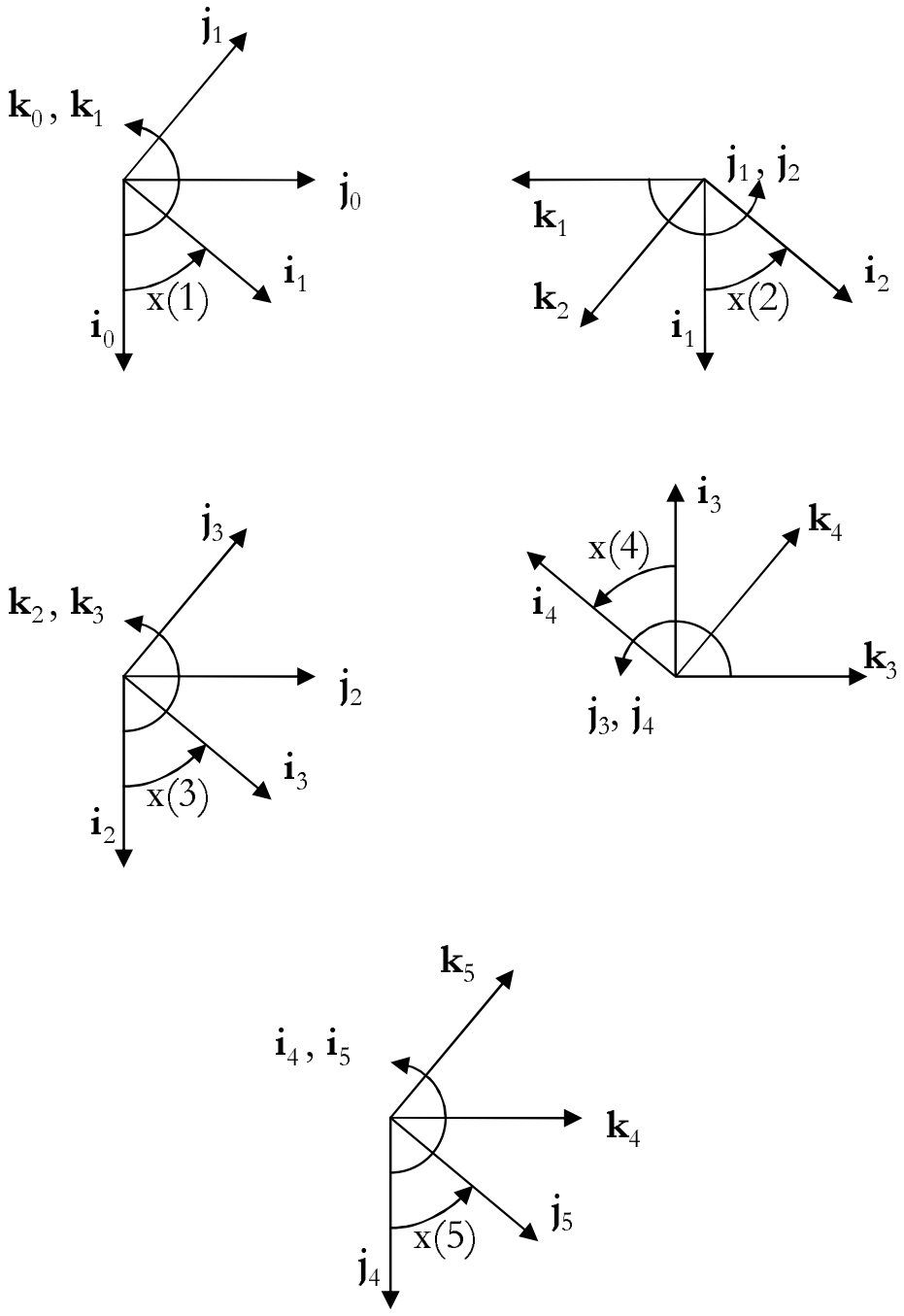


Figure 2.8: Coordinate System Transformations

# Chapter 3

# Physical Model

In order to validate the computer simulation developed, a physical model was built to obtain experimental data. Inboard and outboard bodies were constructed and the positions of four markers, all located on the outboard body, were recorded with an Optotrak optical tracking system. Springs were used to provide system stability as well as to test the modeling of externally applied loads. Several physical system properties were measured and used as inputs into the computer simulation. The physical model is shown below in Figure 3.1.

## 3.1 Inboard Body

As described in Chapter 2, the inboard body of the model consists of a stationary, hemi-spherical cut out which is 76.2 $mm$ (3 $in$) in diameter, see Figure 3.2. The body was created from a 127.0 $mm$ (5 $in$) billet of 6061 T6 Al, using a milling machine. The inside of the bowl was polished on a lathe to reduce the amount of friction present and the articulation surface was lubricated with WD 40 prior to testing. The sphericity of the cut out was measured after polishing using a MicroVal 343 coordinate measuring machine (CMM) system [20]. The deviation of the individual points to the calculated sphere was found to be 0.184 $mm$ [20].

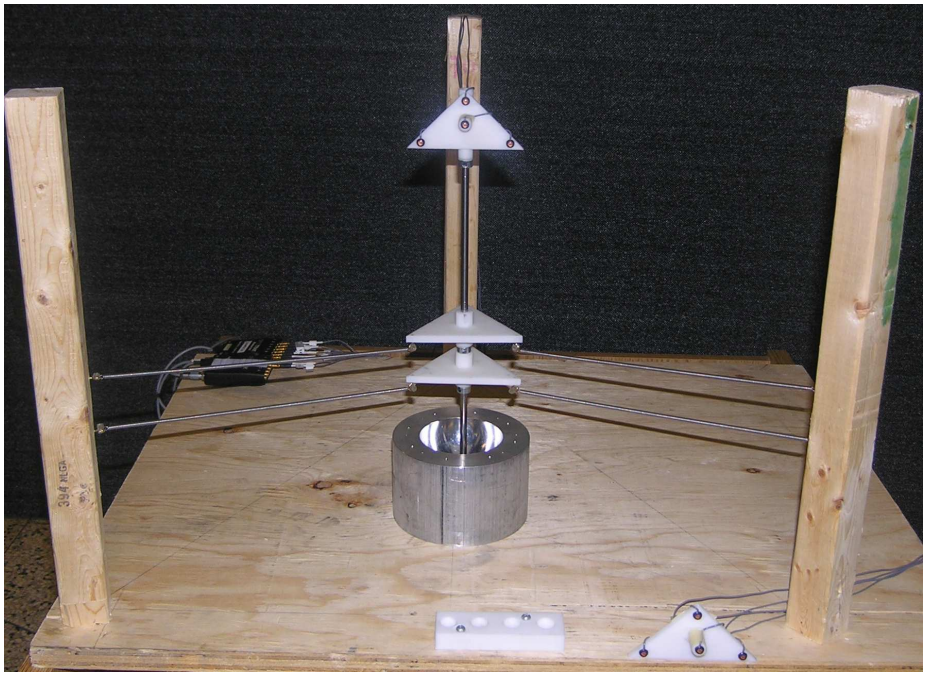

Figure 3.1: Physical Model

Figure 3.2: Inboard Body

## 3.2 Outboard Body

The outboard body, pictured below in Figure 3.3 consists of two main pieces: a spherical articulating piece and a long rigid arm. A case hardened, 1020 carbon steel ball bearing, of diameter 12.7 $mm$ (0.5 $in$), was selected as the spherical articulating piece. A 317.5 $mm$ (12.5 $in$) section of 1060 steel drill rod, of diameter 6.35 $mm$ (0.25 $in$), was selected as the rigid arm. To create a single rigid body, the ball bearing was tapped and the drill rod was threaded.

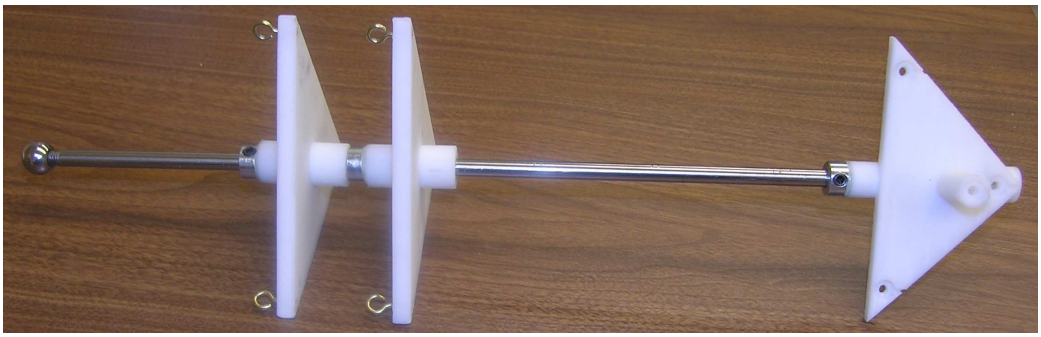

Figure 3.3: Outboard Body

In order to create attachment points on the outboard body for the springs, two equilateral triangular shaped spring attachment bodies, see Figure 3.3 were created using a Dimension 3D rapid prototype printer. The machine deposits a thin filament of ABS plastic according to a solid model file. The parts were designed to provide flexural rigidity to prevent any bending due to the applied spring loads. The springs were attached to the plastic body by eye hooks. Small holes were included in the corners of the parts to provide a location to mount the eye hooks. To prevent the spring ends from sliding around on the eye hooks during the simulation, small pieces of plastic tubing were inserted into the eye hooks once the springs were attached and the hooks were clamped. The spring attachment bodies were made on the rapid prototype machine because lightweight and accurate parts were required. Shaft collars, shown in Figure 3.4 were used to rigidly fix the spring attachment bodies to the rigid arm.

Figure 3.4: Shaft Collar

## 3.3 Springs and Structural Support

Six springs were needed to provide stability to the moving outboard body. Zinc-plated, tempered steel extension springs, 203.2 $mm$ (8 $in$) length, 3.2 $mm$ (0.125 $in$) outer diameter, 0.4 $mm$ (0.016 $in$) wire diameter, were selected and one is shown in Figure 3.5. The springs were attached to the outboard body and the ground fixed testing rig by eye hooks.

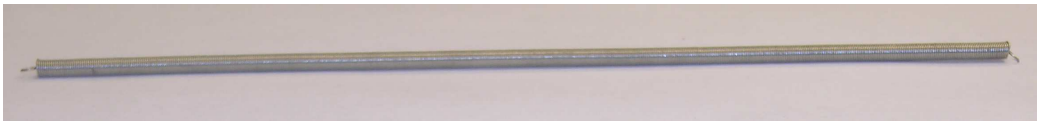

Figure 3.5: Springs

The testing rig consisted of a large plywood base, with three 500 $mm$ (20 $in$) long 2"X2" posts, standing upright, used to provide the ground fixed spring attachment points. The posts were rigidly attached to the base structure, assembled in a circular pattern, with an approximate radius of 380 $mm$ (15 $in$), 120 degrees from each other. Eye hooks, located a vertical distance of 150 $mm$ (6 $in$) and 200 $mm$ (8 $in$) from the base on each post, were used to attach the springs to the ground fixed base, see Figure 3.6.

The base structure was leveled before beginning testing to ensure the ground fixed coordinate system was oriented appropriately.

Figure 3.6: Ground Fixed Spring Attachment

## 3.4 Optotrak 3020 Motion Tracking System

Position locations on the outboard body were captured during the physical testing through the implementation of the Optotrak 3020 motion tracking system (Northern Digital) [24]. The testing took place at the Human Mobility Research Center at Queen's University, Kington Ontario, Canada. The positions of a ground fixed reference body were also monitored to allow for the creation of a ground fixed coordinate system. The motion tracking system has four main components: the position sensor unit, the system control unit, the strober units, and the markers. The raw data were collected and converted to three dimensional position data in a preset camera coordinate system using a computer running Toolbench (Northern Digital) software. The Opotrak system has an accuracy of 0.1 $mm$ for position measurements in the vertical and horizontal direction, and an accuracy of 0.15 $mm$ for position measurements toward and away from the camera.

### 3.4.1 Position Sensor Unit

Infrared light emitting diodes (IREDS), encased in markers located on the outboard body and the ground reference body, were monitored by three lens assemblies located in a position sensor unit, see Figure 3.7. The position sensor unit transmits the data

collected to the system control unit through a 10-pin (Lemo) communication cable [24].

Figure 3.7: Position Sensor

### 3.4.2 System Control Unit

The purpose of the system control unit is to control the firing sequences of the markers and to send data collected by the position sensor unit to a computer station [24]. The system control unit is shown below in Figure 3.8.

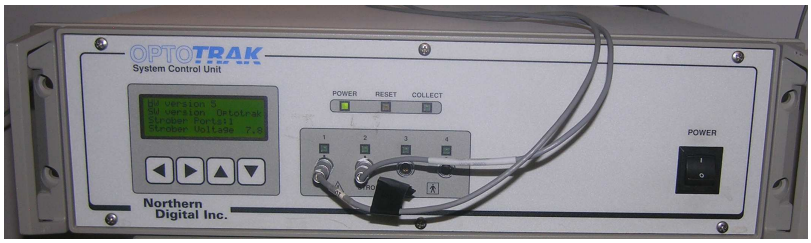


Figure 3.8: System Control Unit

### 3.4.3 Strober Units

The strober units, see Figure 3.9, receive signals and power from the system control unit through a four-pin (Lemo) strober cable. A maximum of six markers can be connected to each strober unit through six coxial (Lemo) receptacles [24].


Figure 3.9: Strobers

The strober also has a four-pin (Lemo) receptacle which can be linked up with another strober. Up to four strobers can be connected together. The purpose of the strober is to transmit the signals and power from the system control unit to each of the markers.

### 3.4.4 Markers

The markers, see Figure 3.10, connected to the strobers through a coxial (Lemo) marker cable, were fixed to the outboard body and ground reference system. The IRED, embedded in the marker, transmits an infrared signal which is observed and recorded by the position sensor unit [24].

Figure 3.10: Marker

## 3.5 Reference Bodies

The main purpose of the reference bodies was to: 1) provide unit vector directions for the ground fixed and body fixed coordinate systems and 2) provide a mounting location for the IRED which indicated the location of the body in three dimensional space with respect to time. Two reference bodies were created using a Dimension 3D rapid prototype printer to assist in transforming the data obtained in camera coordinates into data meaningful to the system. One reference body was designed to be attached to the outboard body, see Figure 3.11, to track the position of the outboard body over time.

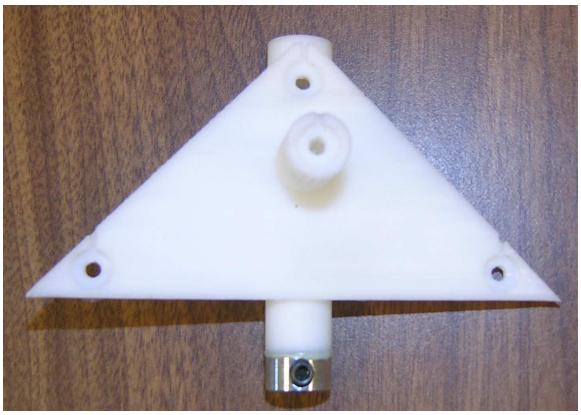

Figure 3.11: Body Fixed Reference Body

The body fixed coordinate system, $(\hat{i_5}, \hat{j_5}, \hat{k_5})$, was created based on the location of the body fixed IRED's relative to one another. A ground fixed body, shown in Figure 3.12, was fixed to the testing table and the ground fixed coordinate system, $(\hat{i_0}, \hat{j_0}, \hat{k_0})$, was created based on the location of the ground fixed IRED's relative to one another. Please see Appendix C for the coordinate system formulations.

Figure 3.12: Ground Fixed Reference Body

## 3.6 Process of Digitization

It was critical to accurately identify the location of a number of points on the physical model in order to obtain all of the information required as inputs into the computer simulation. Knowing the exact location of these points, either in body fixed or ground fixed coordinates, was extremely important in order to accurately compare the computer simulation to the physical model results. A pointer tool, with six markers, was used to identify the points, see Figure 3.13 below.

The pointer was held with the tip touching the point requiring digitization and data were recorded for $3s$. The raw data collected from each of the markers on the pointer were transformed to three dimensional position data in camera coordinates using the Toolbench software package. The data were processed to obtain the three dimensional location of the point in camera coordinates, see Appendix C.

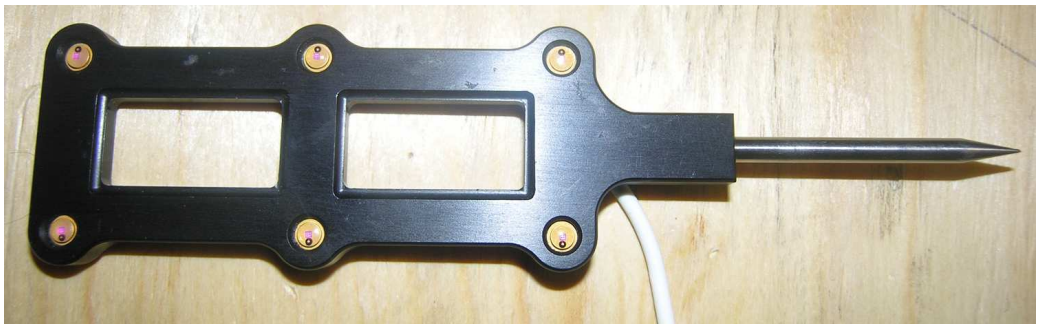

Figure 3.13: Pointer

## 3.7 Physical Properties

Several physical properties of the experimental model were required to produce a computer simulation that could be compared to the experimental testing. A description of each property and how it was measured is given below. Also, several points on the model were digitized as described above. The points include: the center of mass of the outboard body, the spring attachment locations, locating points for the center of rotation for the inboard body, the center of rotation of the outboard body, and locating points for all the parts on the outboard body.

### 3.7.1 Mass of Outboard Body

The mass of the outboard body was determined by weighing the body on a digital scale. The springs were not included in the mass; however, all components which hold the spring to the outboard body were included. The markers were also included in the mass.

### 3.7.2 Center of Mass of Outboard Body

The center of mass of the outboard body was determined by the following method. The body was suspended from a single point and a photograph was taken of the system. A plumb bob was hung beside the body to indicate true vertical. This process was repeated two more times with the body hung from different points in

each photo. The photos were analyzed and a line parallel to the true vertical line was drawn from the point of suspension. The intersection of the three lines indicated the center of mass. Figure 3.14 shows this process.

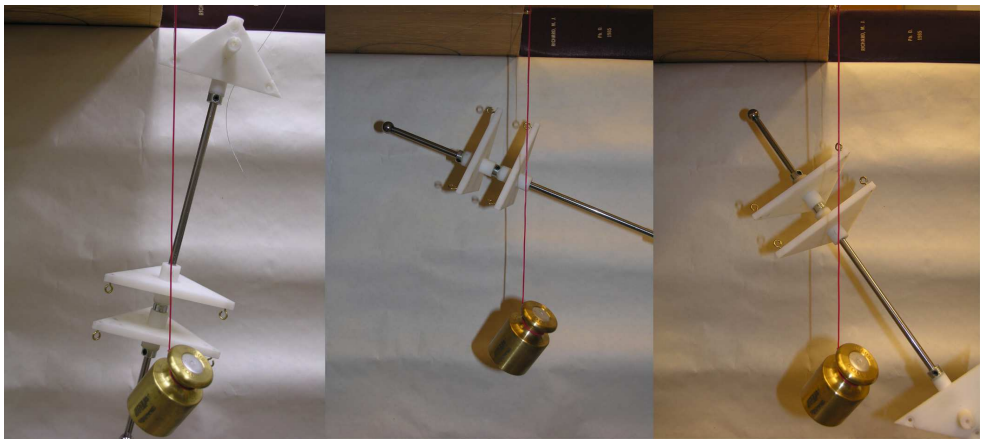

Figure 3.14: Determination of the Center of Mass of the Outboard Body

This point was marked on the body and later digitized using the optical measurement system to determine the center of mass relative to the fifth coordinate system located in the body.

### 3.7.3 Spring Stiffness

The spring stiffness was determined by vertically loading each spring with a series of calibrated masses. The springs were preloaded with a 200 $g$ weight to overcome the initial tension. Plots of force versus spring length are included for each spring in Appendix E. A line of best fit was plotted for each data set, and the spring stiffness, given by the slope of the curve, is shown below in Table 3.1 below.

| Spring | E | F | G | H | I | J |
|---|---|---|---|---|---|---|
| Stiffness $(\frac{N}{m})$ | 13.26 | 13.26 | 14.00 | 13.24 | 13.44 | 12.91 |

Table 3.1: Spring Stiffnesses.

### 3.7.4 Zero Force Spring Length

Since the springs selected had an inherent initial tension, it was necessary to determine the zero force spring length and not just the undeflected spring length. This is because in order to surpass the undeflected spring length, a force as least equal to the initial tension force had to be applied to the spring. The zero force spring lengths were found by determining the horizontal intercepts of the spring stiffness plots in Appendix E, and the values are tabulated below in Table 3.2

| Spring | E | F | G | H | I | J |
|---|---|---|---|---|---|---|
| Length ($m$) | 0.064 | 0.062 | 0.062 | 0.067 | 0.062 | 0.060 |

Table 3.2: Zero Force Spring Lengths.

### 3.7.5 Spring Attachment Locations

The spring attachment locations were determined by digitizing the locations with the pointer shown in Figure 3.13. The body fixed spring attachment locations are depicted in Figure 3.15. The ground fixed locations are shown in Figure 3.16. Figure 3.17 shows the pointer being used to digitize a body fixed spring attachment location.

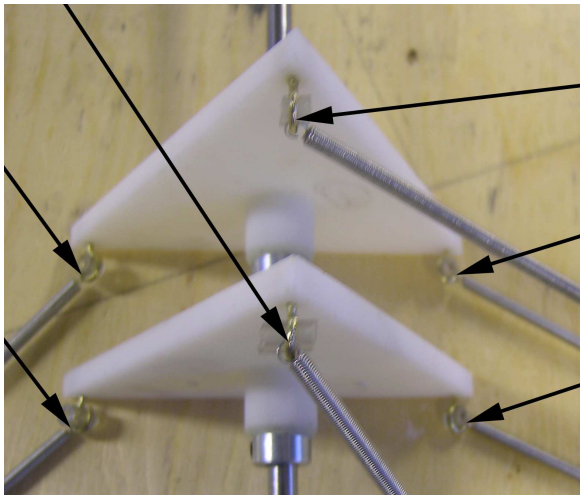

Figure 3.15: Body Fixed Spring Attachment Points

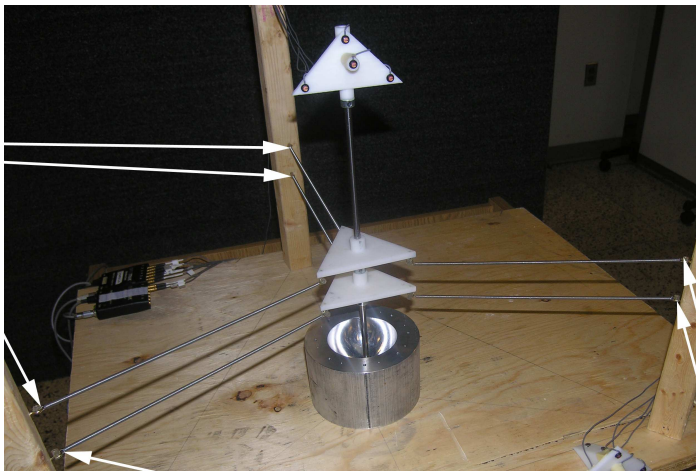

Figure 3.16: Ground Fixed Spring Attachment Points

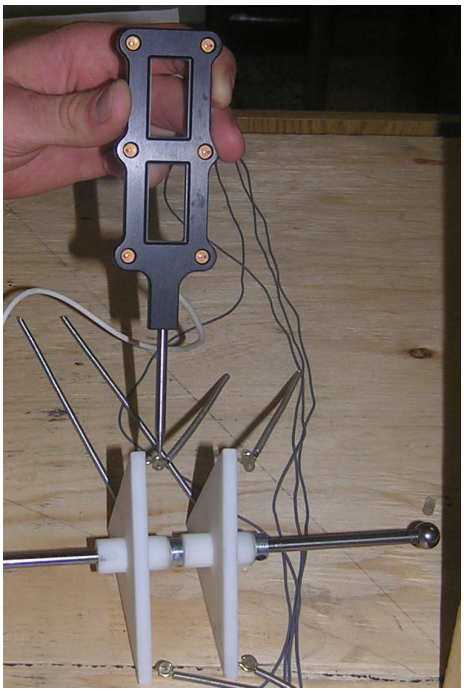

Figure 3.17: Pointer Digitizing A Body Fixed Attachment Point

### 3.7.6 Center of Rotation of Inboard Body

The center of rotation of the inboard spherical cutout was determined through digitizing eight center punch holes, located in a hole pattern of radius $4in$, and finding the average midpoint of the four diametrical pairs. The center punch holes can be seen between the deeper holes in Figure 3.2.

### 3.7.7 Center of Rotation of Outboard Body

The center of rotation for the outboard body was found using the 6D Architect (Northern Digital) software. A spherical cut out was produced on the rapid prototyping machine to match the radius of the spherical ball bearing. The outboard body was inserted into the cutout and data were obtained as the body was rotated in the cut out, see Figure 3.18. A body fixed coordinate system was defined based on the sensor data obtained, and the coordinates of each marker were given relative to the center of rotation. The center of rotation of the outboard body was defined as the origin for the body fixed coordinate system and, as such, it was required to know the location of this point, as all the body fixed inputs in the computer simulation were required in reference to this point.

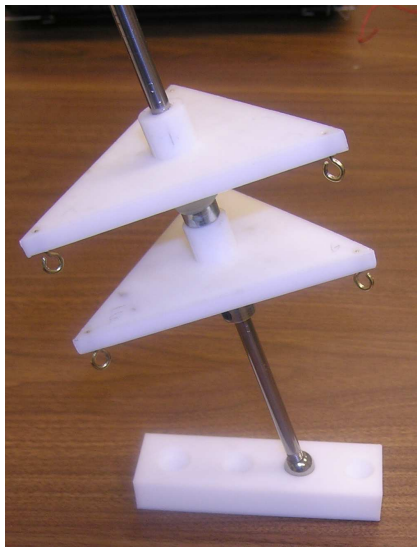

Figure 3.18: Determining the Center of Rotation of the Outboard Body

### 3.7.8 Inertia Tensor of Outboard Body

Several steps were required to calculate the inertia tensor. In order to accurately predict this property, 13 locating points on the outboard body were digitized to identify the location and orientation, relative to the center of mass in body fixed coordinates, of each part on the body. The center of mass location was also digitized. As shown above in Figure 3.3, the outboard body comprised eight parts: the reference body, two spring attachment bodies, the spherical articulating body, the rigid rod, and three shaft collars. Each part is discussed separately below. The parts were all modeled in Solid Edge (USG) and this software was used to define the inertia tensor for each body. The mass of each part was measured individually and a uniform density was assumed for each part. Since the location of each digitized point in the computer model was known, a transformation matrix was defined to convert from body fixed coordinates to the coordinates defined in each computer model. The center of mass of the outboard body was defined in each file, a coordinate system aligned with the body fixed system was assigned, and the mass moments and products of inertia were found. The markers and eye hooks were considered to be negligible for the purpose of this calculation. The contributions from each body were summed to yield the inertia tensor for the outboard body about the center of mass in the body fixed coordinate system. The moment and product of inertia values for each body and the totals are tabulated below, see Tables 3.3 and 3.4.

#### Reference Body

Three points were digitized on the reference body, as shown below in Figure 3.19, and transformed to body fixed coordinates. The transformation matrix from body fixed coordinates to the computer model coordinates was defined and the center of mass was located in the computer model.

#### Spring Attachment Bodies

Three points on each spring attachment body were digitized, as shown in Figure 3.20. These points were used to define the transformation matrix from body fixed

| Part | Ixx $(kg \cdot m^2)$ | Iyy $(kg \cdot m^2)$ | Izz$(kg \cdot m^2)$ |
|---|---|---|---|
| Reference Body | $4.55(10)^{-6}$ | $3.91(10)^{-4}$ | $3.94(10)^{-4}$ |
| Shaft Collar 1 | $6.76(10)^{-7}$ | $9.64(10)^{-5}$ | $9.59(10)^{-5}$ |
| Spring Attachment Body 1 | $2.82(10)^{-5}$ | $2.45(10)^{-5}$ | $2.12(10)^{-5}$ |
| Shaft Collar 2 | $7.33(10)^{-7}$ | $7.35(10)^{-}6$ | $6.83(10)^{-6}$ |
| Spring Attachment Body 2 | $2.86(10)^{-5}$ | $1.13(10)^{-4}$ | $1.09(10)^{-4}$ |
| Shaft Collar 3 | $7.00(10)^{-7}$ | $2.99(10)^{-5}$ | $2.94(10)^{-5}$ |
| Sphere | $5.74(10)^{-7}$ | $1.57(10)^{-4}$ | $1.56(10)^{-4}$ |
| Rod | $6.69(10)^{-6}$ | $6.27(10)^{-4}$ | $6.21(10)^{-4}$ |
| TOTAL | $7.08(10)^{-5}$ | $1.45(10)^{-3}$ | $1.43(10)^{-3}$ |

Table 3.3: Moments of Inertia for Outboard Body in Body Fixed Coordinates

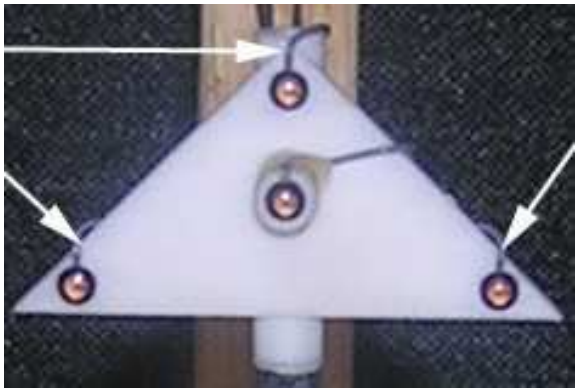

Figure 3.19: Points Digitized on the Reference Body

coordinates to computer model coordinates for each body. The center of mass of the outboard body was defined for each spring attachment body and the inertia tensor contributions were determined.

### Spherical Articulating Body

The contribution of the spherical articulating body to the inertia matrix was determined by using the center of rotation found earlier to locate the sphere relative to the center of mass.

| Part | Ixy $(kg \cdot m^2)$ | Ixz $(kg \cdot m^2)$ | Iyz $(kg \cdot m^2)$ |
|---|---|---|---|
| Reference Body | $-3.67(10)^{-6}$ | $-9.90(10)^{-6}$ | $1.97(10)^{-7}$ |
| Shaft Collar 1 | $-9.08(10)^{-7}$ | $-7.15(10)^{-6}$ | $6.78(10)^{-8}$ |
| Spring Attachment Body 1 | $1.15(10)^{-6}$ | $4.94(10)^{-6}$ | $7.94(10)^{-7}$ |
| Shaft Collar 2 | $4.91(10)^{-7}$ | $1.94(10)^{-}6$ | $1.42(10)^{-6}$ |
| Spring Attachment Body 2 | $4.10(10)^{-6}$ | $1.90(10)^{-5}$ | $7.97(10)^{-7}$ |
| Shaft Collar 3 | $8.19(10)^{-7}$ | $3.99(10)^{-6}$ | $1.12(10)^{-7}$ |
| Sphere | $3.17(10)^{-6}$ | $7.73(10)^{-6}$ | $1.57(10)^{-7}$ |
| Rod | $-5.34(10)^{-6}$ | $2.86(10)^{-6}$ | $5.56(10)^{-7}$ |
| TOTAL | $-1.88(10)^{-7}$ | $2.34(10)^{-5}$ | $2.82(10)^{-6}$ |

Table 3.4: Products of Inertia for Outboard Body in Body Fixed Coordinates

### Rigid Rod

The rod was located by digitizing four points. A center punch mark was machined on the end of the rod using a lathe and this was the first point digitized. Three additional points, forming a circle immediately above the second spring attachment body, were also digitized, see Figure 3.21.

The center of the rod at this location was determined from these three points. Using the two rod center locations, the orientation of the long axis of the rod was determined. The contributions of the rod to the inertia matrix relative to the center of mass was then found.

### Shaft Collars

Three shaft collars were used in the physical model to rigidly fix the parts produced on the rapid prototyping machine to the outboard body. Using the technical specifications, a computer model of the shaft collar was produced. The shaft collars were assumed to be aligned with the long rigid rod, and were located at the base of each respective rapid prototype body.

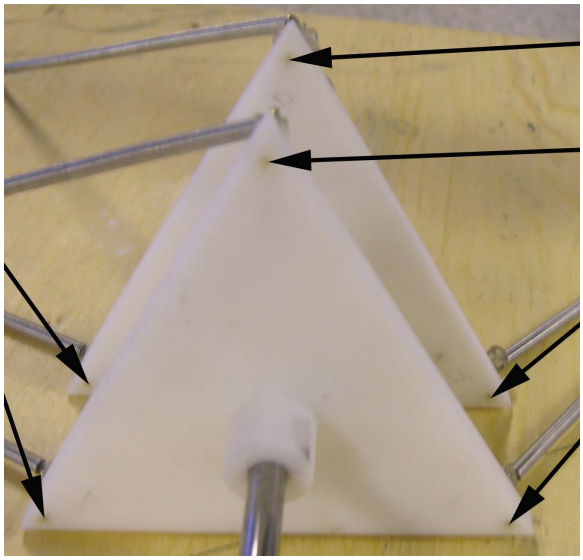

Figure 3.20: Points Digitized on the Spring Attachment Bodies

## 3.8 Testing Protocol

The following section gives an overview of the experimental testing procedure, which can be subdivided into four main components: set-up, digitization, static trials and dynamic trials. Each of these components of the testing protocol is discussed in detail.

### 3.8.1 Set Up

The set up phase of the testing protocol involved first turning on the Optotrak position sensor unit and system control unit, and placing the testing table in the field of view of the position sensor unit. The testing table was leveled and fixed to prevent motion in the camera coordinate system. Markers were attached to the body fixed and ground fixed reference bodies and connected to one of two strober units. The pointer was also connected to one of the strober units.

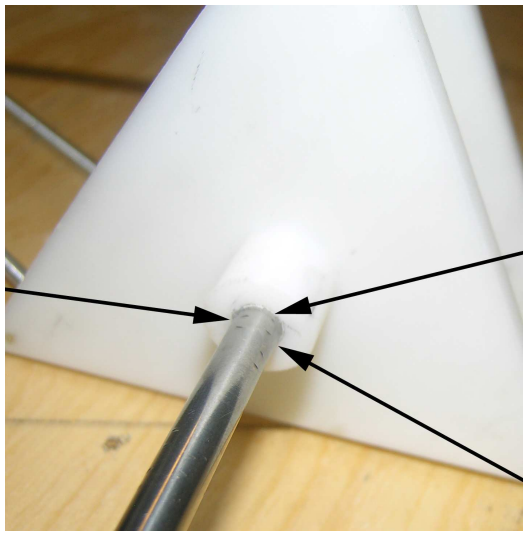

Figure 3.21: Points Digitized on the Rod

### 3.8.2 Digitization

In the digitization phase, 10 body fixed and 14 ground fixed positions were determined through digitization with the pointer. Data collection for the digitization trials occurred for 3 seconds at a sampling rate of 157 Hz. The body fixed positions were digitized first, with the outboard body in a static position on the testing table as shown in Figure 3.17. Next the center of rotation of the outboard body was determined by using the 6D Architect (Northern Digital) software and a 20 second trial, where the outboard body was rotated in the spherical cutout shown in Figure 3.18. Lastly, the outboard body was positioned in the inboard body, the springs were attached to the ground fixed attachment points, and the 14 ground fixed positions were digitized.

### 3.8.3 Static Trials

Three static trials were recorded to compare the equilibrium position predicted by the simulation to that observed during experimental testing. Data collection occurred for 10 seconds, at a sampling rate of 157 Hz. Photographs of the equilibrium position were also obtained.

### 3.8.4 Dynamic Trials

Several dynamic trials were recorded, each for a length of 10 seconds at a sampling rate of 157 Hz. This sampling rate was selected in order to avoid aliasing. Based on qualitatively observing the motion of the model, is was determined that the frequency of oscillation would be under 80 Hz. In order to maintain the initial conditions of zero angular velocity, the outboard body was displaced from equilibrium and held in this position by a taut string fixed to the testing table. Photographs of each starting condition were obtained to assist with determining the initial condition angles. The exact starting location of the system did not need to be repeatable because the initial conditions were determined based on the starting marker positions recorded for each trial. Approximately one or two seconds of static data were collected at the beginning of the dynamic trial to ensure that the initial marker positions could be determined. After this time passed, the string was cut and the dynamic portion of the trial commenced. To ensure that the cutting of the string did not interfere with the trial, the string was cut as close to the testing table as possible. The added mass of string was considered to be negligible.

# Chapter 4

# Comparison of Results

## 4.1 Input Files

In order to compare the experimental results obtained through testing to a simulated solution, two input files were required. Firstly, a constant input file was created after obtaining the physical property data for the experimental model, as explained in Chapter 3. This file, found in Appendix F, contained all of the experimental model data that did not change throughout the testing process as well as the simulation time and output time step.

The second input file contained the initial conditions for each specific trial. The initial conditions are simply the configuration coordinates, $x(1)$, $x(2)$, $x(3)$, $x(4)$, and $x(5)$, and generalized speeds, $x(6)$, $x(7)$, $x(8)$, $x(9)$, and $x(10)$ - or in simpler terms, the starting rotation angles and angular velocities. Since the trials were initiated from a static position, the generalized speed terms were all zero for each trial. The determination of the configuration coordinates, based on experimentally collected body fixed marker position data, seems trivial; however, due to the complexity of the system this proved to be a very difficult challenge. The process of determining the starting angles is described later in this chapter.

## 4.2 Comparing the Equilibrium State

### 4.2.1 Using Simulation With Damping to Predict Equilibrium Angles

The first step in comparing the experimental results collected through the physical model and the computer simulation was to determine if the static three dimensional equilibrium position of each of the four markers could be matched. In order to determine the equilibrium angles for the computer simulation, damping was added to identify where the model would naturally come to rest. Damping was included in the model by adding forces proportional to velocity to each of the body fixed spring attachment points. An arbitrary condition, where $x(1) = 20°$, $x(2) = 20°$, $x(3) = 160°$, $x(4) = 20°$, and $x(5) = 10°$, was selected and the damped simulation was used to determine the equilibrium position for the system. These angles were used in the initial condition file and the results from the simulation are shown below in Figures 4.1, 4.2, 4.3, 4.4, and 4.5.

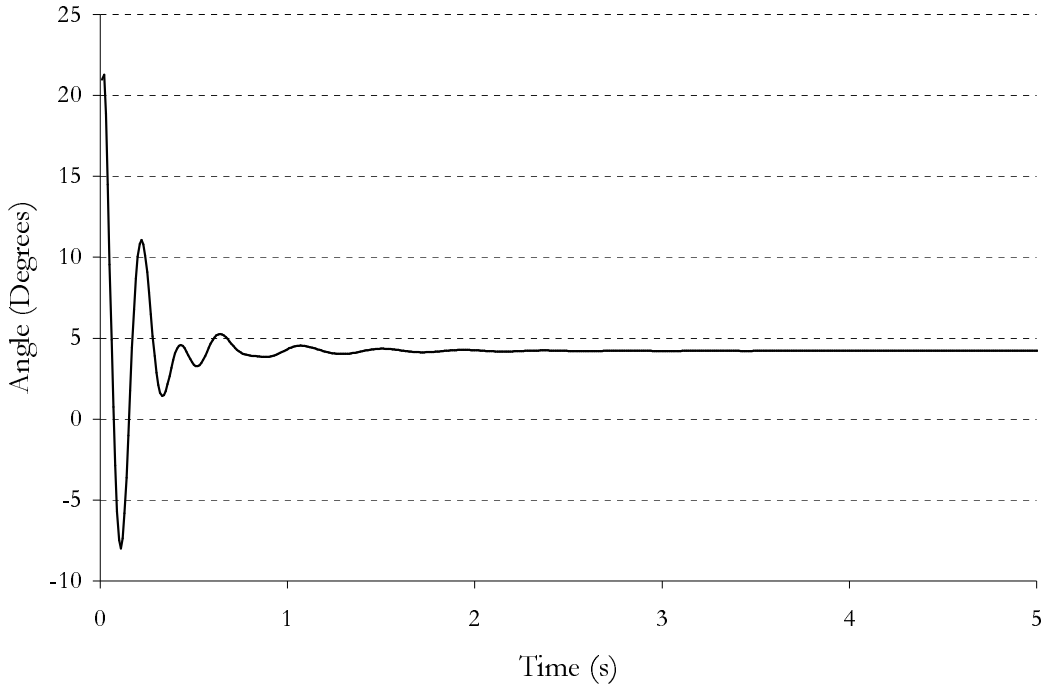


Figure 4.1: Damped Response of x(1)

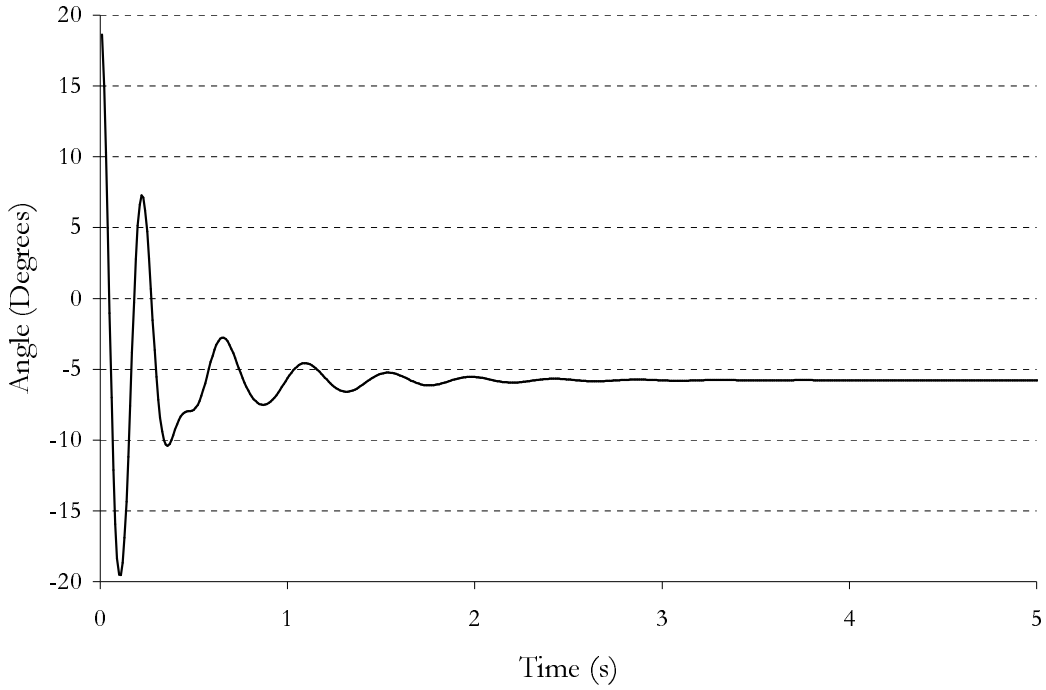


Figure 4.2: Damped Response of x(2)

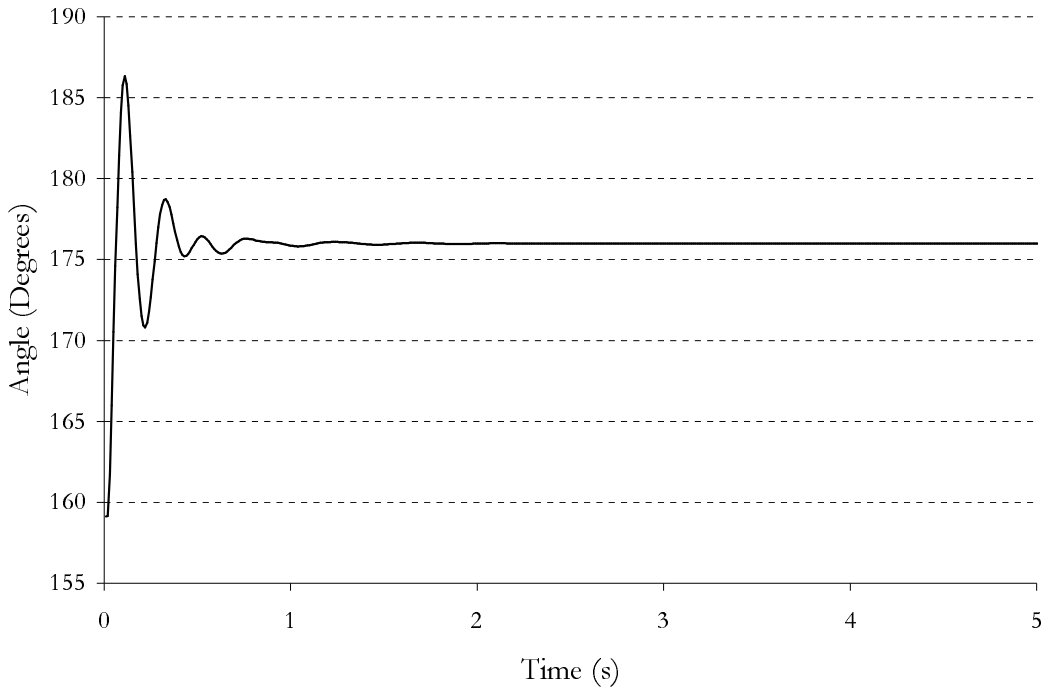


Figure 4.3: Damped Response of x(3)

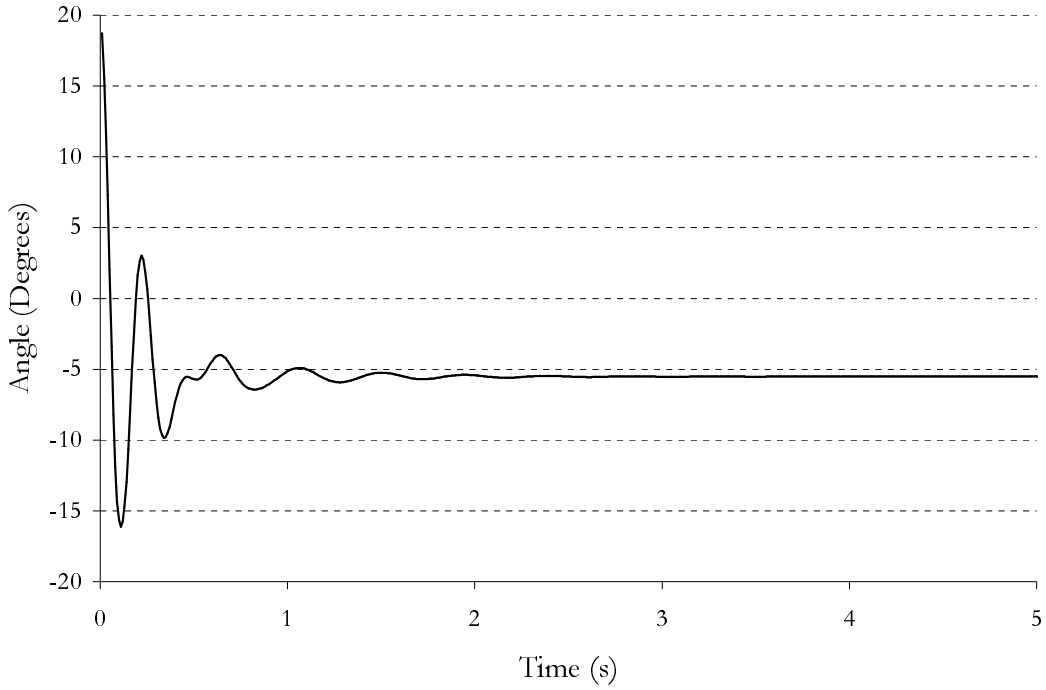


Figure 4.4: Damped Response of x(4)

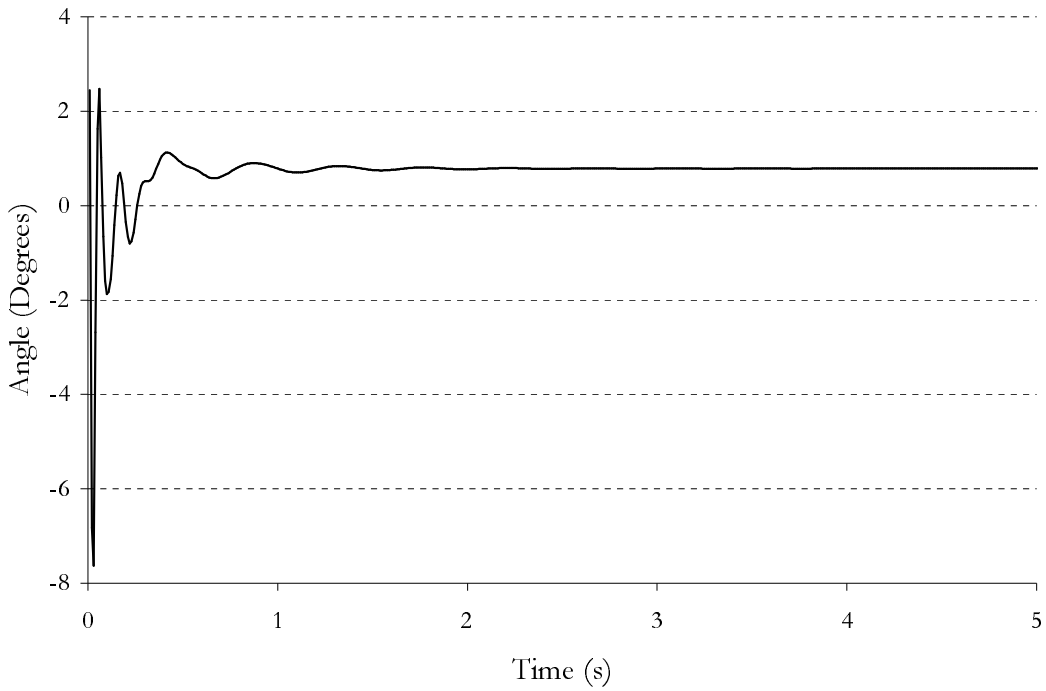


Figure 4.5: Damped Response of x(5)

It is clear from Figures 4.1 - 4.5 that the damping program is working as expected and that by at least the four second mark all of the angles remain relatively unchanged for the remainder of the simulation. This suggested that the system had settled into an equilibrium position. To determine if this was actually the case, the configuration coordinates were each averaged over the last second of the simulation to obtain new initial conditions as follows, $x(1) = 4.2°$, $x(2) = -5.8°$, $x(3) = 176.0°$, $x(4) = -5.5°$, and $x(5) = 0.8°$. When these angles were compared to the photographs taken during the static trial, see Figure 4.6 below, they agree qualitatively, as a negative $x(2)$ value indicates a clockwise rotation about the ground fixed $j_0$ axis, which points to the right in the front view and into the page in the side view of Figure 4.6.


Figure 4.6: Side View and Front View of Physical Model in Equilibrium Position

These initial conditions were used to run a new simulation without damping, and the position predicted for each of the four markers in ground fixed, $(\hat{i_0}, \hat{j_0}, \hat{k_0})$, coordinates was compared to the experimental static trial data. It is important to note that several static trials were obtained between dynamic trials and the experimental results for the equilibrium position were found to be repeatable. The marker positions, in the $(\hat{i_0}, \hat{j_0}, \hat{k_0})$ coordinates, are shown in Figures, 4.7 to 4.10 below. The components for marker 1 are shown in a larger scale in Figures 4.11 and 4.12.

From Figures 4.7 to 4.10 two observations can be made. Firstly, just considering the simulation data, it is clear that the configuration coordinates predicted by the damped model do in fact identify an equilibrium position in the simulation. Furthermore, the results from the simulation closely match that of the experimental equilibrium trial.

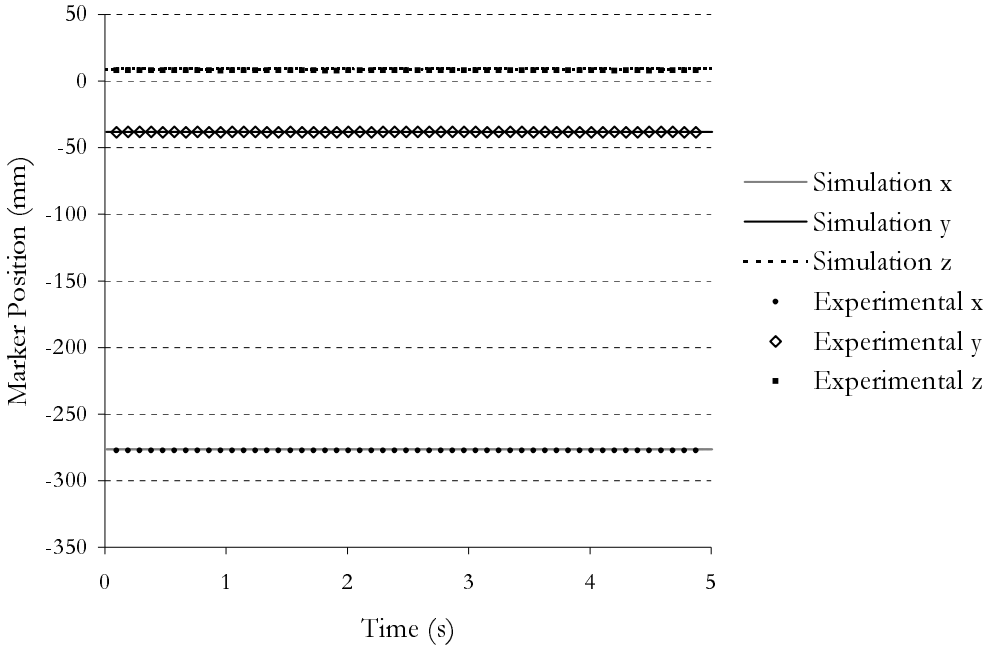


Figure 4.7: Comparison of Marker 1 Equilibrium Position: System Damping Technique

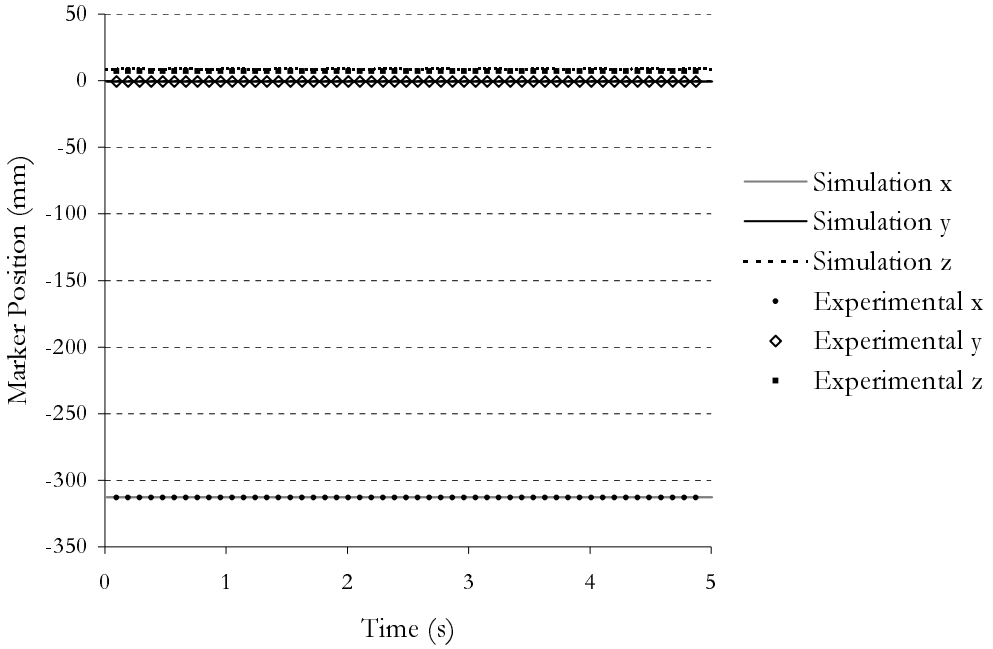


Figure 4.8: Comparison of Marker 2 Equilibrium Position: System Damping Technique

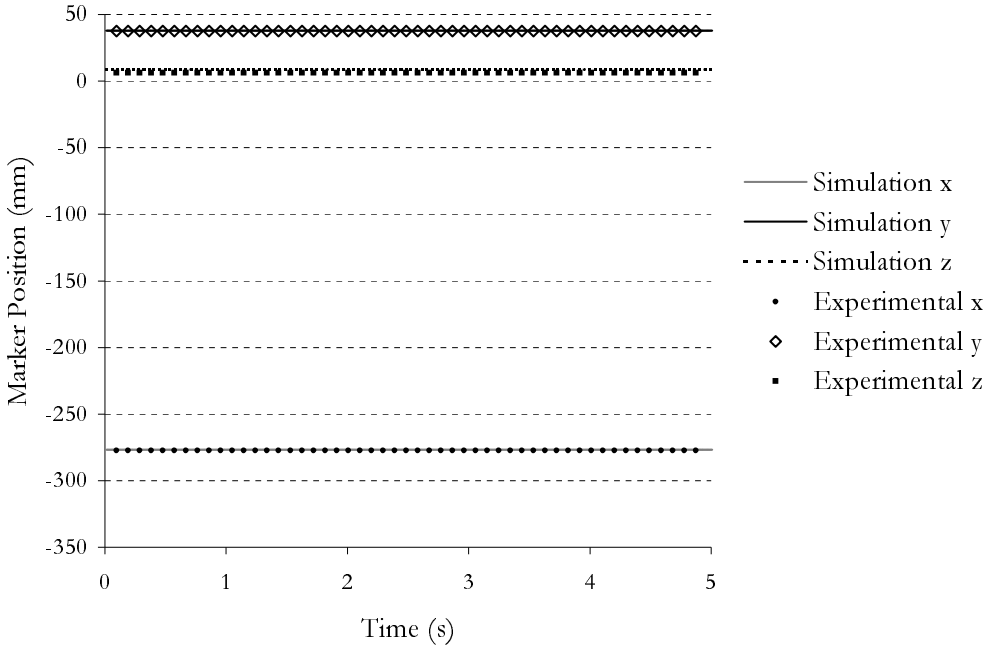


Figure 4.9: Comparison of Marker 3 Equilibrium Position: System Damping Technique

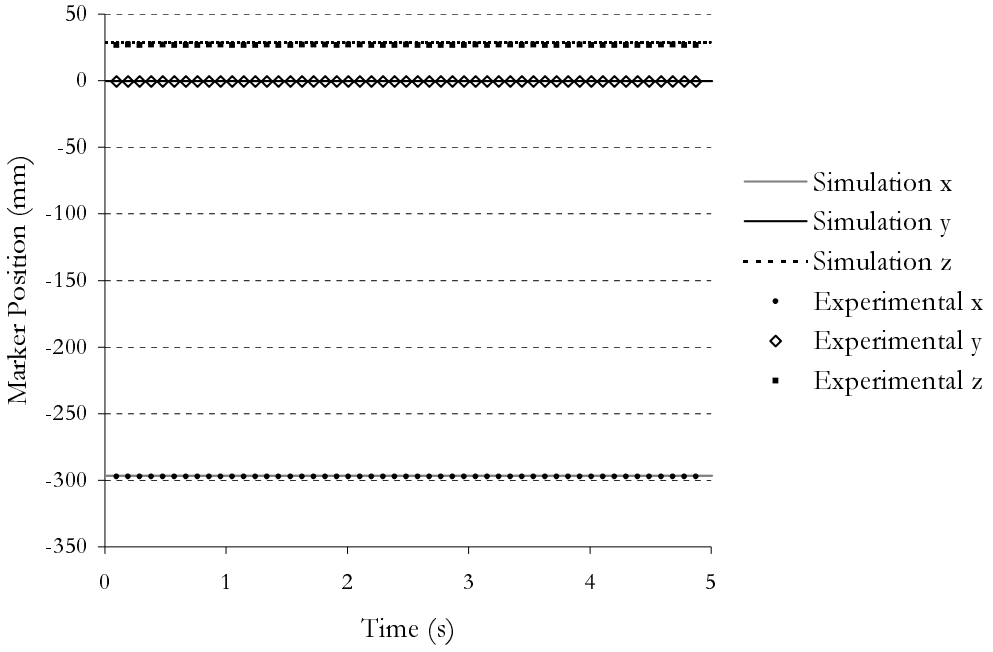


Figure 4.10: Comparison of Marker 4 Equilibrium Position: System Damping Technique

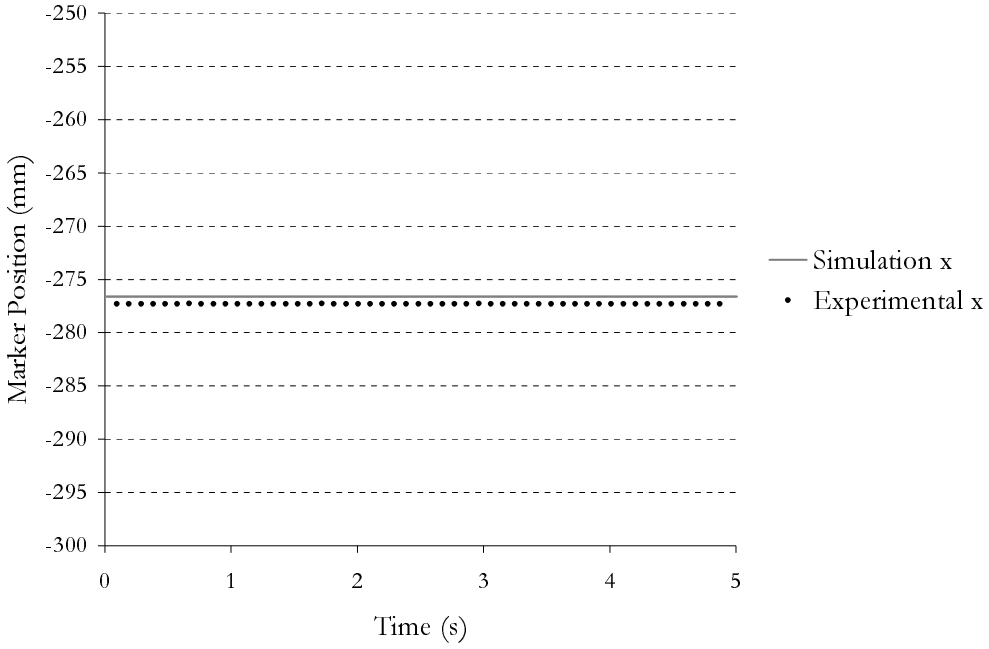


Figure 4.11: Comparison of Marker 1 Equilibrium Position: System Damping Technique

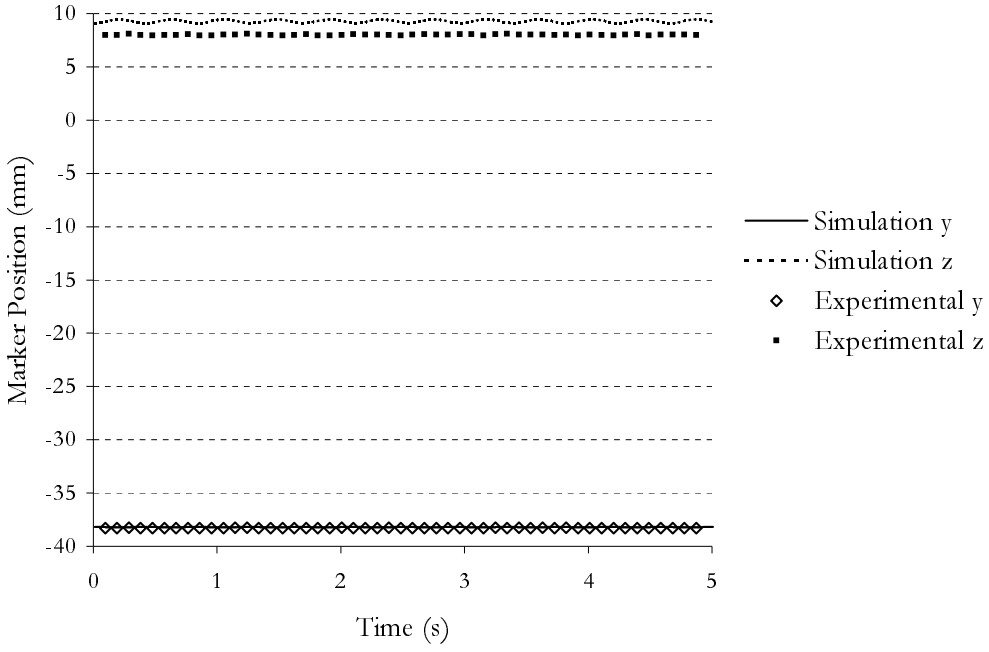


Figure 4.12: Comparison of Marker 1 Equilibrium Position: System Damping Technique

### 4.2.2 Using A Numerical Technique to Predict Equilibrium

Next the equilibrium angles necessary for the computer simulation were determined through another method, a modified Newton-Raphson process. This iterative numerical solution technique can be used to solve a system of equations in the following way: first a set of independent variables are assumed and this is used to calculate an approximate solution. The approximate solution is compared to an actual known solution, and the set of independent variables assumed is modified to attempt to minimize the error between the two solutions. The process is iterated until the error between the two solutions is deemed acceptable. In the equilibrium position, configuration coordinates $x(1)$, $x(2)$, $x(4)$ and $x(5)$ were expected to be close to zero and coordinate $x(3)$ was expected to be close to 180 degrees. Angles of $x(1) = 0°$, $x(2) = 0°$, $x(3) = 180°$, $x(4) = 0°$, and $x(5) = 0°$, were used to start the solution process. The computer simulation was used to determine the marker positions at time t=0. These results were compared to the desired marker positions, given by the experimental data, and attempts were made to minimize the error between the two solutions. Once the solution converged, the angles were used as the initial conditions for the equilibrium computer simulation. The initial angles were predicted to be $x(1) = 0.23°$, $x(2) = 9.3°$, $x(3) = 179.7°$, $x(4) = 8.7°$, and $x(5) = 1.8°$.

The results are shown below in Figures 4.13, 4.14, 4.15, and 4.16 where is can be seen that the simulation is not quite at equilibrium. This brings to light the fact that although the numerical routine may be able to very accurately predict a solution, it may in fact be converging on another set of angles with a similar resultant position. Since the system is comprised of non-linear algebraic equations, there may be multiple solutions to any given initial starting position. The complexity in the system results from following the specific articulation path. Since four markers were traced, there are twelve pieces of initial condition information known about the system: the x, y, and z components of each marker position in the ground fixed coordinate system. The system; however, only has five degrees of freedom, which means that only five of the 12 positions can be minimized using the Newton-Raphson method. The other seven components are not used and can only be predicted once the iterative process has converged on a set of starting angles. There is no way to minimize the results

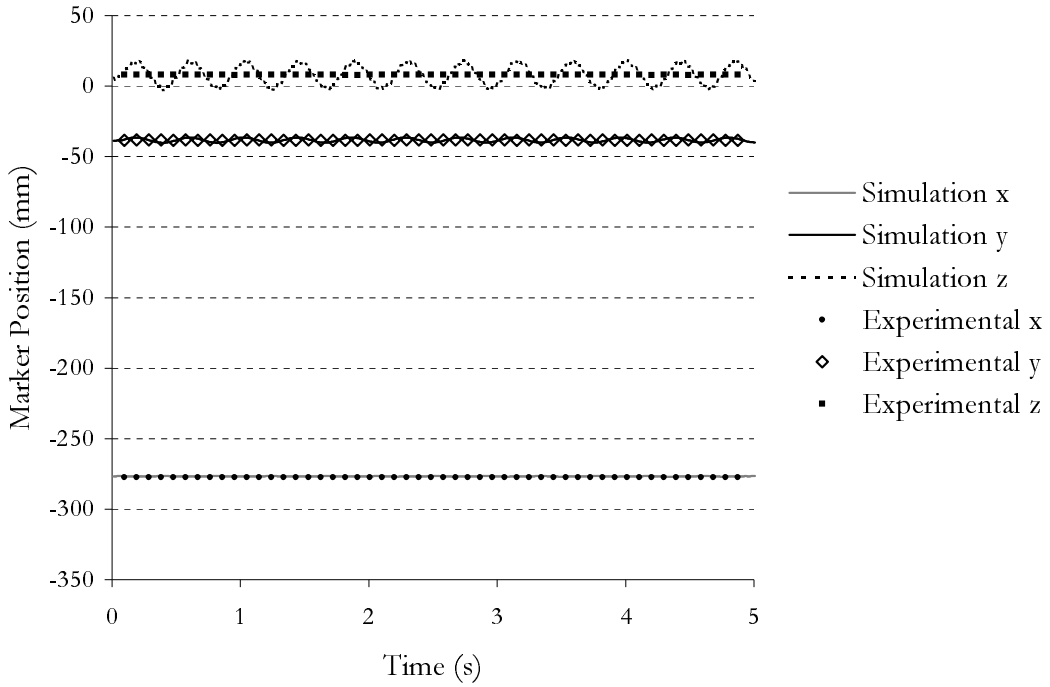


Figure 4.13: Comparison of Marker 1 Equilibrium Position: Newton Raphson IC's

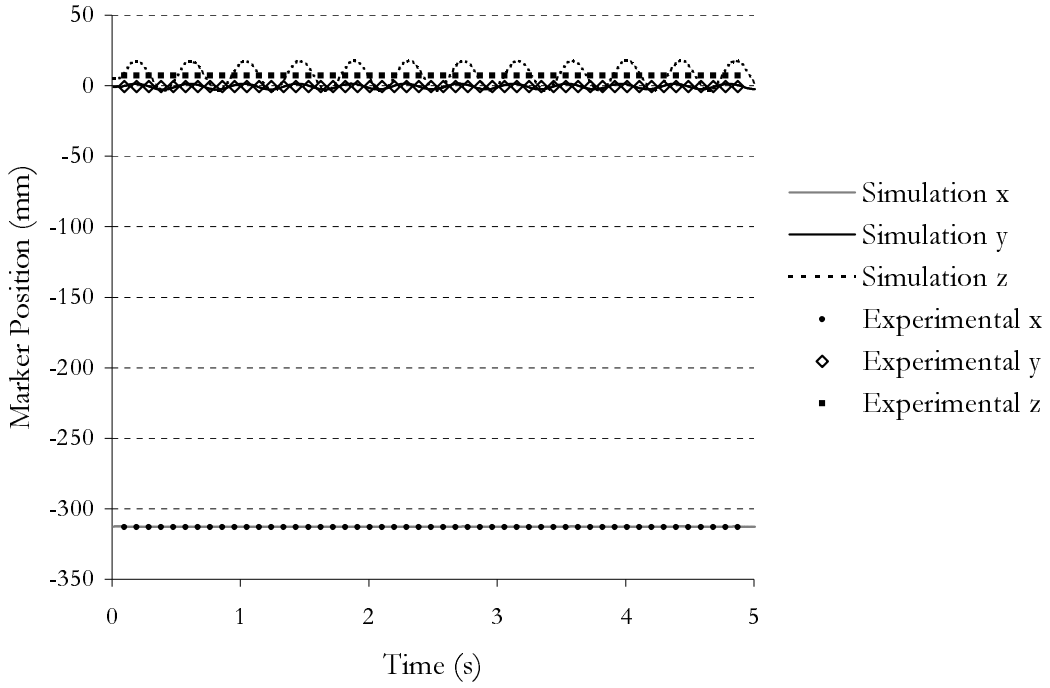


Figure 4.14: Comparison of Marker 2 Equilibrium Position: Newton Raphson IC's

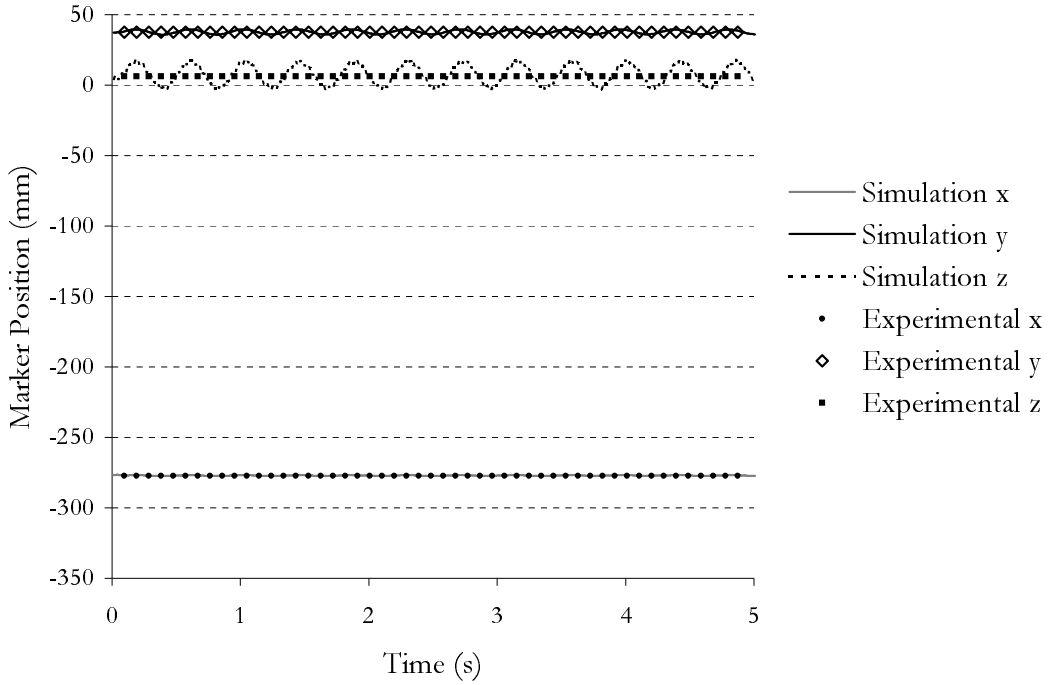


Figure 4.15: Comparison of Marker 3 Equilibrium Position: Newton Raphson IC's

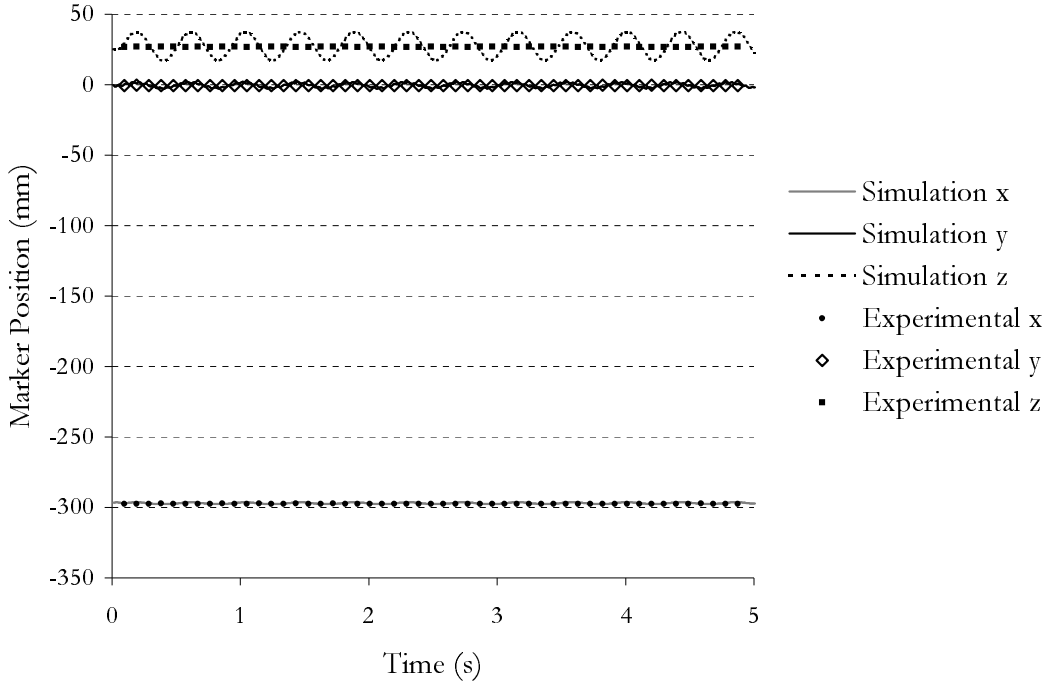


Figure 4.16: Comparison of Marker 4 Equilibrium Position: Newton Raphson IC's

obtained with these starting angles for the seven left over pieces of information. Also, because the system is comprised of non-linear algebraic equations, it is impossible to tell which pieces of information are best to use in the minimization, and which can be left out. The five piece of position information used for analysis was varied and it was found that the angles predicted did changed slightly. Dealing with finding the initial conditions for the set of non-linear equations of motion for a five degree of freedom system proved to be much more difficult then originally thought. At first, a least squares error minimization was considered. If the system was comprised of linear algebraic equations, the least squares method could have been easily implemented. The presence of trigonometric functions requires the use of an iterative Newton-Raphson solution and as such, least squares minimization could not be used. The Newton-Raphson technique may not provide the best method of solving for initial conditions of this non-linear system. Since the position measurements for the markers have errors associated with them, forcing the error on five of the pieces of position information to zero may not yield the best possible set of initial angles. This leaves no way to account for error in the measurement system.

## 4.3 Comparing Dynamic Simulations

The initial angles for each of the dynamics simulations were determined using the Newton-Raphson method described above, as it was found to be impossible to determine them any other way. Several experimental dynamic trials were performed, and the trial with the largest amplitude of motions, Trial 5, was selected for analysis and comparison to the computer simulation. The starting condition is shown for this trial in Figure 4.17 below. The initial angles were determined to be $x(1) = -20.5°$, $x(2) = 17.3°$, $x(3) = 186.5°$, $x(4) = 16.2°$, and $x(5) = 2.7°$. These angles appear to agree qualitatively with the set up shown in Figure 4.17. The simulation was run using these initial angles and the solution was compared to that of the experimental trial, and the following results for marker position were obtained. Figures 4.18 to 4.20 were analyzed to quantify the comparison under the following criteria: initial response, relative amplitude of motion, and frequency of oscillation.

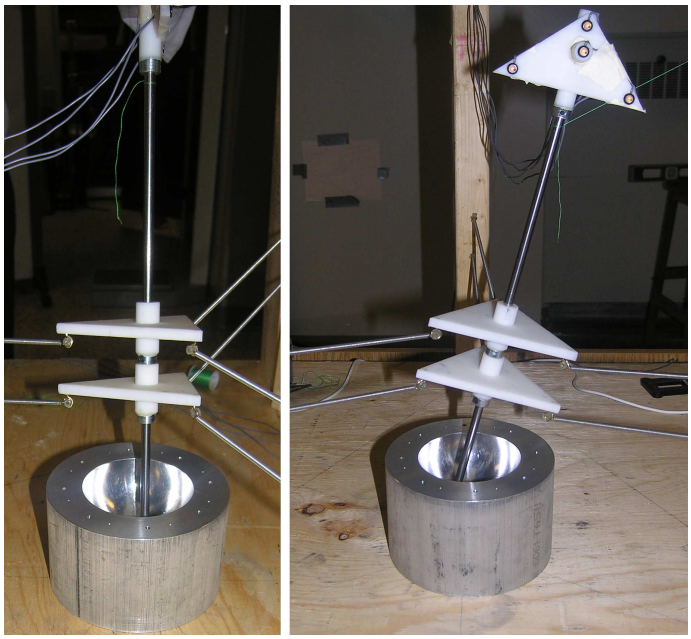

Figure 4.17: Side View and Front View of Dynamic Trial Analyzed

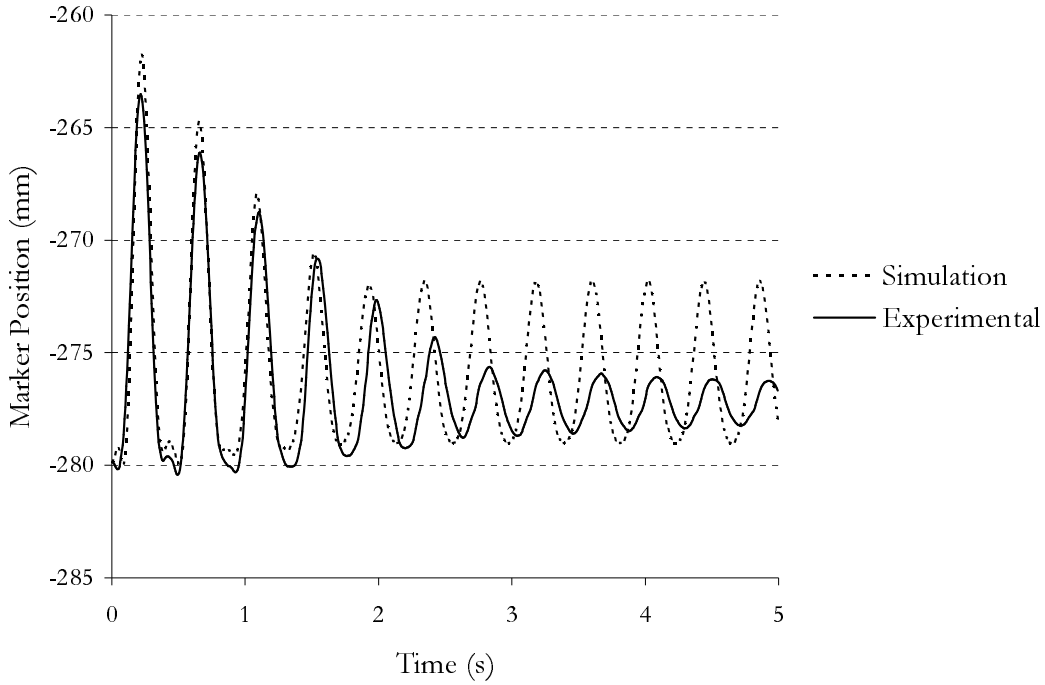


Figure 4.18: Comparison of Marker 1 X Position: Trial 5

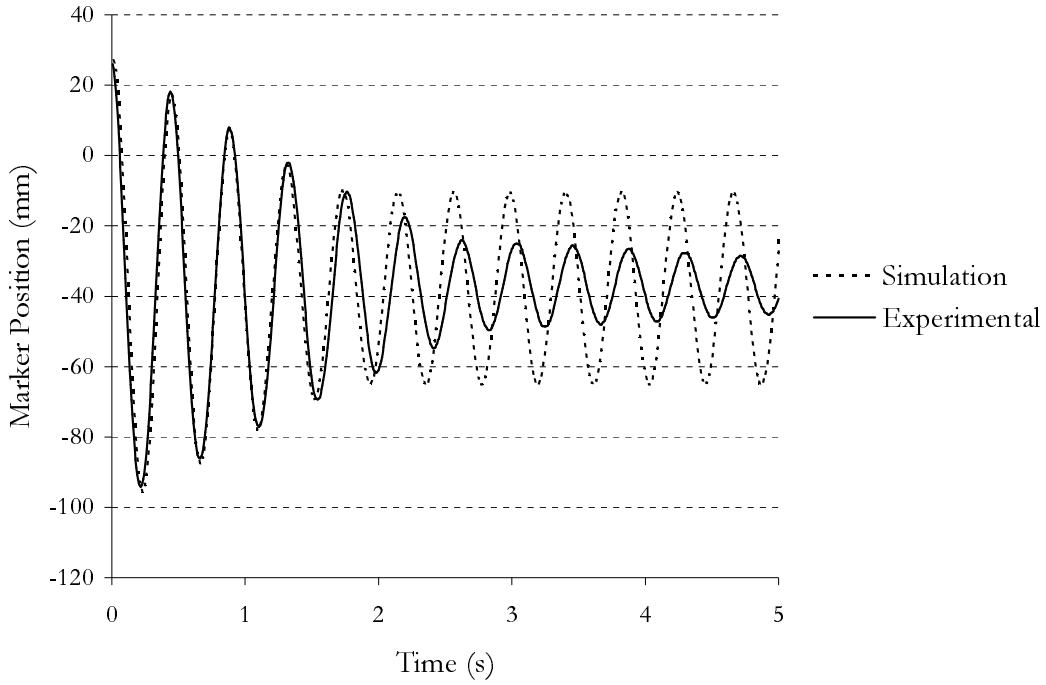


Figure 4.19: Comparison of Marker 1 Y Position: Trial 5

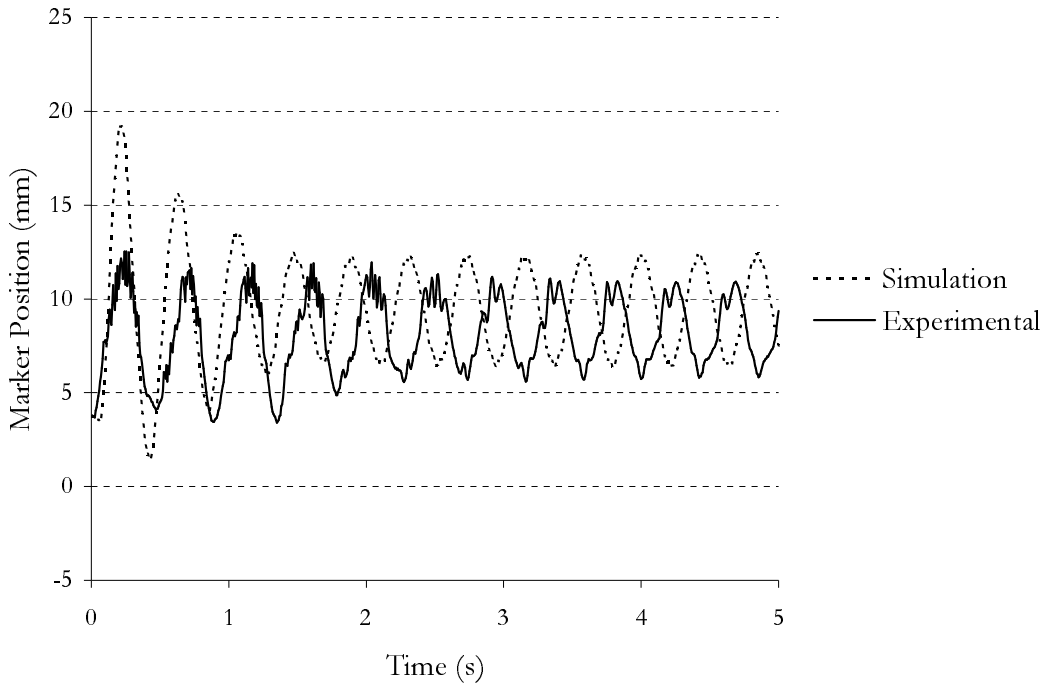


Figure 4.20: Comparison of Marker 1 Z Position: Trial 5

It was not possible to apply system damping to determine the initial conditions because for the dynamic trials, the system was not initially held in the equilibrium position. The error on the x positions of markers 1 and 2, the y positions of markers 1 and 3 and the z position of marker 2 were selected to be minimized to determine the initial conditions.

### 4.3.1 Initial Response

It is noted that generally the x and y marker positions determined through the simulation closely agreed to the experimental results. This is especially true when considering the initial response of the system. Plots of the x,y and z positions of the first marker over the first 0.3 $s$ of the trial are shown in Figures 4.21, 4.22, 4.23, respectively.

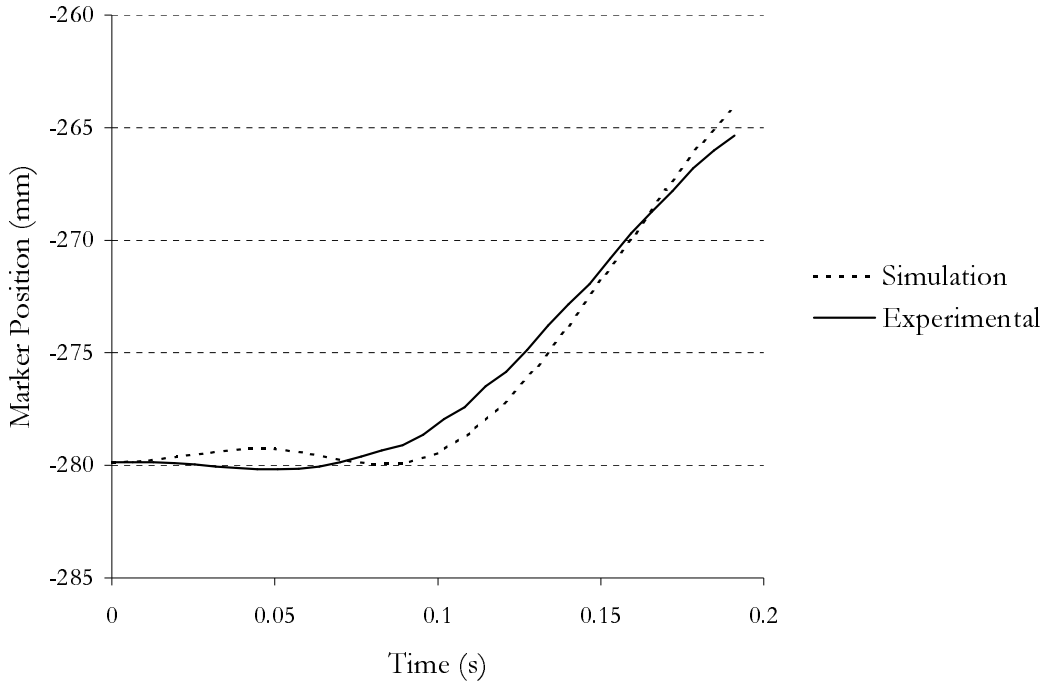


Figure 4.21: Initial x Response of Marker 1

These plots show that the initial response of the computer simulation closely matches that of the experimental trial.

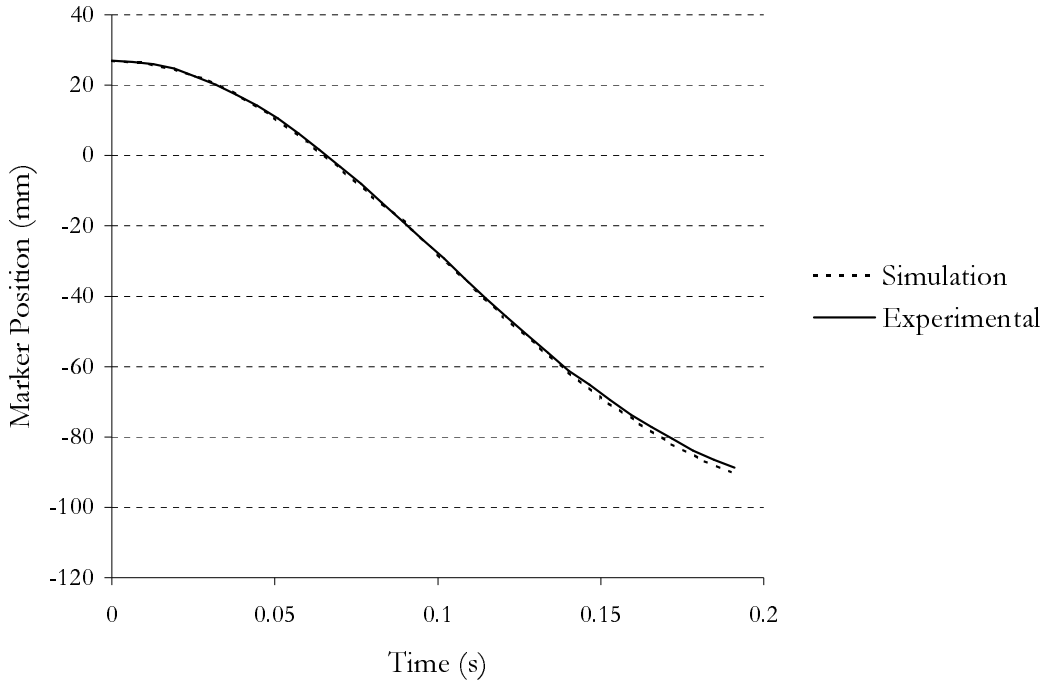


Figure 4.22: Initial y Response of Marker 1

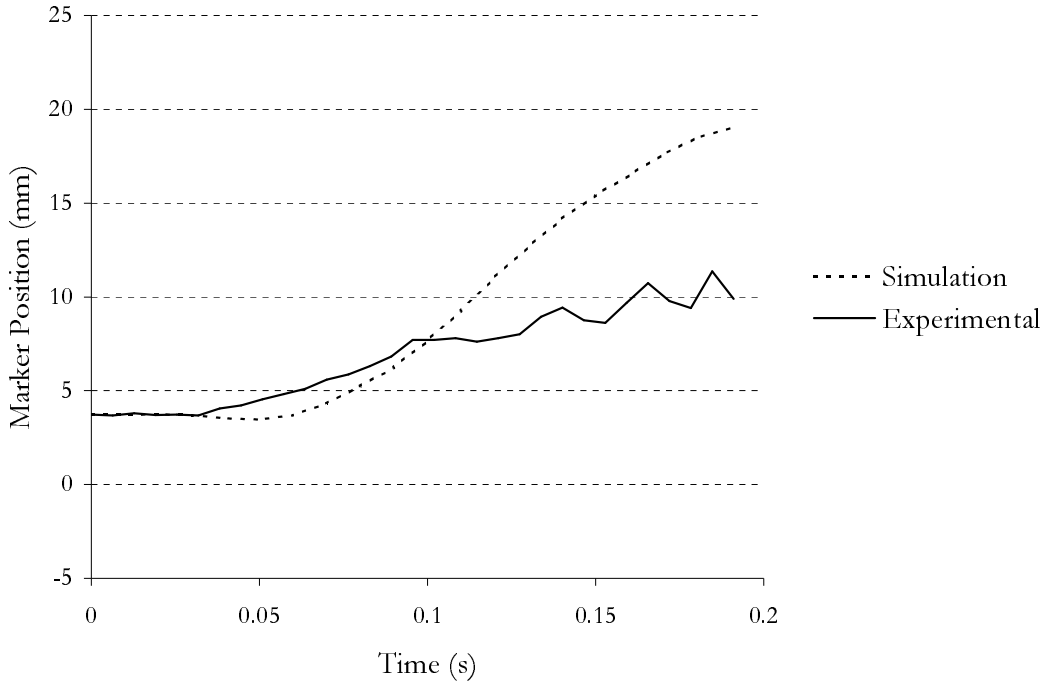


Figure 4.23: Initial z Response of Marker 1

### 4.3.2 Relative Amplitude of Motion

As shown in Figures 4.18 to 4.20, the amplitudes of the x and y motions predicted by the computer simulation closely match that of the experimental trial, especially for the first few seconds. As time elapses, viscous damping effects in the physical model cause the amplitude of motion to decrease. Viscous damping was not modeled in the computer simulation so the response predicted does not drop off. The z motion predicted by the computer simulation was found to be approximately twice that of the physical model. One explanation for this is the fact that initial positions of some of the markers, determined by using the angles predicted by the Newton Raphson method, were found to be slightly off from the experimental trial. Since there are only five degrees of freedom, the Newton Raphson method can only minimize the error in five of the twelve pieces of position information for the four markers. As such, the seven remaining positions could only be predicted once the solution converged on a set of starting angles.

### 4.3.3 Frequency of Oscillation

The trial examined was dominated by motion in the y direction and as such, Figure 4.19 was used to determine the frequency of oscillation. Two peaks were identified at $t_1 = 0.44\ s$ and $t_2 = 3.88\ s$ for the experimental trial, and at $t_3 = 0.44\ s$ and $t_4 = 3.81\ s$ for the simulation, with 8 cycles between the peaks for both. The frequency of the experimental oscillation was calculated to be $\omega_e = 2.33\ Hz$. The frequency for the simulation was calculated to be $\omega_s = 2.37\ Hz$.

## 4.4 Incorporating System Damping

Incorporating system damping into the computer simulation was found to be quite a difficult task. Firstly, no suitable method for experimentally measuring the damping was available. This is due to the complex nature of the problem. Several different types of damping are acting on the system and it is difficult to model the exact behaviour.

### 4.4.1 Coulomb Damping

Coulomb damping, sometimes known as dry friction damping, results when two surfaces are in contact and are moving relative to one another. The force of friction between the two surfaces is constant and acts in opposition of the motion. Since no feasible method was found to experimentally measure the friction force or the normal force between the articulating bodies in the physical system, attempts were made to minimize the dry friction. This was accomplished by polishing and lubricating the contact surface of the inboard body. Despite these efforts, Coulomb damping was still visibly present in the experimental results, as is shown by the linear decrease in the amplitude of oscillations in Figure 4.24. Parameter estimation was performed in order to incorporate the Coulomb damping into the computer simulation. A constant force acting in the negative direction of the velocity vector at the point of contact was included in the model, and the value of the force was varied until the simulation was found to behave similarly to the experimental trials. It is important to note that Coulomb damping was only incorporated into the model while the velocity of the outboard body at the point of contact was not zero, and this why the effects of dry friction are only present for the first few seconds of the simulation.

### 4.4.2 Viscous Damping

Attempts were made to minimize the contact friction at the articulation surface by polishing and lubricating the inboard surface. Although these techniques did tend to reduce the amount of Coloumb damping, the addition of the lubricating oil may have added viscous damping effects to the model. Also, viscous damping effects may have resulted from air resistance. This is a cause for concern because air resistance acts over the whole model, and can not be modeled as having a single point of application for the viscous force.

Viscous damping, unlike Coulomb damping, tends to slow the frequency of oscillation and this can help explain why the frequency of oscillation for the simulation is slightly higher then that of the experiment. An approximate damping coefficient was calculated based on the frequency found for the experimental trial to be $\zeta = 0.219$,

as shown in Appendix D. The exponential decay predicted by this damping ratio was plotted against the experimental data and is shown below in Figure 4.24, which shows that the estimation of the damping ratio was reasonable. Using the damping coefficient and the natural frequency of the simulation, found in Section 4.3.3, a simulation with equivalent damping would have a damped frequency of $\omega_d = 2.316\ Hz$. This damped frequency is very close to the experimental frequency calculated.

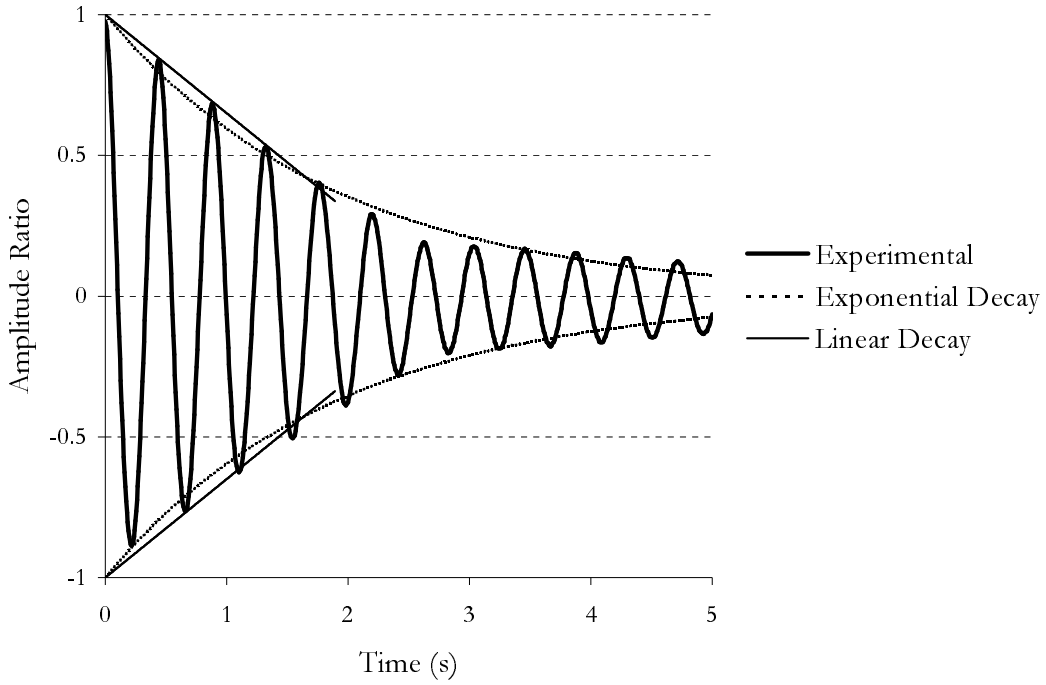


Figure 4.24: Estimation of Damping in the Experimental Data

## 4.5 Other Sources of Error

One notable source of error, other then damping effects, in the experimental trial was found to be from the body fixed marker wires. Although the wires were fairly light and were supported by a vertical post on the testing board, they tended to sway back and forth throughout the trial, essentially creating an additional forcing function acting on the outboard body. With no way of quantifying this forcing function, the simulation did not include the effects of the wire sway. Adding a forcing function to the model would change both the amplitude and frequency of the system response.

Another source of error is that the mass of the springs was neglected in the calculation of the total mass and inertia matrix. Initially the outboard body was treated as a single rigid body; however, after reviewing the experimental results the effects of the additional mass of the springs was considered. An approximation for the natural frequency of a system that includes mass of springs is given by the following equation [26],

$$\omega_{n_s} = \sqrt{\frac{K_{eqv}}{M + \frac{M_s}{3}}} \tag{4.1}$$

Where $K_{eqv}$ is the equivalent stiffness, $M$ is the mass of the system without considering the springs, and $M_s$ is the mass of the spring.

The equivalent stiffness term was estimated by the following,

$$K_{eqv} = {\omega_n}^2 M \tag{4.2}$$

Combining equations 4.1 and 4.2, the approximate natural frequency with spring masses for the simulated system was calculated to be $\omega_{n_s} = 2.317Hz$. This frequency is comparable to that of the experimental data and as such, the mass of the springs should be incorporated into the into the simulation.

# Chapter 5

# Conclusions and Recommendations

## 5.1 Conclusions

As discussed in the research outline, the two main goals of this project were to: develop a new special case computer simulation for the three dimensional dynamic equations of motion of a five degree of freedom point contact joint and validate the simulation with data collected from a physical model. The equations of motion were derived using Kane's method in order to allow for efficient computer implementation. A potential application of this research is in the area of biomechanical knee joint models.

In order to validate the computer simulation, an operational physical model was required. The system was designed to provide stable articulation over large angles. Sphere in sphere contact was used: a smaller outboard body articulates within a larger spherical cutout (inboard body) in both a rolling (rotational) and sliding (translational) manner. The spherical contact surface greatly simplifies the computer simulation model. Springs were added to the system to provide stability by connecting the outboard body to ground.

The first task was broken down into two stages: two dimensional planar modeling and three dimensional modeling. In the first stage, a two dimensional planar point contact joint was modeled. The equations of motion were derived using both Kane's approach and the Lagrangian method. The results from the two simulations agreed exactly,

within the tolerances of the integrator used, indicating that the Kane's model was predicting accurate system dynamics. The total energy of the system was predicted using both simulations and under ideal conditions, each method was found to maintain constant energy, further strengthening the proof of the functionality of the Kane's model.

In the next computer modeling stage, the simulation was expanded to three dimensions. Five rotational degrees of freedom were assigned and the fully non-linear dynamic equations of motion were derived for the system using the Kane's approach. Six coordinate systems were assigned to the model - the most important being the ground fixed system, $(\vec{i}_0, \vec{j}_0, \vec{k}_0)$, and the body fixed system, $(\vec{i}_5, \vec{j}_5, \vec{k}_5)$. The equations of motion were integrated using a fourth/fifth order, variable time step Runge-Kutta integrator to yield a numerical solution for the system. The positions of four markers, located on the outboard body of the system, were predicted in ground fixed coordinates by the solution routine.

The second goal of this research was to validate the three dimensional computer simulation with data collected from a physical system. No experimental validations are known to exist for spatial higher order pairs at this time, so reaching the objectives in this phase was very important. A physical model of the system was constructed and analysis of the motions of the joint was performed. Position locations of four markers located on the outboard body were captured during the physical testing through the implementation of the Optotrak 3020 motion tracking system (Northern Digital) [24]. A ground fixed coordinate system was also identified by monitoring four ground fixed markers. The positions of four markers on the outboard body were transformed into the ground fixed coordinate system and the results were compared to those obtained through the computer implementation.

Both static and dynamic trials were performed and compared to the simulation. The equilibrium position of the computer system was found by adding damping to the system to determine where it would naturally come to rest. Under arbitrary initial conditions, the system settled at the following set of angles $x(1) = 4.2°$, $x(2) = -5.8°$, $x(3) = 176.0°$, $x(4) = -5.5°$, and $x(5) = 0.8°$. These angles were then used in the undamped simulation and the results closely matched those obtained from a static

experimental trial. Another method, the Newton-Raphson technique, was also used to determine the initial conditions of the equilibrium position. The following set of angles were obtained, $x(1) = 0.23°$, $x(2) = 9.3°$, $x(3) = 179.7°$, $x(4) = 8.7°$, and $x(5) = 1.8°$. These results were not found to provide a stable equilibrium in the computer implementation. This identified an important problem with determining the initial conditions for the five degree of freedom system: due to the non-linear equations of motion multiple angle set may be attainable for a desired marker position solution. Although this was identified as a problem, the Newton-Raphson iterative process was the only way to determine the initial conditions for the dynamic test trials.

The dynamic test trial with the largest amplitudes of motion, Trial 5, was selected for comparison to the computer simulation. The following initial angles were predicted by the Newton-Raphson method for this trial: $x(1) = -20.5°$, $x(2) = 17.3°$, $x(3) = 186.5°$, $x(4) = 16.2°$, and $x(5) = 2.7°$. In comparing the computer simulation to the experimental results, a very close match was found. The initial response of the markers in the x, y and z directions were found to agree and the relative amplitude of motion was comparable for the x and y directions, especially during the first few seconds before viscous damping begins to dominate the experimental model. The amplitude of motion of the z position of the marker was found to be overestimated by the simulation, potentially due to slightly incorrect initial conditions. Trial 5 was dominated by motion in the y direction so the frequency of oscillation in this direction was considered. The experimental data frequency of oscillation was found to be $\omega_e = 2.33\ Hz$ and the simulation frequency was found to be $\omega_s = 2.37\ Hz$. Several sources for the discrepancies include viscous damping, a possible additional forcing function caused by lead wire sway, and neglecting the mass of the systems springs. Coulomb damping was included in the simulation.

The results indicate that the fundamental dynamics of the system are being accurately predicted by the computer simulation, but several additional factors, such as viscous damping and spring masses, may need to be added to the simulation in order to increase the accuracy.

## 5.2 Recommendations

The following items should be addressed in order to increase the accuracy of the computer simulation.

The method used to determine the initial conditions needs to be reconsidered as currently there are discrepancies as shown the prediction of the equilibrium position. This issue is much more complex then originally thought and a separate project should be devoted to research methods of predicting solution sets for non-linear equations, given desired outcomes.

Another point to consider is the implementation of viscous forces in the computer simulation. Without a known point of application, this problem proves to be difficult to address and may require the combination of fluid mechanics and aerodynamics specialists, to help model the viscous forces of the lubrication film and air resistance.

While the optical measuring system was very accurate, the outboard body marker wire sway was found to be quite significant and could have unknown effects on the experimental data. To avoid having to model this in the computer simulation, the implementation of wireless sensors should be considered.

Lastly, it is important to consider the next step in the progression of this project for the potential use in biomechanical knee models: introducing a new contact surface with a changing radius of curvature. This new contact surface will undoubtedly introduce many new challenges and it is recommended that a two dimensional model first be considered. Computer simulation, along with experimental validation will ensure that accurate system dynamics are being predicted.

# References


[1] E. M. Abdel-Rahman and M. S. Hefzy. Three Dimensional Dynamic Behaviour of the Human Knee Joint Under Impact Loading. *Medical Engineering and Physics*, 20(4):276–290, June 1998.

[2] R. J. Anderson. The Practice of Engineering Dynamics: Mech 821 Course Notes. Queen's University, 2003.

[3] Y. Bei. *Dynamic Simulation of Knee Joint Contact During Human Motion*. PhD thesis, University of Florida - Department of Mechanical and Aerospace Engineering, Gainesville, Florida, 2003.

[4] Y. Bei and B. J. Fregly. Multibody Dynamic Simulation of Knee Contact Mechanics. *Medical Engineering and Physics*, 26(9):777–789, November 2004.

[5] L. Blankevoort, J. H. Kuiper, R. Huiskes, and H. J. Grootenboer. Articular Contact in a Three Dimensionional Model of the Knee. *Journal of Biomechanics*, 24(11):1019–1031, 1991.

[6] D. I. Caruntu and M. S. Hefzy. 3-D Anatomically Based Dynamic Modeling of the Human Knee Joint to Include Tibio-Femoral and Patello-Femoral Joints. *Journal of Biomechanical Engineering*, 126(1):44–54, February 2004.

[7] S. L. Delp, F. C. Anderson, A. S. Arnold, P. Loan, A. Habib, T. J. Chand, E. Guendelman, and D.G. Thelen. Opensim: Open-source Software to Create and Analyze Dynamic Simulations of Movement. *IEEE Transactions on Biomedical Engineering*, In Press.

[8] Elite Consulting. PRO/Mechanica Motion. [Online], 2007. Available from: $\langle http://www.elite-consulting.com/\rangle$ [Accessed March 2007].

[9] J. R. Essinger, P. F. Leyvraz, J. H. Heegard, and D. D. Robertson. A Mathmatical Model for the Evaluation of the Behaviour During Flexion of Condylar-Type Knee Prostheses. *Journal of Biomechanics*, 22(11/12):1019–1241, 1989.

[10] V. L. Giddings, S. M. Kurtz, and A. A. Edidin. Total Knee Replacement Polyethylene Stresses During Loading in a Knee Simulator. *Journal of Tribology*, 123(4):842–847, October 2001.

[11] A. C. Goedest, M. Beaugonin, E. Haug, M. Taylor, and P. J. Gregson. Simulation of a Knee Joint Replacement During a Gait Cycle Using Explicit Finite Element Analysis. *Journal of Biomechanics*, 35(2):267–275, February 2002.

[12] J. P. Halloran, A. J. Petrella, and P. J. Rullkoetter. Explicit Finite Element Modeling of Total Knee Replacement Mechanics. *Journal of Biomechanics*, 38(2):323–331, February 2005.

[13] M. S. Hefzy and T. D. C. Cooke. Review of Knee Models: 1996 Update. *Applied Mechanics Reviews*, 49(10: Part 2):S187–S193, October 1996.

[14] M. S. Hefzy and E. S. Grood. Review of Knee Models. *Applied Mechanics Reviews*, 41(1):1–13, January 1988.

[15] T. R. Kane and Levinson D. A. *Dynamics: Theory and Applications*. McGraw-Hill Book Company, New York, New York, 1985.

[16] J. D. Kempson. Two Spheres: A Higher Pair Joint Formulation Using Kane's Equation. Master's thesis, Queen's University - Department of Mechanical and Materials Engineering, Kingston, Ontario, 2006.

[17] P. K. Levangie. *Joint Structure and Function: A Comprensive Analysis 4th Edition*. F.A. Davis Company, Philadelphia, Pennsylvania, 2005.

[18] LSDYNA:. 3D User's Manual. Technical report, Livermore Software Technology Corporation, Livermore, California, 1995.

[19] J. L. Meriam and Kraige L. G. *Engineering Mechanics Volume 2 Dynamics - Fifth Edition*. John Wiley and Sons, Incorperated, New York, New York, 2003.

[20] Micromeasure II+ and III:. Software Manual. Technical report, Brown and Sharpe Mfg. Co., North Kingstown, Rhode Island, 1994.

[21] M. H. Moeinzadeh, A. E. Engin, and N. Akkas. Two Dimensional Dynamic Modelling of Human Knee Joint. *Journal of Biomechanics*, 16(4):253–264, 1983.

[22] MSC. ADAMS: User's Manual. Technical report, MSC Software Corporation, Santa Ana, California, 2005.

[23] Musculographics Inc. SIMM and the Dynamics Pipeline. [Online], 2007. Available from: $\langle http://www.musculographics.com/\rangle$ [Accessed February 2007].

[24] Opototrak. 3020: System Guide. Technical report, Northern Digital Inc., Waterloo, Ontario, 1994.

[25] S. J. Piazza and S. L. Delp. Three Dimensional Dynamic Simulation of Total Knee Replacement Motion During a Step-Up Task. *Journal of Biomechanical Engineering*, 123(6):599–606, December 2001.

[26] S. S. Rao. *Mechanical Vibrations - Fourth Edition*. Pearson Eduation, Incorperated, Upper Saddle River, New Jersey, 2004.

[27] B. H. Tongue. *Principles of Vibrations - Second Edition*. Oxford University Press, New York, New York, 2002.

[28] J. Wismans, F. Veldpaus, and J. Janssen. A Three Dimensionional Mathmatical Model of the Knee Joint. *Journal of Biomechanics*, 13(8):677–685, 1980.

[29] U. P. Wyss. Mech 491: Design of Biomechanical Devices. Queen's University, 2005.

[30] Zimmer Product Website. Knee Replacements. [Online], 2007. Available from: $\langle http://www.zimmer.com\rangle$ [Accessed August 2007].

# Appendix A

# Two Dimensional Lagrange Model

The Lagrange equations of motion are based on energy and are of the form [2],

$$\frac{d}{dt}\left(\frac{\partial T}{\partial \dot{q}}\right) - \frac{\partial T}{\partial\ q} + \frac{\partial U}{\partial\ q} = Q_q \tag{A.1}$$

The kinetic energy term, T, is given by the following,

$$T = \frac{1}{2} m \vec{v}_{G2} \cdot \vec{v}_{G2} + \frac{1}{2} I_{G2} \vec{\omega_2} \cdot \vec{\omega_2} \tag{A.2}$$

By simplifying the velocity of the center of mass of the outboard body calculated in equation 2.42 and substituting the absolute angular velocity calculated in equation 2.29, the kinetic energy term becomes,

$$\begin{aligned} T &= \frac{1}{2} m x(3)^2 \left(RA - RB\right)^2 - mbx(3)^2 \left(RA - RB\right) \cos x(2) \\ &- mbx(3)x(4) \left(RA - RB\right) \cos x(2) + mb^2 \left(x(3) + x(4)\right)^2 \\ &+ I_{G2} \left(x(3) + x(4)\right)^2 \end{aligned} \tag{A.3}$$

The model has two contributors to the potential energy term, U: gravitational potential, $U_g$, and elastic potential, $U_e$. The gravitational potential term requires the change in height of the center of mass of the outboard body with respect to a fixed

datum. The center of rotation of the inboard body was selected to be the datum, and the position to the outboard body center of mass is given by the following,

$$\vec{P}_{G2} = \vec{R1}^{T} \begin{Bmatrix} \hat{i_0} \\ \hat{j_0} \\ \hat{k_0} \end{Bmatrix} - \vec{R2}^{T} [TT] \begin{Bmatrix} \hat{i_0} \\ \hat{j_0} \\ \hat{k_0} \end{Bmatrix} - \vec{B}^{T} [TT] \begin{Bmatrix} \hat{i_0} \\ \hat{j_0} \\ \hat{k_0} \end{Bmatrix} \tag{A.4}$$

This simplifies to the following,

$$\begin{aligned} \vec{P}_{G2} &= [(RA - RB)\cos x(1) - b\cos x(1)\cos x(2) + b\sin x(1)\sin x(2)]\,\vec{i_0} \\ &+ [(RA - RB)\sin x(1) - b\sin x(1)\cos x(2) - b\cos x(1)\sin x(2)]\,\vec{j_0} \end{aligned} \tag{A.5}$$

Therefore, the gravitational potential energy is given by,

$$U_g = mg(RA - RB)\cos x(1) - mgb\cos x(1)\cos x(2) + mgb\sin x(1)\sin x(2) \tag{A.6}$$

The elastic potential energy depends on the deflections of the springs in the systems. The elastic potential energy is given by the following,

$$U_e = \frac{1}{2}K_E\delta_E^2 + \frac{1}{2}K_F\delta_F^2 \tag{A.7}$$

Since the dependence on the generalized coordinates is not apparent in the above equation, the spring deflections were separated as given by equations 2.87 and 2.88.

$$\begin{aligned} U_e &= \frac{1}{2}K_E\left({P_{ED_x}}^2 + {P_{ED_y}}^2\right) - \frac{1}{2}K_E ED\sqrt{{P_{ED_x}}^2 + {P_{ED_y}}^2} + \frac{1}{2}K_E\,(ED)^2 \\ &+ \frac{1}{2}K_F\left({P_{FD_x}}^2 + {P_{FD_y}}^2\right)^2 - \frac{1}{2}K_F FD\sqrt{{P_{FD_x}}^2 + {P_{FD_y}}^2} + \frac{1}{2}K_{EF}\,(FD)^2 \end{aligned} \tag{A.8}$$

where:

$$P_{ED_x} = -LE_x + (RA - RB)\cos x(1) - b\cos(x(1) + x(2)) + d\cos(x(1) + x(2))$$

$$P_{ED_y} = -LE_y + (RA - RB)\sin x(1) - b\sin(x(1) + x(2)) + d\sin(x(1) + x(2))$$

$$P_{FD_x} = -LF_x + (RA - RB)\cos x(1) - b\cos(x(1) + x(2)) + d\cos(x(1) + x(2))$$

$$P_{FD_y} = -LF_y + (RA - RB)\sin x(1) - b\sin(x(1) + x(2)) + d\sin(x(1) + x(2))$$

At this point Lagrange's Equation can be applied to the model. The configuration coordinates are the same as for the Kane's formulation, x(1) and x(2), and the first derivatives are given by x(3) and x(4), respectively. For the first configuration coordinate, applying equation A.1 yields the following,

$$\begin{aligned} \frac{\partial T}{\partial x(3)} &= mx(3)\left(RA - RB\right)^2 - 2mbx(3)\left(RA - RB\right)\cos x(2) \\ &+ -mbx(4)\left(RA - RB\right)\cos x(2) + mb^2\left(x(3) + x(4)\right) \\ &+ I_{G2}\left(x(3) + x(4)\right) \end{aligned} \tag{A.9}$$

$$\begin{aligned} \frac{d}{dt}\left(\frac{\partial T}{\partial x(3)}\right) &= m\dot{x}(3)\left(RA - RB\right)^2 + 2mbx(3)x(4)\left(RA - RB\right)\sin x(2) \\ &- 2mb\dot{x}(3)\left(RA - RB\right)\cos x(2) + mbx(4)^2\left(RA - RB\right)\sin x(2) \\ &- mb\dot{x}(4)\left(RA - RB\right)\cos x(2) + mb^2\left(\dot{x}(3) + \dot{x}(4)\right) + I_{G2}\left(\dot{x}(3) + \dot{x}(4)\right) \end{aligned} \tag{A.10}$$

$$\frac{\partial T}{\partial x(1)} = 0 \tag{A.11}$$

$$\frac{\partial U_g}{\partial x(1)} = -mg(RA - RB)\sin x(1) + mgb\sin x(1)\cos x(2) + mgb\cos x(1)\sin x(2) \tag{A.12}$$

$$\begin{aligned}\frac{\partial U_e}{\partial x(1)} &= K_E P_{ED_x}\frac{\partial P_{ED_x}}{\partial x(1)} + K_E P_{ED_y}\frac{\partial P_{ED_y}}{\partial x(1)} \\ &- \frac{K_E ED}{\sqrt{{P_{ED_x}}^2 + {P_{ED_y}}^2}}\left(\frac{\partial P_{ED_x}}{\partial x(1)} + \frac{\partial P_{ED_y}}{\partial x(1)}\right) \\ &+ K_F P_{FD_x}\frac{\partial P_{FD_x}}{\partial x(1)} + K_F P_{FD_x}\frac{\partial P_{FD_y}}{\partial x(1)} \\ &- \frac{K_F FD}{\sqrt{{P_{FD_x}}^2 + {P_{FD_y}}^2}}\left(\frac{\partial P_{FD_x}}{\partial x(1)} + \frac{\partial P_{FD_y}}{\partial x(1)}\right)\end{aligned} \tag{A.13}$$

where:

$$\frac{\partial P_{ED_x}}{\partial x(1)} = -(RA - RB)\sin x(1) + b\sin\left(x(1) + x(2)\right) - d\sin\left(x(1) + x(2)\right)$$

$$\frac{\partial P_{ED_y}}{\partial x(1)} = (RA - RB)\cos x(1) - b\cos\left(x(1) + x(2)\right) + d\cos\left(x(1) + x(2)\right)$$

$$\frac{\partial P_{FD_x}}{\partial x(1)} = -(RA - RB)\sin x(1) + b\sin\left(x(1) + x(2)\right) - d\sin\left(x(1) + x(2)\right)$$

$$\frac{\partial P_{FD_y}}{\partial x(1)} = (RA - RB)\cos x(1) - b\cos\left(x(1) + x(2)\right) + d\cos\left(x(1) + x(2)\right)$$

Similarly, for the second configuration coordinate, applying equation A.1 yields the following,

$$\begin{aligned}\frac{\partial T}{\partial x(4)} &= -mbx(3)\left(RA - RB\right)\cos x(2) + mb^2\left(x(3) + x(4)\right) \\ &+ I_{G2}\left(x(3) + x(4)\right)\end{aligned} \tag{A.14}$$

$$\begin{aligned}\frac{d}{dt}\left(\frac{\partial T}{\partial x(4)}\right) &= mbx(3)x(4)^2\left(RA - RB\right)\sin x(2) \\ &- mb\dot{x}(3)\left(RA - RB\right)\cos x(2) \\ &+ mb^2\left(\dot{x}(3) + \dot{x}(4)\right) + I_{G2}\left(\dot{x}(3) + \dot{x}(4)\right)\end{aligned} \tag{A.15}$$

$$\begin{aligned}\frac{\partial T}{\partial x(2)} &= mb\left(x(3)\right)^2\left(RA-RB\right)\sin x(2) \\ &+ mbx(3)x(4)\left(RA-RB\right)\sin x(2)\end{aligned} \tag{A.16}$$

$$\frac{\partial U_g}{\partial x(2)} = mgb\cos x(1)\sin x(2) + mgb\sin x(1)\cos x(2) \tag{A.17}$$

$$\begin{aligned}\frac{\partial U_e}{\partial x(2)} &= K_E P_{ED_x}\frac{\partial P_{ED_x}}{\partial x(2)} + K_E P_{ED_y}\frac{\partial P_{ED_y}}{\partial x(2)} \\ &- \frac{K_E ED}{\sqrt{{P_{ED_x}}^2 + {P_{ED_y}}^2}}\left(\frac{\partial P_{ED_x}}{\partial x(2)} + \frac{\partial P_{ED_y}}{\partial x(2)}\right) \\ &+ K_F P_{FD_x}\frac{\partial P_{FD_x}}{\partial x(2)} + K_F P_{FD_x}\frac{\partial P_{FD_y}}{\partial x(2)} \\ &- \frac{K_F FD}{\sqrt{{P_{FD_x}}^2 + {P_{FD_y}}^2}}\left(\frac{\partial P_{FD_x}}{\partial x(2)} + \frac{\partial P_{FD_y}}{\partial x(2)}\right)\end{aligned} \tag{A.18}$$

where:

$$\frac{\partial P_{ED_x}}{\partial x(2)} = b\sin\left(x(1)+x(2)\right) - d\sin\left(x(1)+x(2)\right)$$

$$\frac{\partial P_{ED_y}}{\partial x(2)} = -b\cos\left(x(1)+x(2)\right) + d\cos\left(x(1)+x(2)\right)$$

$$\frac{\partial P_{FD_x}}{\partial x(2)} = b\sin\left(x(1)+x(2)\right) - d\sin\left(x(1)+x(2)\right)$$

$$\frac{\partial P_{FD_y}}{\partial x(2)} = -b\cos\left(x(1)+x(2)\right) + d\cos\left(x(1)+x(2)\right)$$

# Appendix B

# Three Dimensional Model Formulation

### Transformation Matrices

In this model it is desired to be able to transform both from ground fixed to body fixed coordinates and from body fixed to ground fixed coordinates. The transformation from ground fixed coordinates to body fixed coordinates requires five rotations. The rotation from the ground fixed coordinate system, $(\hat{i_0}, \hat{j_0}, \hat{k_0})$, to the intermediate coordinate system, $(\hat{i_1}, \hat{j_1}, \hat{k_1})$, is represented by the first configuration coordinate, $x(1)$. The transformation matrix from coordinate system $(\hat{i_0}, \hat{j_0}, \hat{k_0})$ to coordinate system $(\hat{i_1}, \hat{j_1}, \hat{k_1})$ is shown below.

$$\left[R_{x(1)}\right] = \begin{bmatrix} \cos x(1) & -\sin x(1) & 0 \\ \sin x(1) & \cos x(1) & 0 \\ 0 & 0 & 1 \end{bmatrix} \tag{B.1}$$

The rotation from the intermediate coordinate system, $(\hat{i_1}, \hat{j_1}, \hat{k_1})$, to the intermediate coordinate system, $(\hat{i_2}, \hat{j_2}, \hat{k_2})$, is represented by the second configuration coordinate, $x(2)$. The transformation matrix from coordinate system $(\hat{i_1}, \hat{j_1}, \hat{k_1})$ to coordinate system $(\hat{i_2}, \hat{j_2}, \hat{k_2})$ is shown below.

$$\left[R_{x(2)}\right] = \begin{bmatrix} \cos x(2) & 0 & \sin x(2) \\ 0 & 1 & 0 \\ -\sin x(2) & 0 & \cos x(2) \end{bmatrix} \tag{B.2}$$

The rotation from the intermediate coordinate system, $(\hat{i_2}, \hat{j_2}, \hat{k_2})$, to the intermediate coordinate system, $(\hat{i_3}, \hat{j_3}, \hat{k_3})$, is represented by the third configuration coordinate, $x(3)$. The transformation matrix from coordinate system $(\hat{i_2}, \hat{j_2}, \hat{k_2})$ to coordinate system $(\hat{i_3}, \hat{j_3}, \hat{k_3})$ is shown below.

$$\left[R_{x(3)}\right] = \begin{bmatrix} \cos x(3) & -\sin x(3) & 0 \\ \sin x(3) & \cos x(3) & 0 \\ 0 & 0 & 1 \end{bmatrix} \tag{B.3}$$

The rotation from the intermediate coordinate system, $(\hat{i_3}, \hat{j_3}, \hat{k_3})$, to the intermediate coordinate system, $(\hat{i_4}, \hat{j_4}, \hat{k_4})$, is represented by the fourth configuration coordinate, $x(4)$. The transformation matrix from coordinate system $(\hat{i_3}, \hat{j_3}, \hat{k_3})$ to coordinate system $(\hat{i_4}, \hat{j_4}, \hat{k_4})$ is shown below.

$$\left[R_{x(4)}\right] = \begin{bmatrix} \cos x(4) & 0 & \sin x(4) \\ 0 & 1 & 0 \\ -\sin x(4) & 0 & \cos x(4) \end{bmatrix} \tag{B.4}$$

The rotation from the intermediate coordinate system, $(\hat{i_4}, \hat{j_4}, \hat{k_4})$, to the body fixed coordinate system, $(\hat{i_5}, \hat{j_5}, \hat{k_5})$, is represented by the fifth configuration coordinate, $x(5)$. The transformation matrix from coordinate system $(\hat{i_4}, \hat{j_4}, \hat{k_4})$ to coordinate system $(\hat{i_5}, \hat{j_5}, \hat{k_5})$ is shown below.

$$\left[R_{x(5)}\right] = \begin{bmatrix} 1 & 0 & 0 \\ 0 & \cos x(5) & -\sin x(5) \\ 0 & \sin x(5) & \cos x(5) \end{bmatrix} = [T1] \tag{B.5}$$

The transformation matrix from the intermediate coordinate system, $(\hat{i_3}, \hat{j_3}, \hat{k_3})$, to the body fixed coordinate system is given by the following,

$$[T2] = \left[R_{x(4)}\right]\left[R_{x(5)}\right] \tag{B.6}$$

The transformation matrix from the intermediate coordinate system, $(\hat{i_2}, \hat{j_2}, \hat{k_2})$, to the body fixed coordinate system is given by the following,

$$[T3] = \left[R_{x(3)}\right]\left[R_{x(4)}\right]\left[R_{x(5)}\right] \tag{B.7}$$

The transformation matrix from the intermediate coordinate system, $(\hat{i_1}, \hat{j_1}, \hat{k_1})$, to the body fixed coordinate system is given by the following,

$$[T4] = \left[R_{x(2)}\right]\left[R_{x(3)}\right]\left[R_{x(4)}\right]\left[R_{x(5)}\right] \tag{B.8}$$

The transformation matrix from the ground fixed coordinate system to the body fixed coordinate system is given by the following,

$$[T5] = \left[R_{x(1)}\right]\left[R_{x(2)}\right]\left[R_{x(3)}\right]\left[R_{x(4)}\right]\left[R_{x(5)}\right] \tag{B.9}$$

The transformation from body fixed coordinates to ground fixed coordinates also requires five rotations. The rotation from the body fixed coordinate system, $(\hat{i_5}, \hat{j_5}, \hat{k_5})$, to the intermediate coordinate system, $(\hat{i_4}, \hat{j_4}, \hat{k_4})$, is represented by a clockwise rotation of the fifth configuration coordinate, $x(5)$. The transformation matrix from coordinate system $(\hat{i_5}, \hat{j_5}, \hat{k_5})$ to coordinate system $(\hat{i_4}, \hat{j_4}, \hat{k_4})$ is shown below.

$$\left[TR_{x(5)}\right] = \begin{bmatrix} 1 & 0 & 0 \\ 0 & \cos x(5) & \sin x(5) \\ 0 & -\sin x(5) & \cos x(5) \end{bmatrix} \tag{B.10}$$

The rotation from the intermediate coordinate system, $(\hat{i_4}, \hat{j_4}, k4)$, to the intermediate coordinate system, $(\hat{i_3}, \hat{j_3}, \hat{k_3})$, is represented by a clockwise rotation of the fourth configuration coordinate, $x(4)$. The transformation matrix from coordinate system $(\hat{i_4}, \hat{j_4}, \hat{k_4})$ to coordinate system $(\hat{i_3}, \hat{j_3}, \hat{k_3})$ is shown below.

$$\left[TR_{x(4)}\right] = \begin{bmatrix} \cos x(4) & 0 & -\sin x(4) \\ 0 & 1 & 0 \\ \sin x(4) & 0 & \cos x(4) \end{bmatrix} \tag{B.11}$$

The rotation from the intermediate coordinate system, $(\hat{i_3}, \hat{j_3}, \hat{k_3})$, to the intermediate coordinate system, $(\hat{i_2}, \hat{j_2}, \hat{k_2})$, is represented by a clockwise rotation of the third configuration coordinate, $x(3)$. The transformation matrix from coordinate system $(\hat{i_3}, \hat{j_3}, \hat{k_3})$ to coordinate system $(\hat{i_2}, \hat{j_2}, \hat{k_2})$ is shown below.

$$\left[TR_{x(3)}\right] = \begin{bmatrix} \cos x(3) & \sin x(3) & 0 \\ -\sin x(3) & \cos x(3) & 0 \\ 0 & 0 & 1 \end{bmatrix} \tag{B.12}$$

The rotation from the intermediate coordinate system, $(\hat{i_2}, \hat{j_2}, \hat{k_2})$, to the intermediate coordinate system, $(\hat{i_1}, \hat{j_1}, \hat{k_1})$, is represented by a clockwise rotation of the second configuration coordinate, $x(2)$. The transformation matrix from coordinate system $(\hat{i_2}, \hat{j_2}, \hat{k_2})$ to coordinate system $(\hat{i_1}, \hat{j_1}, \hat{k_1})$ is shown below.

$$\left[TR_{x(2)}\right] = \begin{bmatrix} \cos x(2) & 0 & -\sin x(2) \\ 0 & 1 & 0 \\ \sin x(2) & 0 & \cos x(2) \end{bmatrix} \tag{B.13}$$

The rotation from the intermediate coordinate system, $(\hat{i_1}, \hat{j_1}, \hat{k_1})$, to the ground fixed coordinate system, $(\hat{i_0}, \hat{j_0}, \hat{k_0})$, is represented by a clockwise rotation of the first configuration coordinate, $x(1)$. The transformation matrix from coordinate system $(\hat{i_1}, \hat{j_1}, \hat{k_1})$ to coordinate system $(\hat{i_0}, \hat{j_0}, \hat{k_0})$ is shown below.

$$\left[TR_{x(1)}\right] = \begin{bmatrix} \cos x(1) & \sin x(1) & 0 \\ -\sin x(1) & \cos x(1) & 0 \\ 0 & 0 & 1 \end{bmatrix} \tag{B.14}$$

The transformation matrix from the body fixed coordinate system to the ground fixed coordinate system is given by the following,

$$[TT] = \left[TR_{x(5)}\right]\left[TR_{x(4)}\right]\left[TR_{x(3)}\right]\left[TR_{x(2)}\right]\left[TR_{x(1)}\right] \tag{B.15}$$

It is also important to note at this point that matrices, $[\dot{T1}]$, $[\dot{T1}]$, $[\dot{T2}]$, $[\dot{T3}]$, $[\dot{T4}]$, and $[\dot{T5}]$, will be needed for the three dimensional analysis. By differentiating the expression for $[T1]$ in equation B.5 with respect to time, the following results,

$$\frac{d\,[T1]}{dt} = \left[\dot{R_{x(5)}}\right] \tag{B.16}$$

The matrix $\left[\dot{R_{x(5)}}\right]$ is found by differentiating the matrix $\left[R_{x(5)}\right]$, equation B.5, with respect to time as follows,

$$\left[\dot{R_{x(5)}}\right] = \begin{bmatrix} 0 & 0 & 0 \\ 0 & -x(10)\sin x(5) & -x(10)\cos x(5) \\ 0 & x(10)\cos x(5) & -x(10)\sin x(5) \end{bmatrix} = [\dot{T1}] \tag{B.17}$$

By differentiating the expression for $[T2]$ in equation B.6 with respect to time, the following results,

$$\frac{d\,[T2]}{dt} = \left[\dot{R_{x(4)}}\right]\left[R_{x(5)}\right] + \left[R_{x(4)}\right]\left[\dot{R_{x(5)}}\right] \tag{B.18}$$

The matrix $\left[\dot{R_{x(4)}}\right]$ is found by differentiating the matrix $\left[R_{x(4)}\right]$, equation B.4, with respect to time as follows,

$$\left[\dot{R_{x(4)}}\right] = \begin{bmatrix} -x(9)\sin x(4) & 0 & x(9)\cos x(4) \\ 0 & 0 & 0 \\ -x(9)\cos x(4) & 0 & -x(9)\sin x(4) \end{bmatrix} \tag{B.19}$$

By differentiating the expression for $[T3]$ in equation B.7 with respect to time, the following results,

$$\frac{d\,[T3]}{dt} = \left[\dot{R_{x(3)}}\right]\left[R_{x(4)}\right]\left[R_{x(5)}\right] + \left[R_{x(3)}\right]\left[\dot{R_{x(4)}}\right]\left[R_{x(5)}\right] + \left[R_{x(3)}\right]\left[R_{x(4)}\right]\left[\dot{R_{x(5)}}\right] \tag{B.20}$$

The matrix $\left[\dot{R_{x(3)}}\right]$ is found by differentiating the matrix $\left[R_{x(3)}\right]$, equation B.3, with respect to time as follows,

$$\left[\dot{R_{x(3)}}\right] = \begin{bmatrix} -x(8)\sin x(3) & -x(8)\cos x(3) & 0 \\ x(8)\cos x(3) & -x(8)\sin x(3) & 0 \\ 0 & 0 & 0 \end{bmatrix} \tag{B.21}$$

By differentiating the expression for $[T4]$ in equation B.8 with respect to time, the following results,

$$\begin{aligned} \frac{d\,[T4]}{dt} = &\left[\dot{R_{x(2)}}\right]\left[R_{x(3)}\right]\left[R_{x(4)}\right]\left[R_{x(5)}\right] + \left[R_{x(2)}\right]\left[\dot{R_{x(3)}}\right]\left[R_{x(4)}\right]\left[R_{x(5)}\right] \\ &+ \left[R_{x(2)}\right]\left[R_{x(3)}\right]\left[\dot{R_{x(4)}}\right]\left[R_{x(5)}\right] + \left[R_{x(2)}\right]\left[R_{x(3)}\right]\left[R_{x(4)}\right]\left[\dot{R_{x(5)}}\right] \end{aligned} \tag{B.22}$$

By differentiating the expression for $[T5]$ in equation B.9 with respect to time, the following results,

$$\begin{aligned} \frac{d\,[T5]}{dt} = &\left[\dot{R_{x(1)}}\right]\left[R_{x(2)}\right]\left[R_{x(3)}\right]\left[R_{x(4)}\right]\left[R_{x(5)}\right] + \left[R_{x(1)}\right]\left[\dot{R_{x(2)}}\right]\left[R_{x(3)}\right]\left[R_{x(4)}\right]\left[R_{x(5)}\right] \\ &+ \left[R_{x(1)}\right]\left[R_{x(2)}\right]\left[\dot{R_{x(3)}}\right]\left[R_{x(4)}\right]\left[R_{x(5)}\right] + \left[R_{x(1)}\right]\left[R_{x(2)}\right]\left[R_{x(3)}\right]\left[\dot{R_{x(4)}}\right]\left[R_{x(5)}\right] \\ &+ \left[R_{x(1)}\right]\left[R_{x(2)}\right]\left[R_{x(3)}\right]\left[R_{x(4)}\right]\left[\dot{R_{x(5)}}\right] \end{aligned} \tag{B.23}$$

**Absolute Angular Velocity of Outboard Body**

The angular velocity of the outboard body is represented by the following equation.

$$\vec{\omega}_2 = \left\{ \begin{array}{ccc} 0 & 0 & x(6) \end{array} \right\} \left\{ \begin{array}{c} \hat{i_0} \\ \hat{j_0} \\ \hat{k_0} \end{array} \right\} + \left\{ \begin{array}{ccc} 0 & x(7) & 0 \end{array} \right\} \left\{ \begin{array}{c} \hat{i_1} \\ \hat{j_1} \\ \hat{k_1} \end{array} \right\}$$
$$+ \left\{ \begin{array}{ccc} 0 & 0 & x(8) \end{array} \right\} \left\{ \begin{array}{c} \hat{i_2} \\ \hat{j_2} \\ \hat{k_2} \end{array} \right\} + \left\{ \begin{array}{ccc} 0 & x(9) & 0 \end{array} \right\} \left\{ \begin{array}{c} \hat{i_3} \\ \hat{j_3} \\ \hat{k_3} \end{array} \right\}$$
$$+ \left\{ \begin{array}{ccc} x(10) & 0 & 0 \end{array} \right\} \left\{ \begin{array}{c} \hat{i_4} \\ \hat{j_4} \\ \hat{k_4} \end{array} \right\} \quad \text{(B.24)}$$

The angular velocity must be represented in one coordinate system, so each of the terms in equation B.24 must be converted to body fixed, $\hat{i_5}, \hat{j_5}, \hat{k_5}$, coordinates.

$$\vec{\omega}_2 = \left\{ \begin{array}{ccc} 0 & 0 & x(6) \end{array} \right\} [T5] \left\{ \begin{array}{c} \hat{i_5} \\ \hat{j_5} \\ \hat{k_5} \end{array} \right\} + \left\{ \begin{array}{ccc} 0 & x(7) & 0 \end{array} \right\} [T4] \left\{ \begin{array}{c} \hat{i_5} \\ \hat{j_5} \\ \hat{k_5} \end{array} \right\}$$
$$+ \left\{ \begin{array}{ccc} 0 & 0 & x(8) \end{array} \right\} [T3] \left\{ \begin{array}{c} \hat{i_5} \\ \hat{j_5} \\ \hat{k_5} \end{array} \right\} + \left\{ \begin{array}{ccc} 0 & x(9) & 0 \end{array} \right\} [T2] \left\{ \begin{array}{c} \hat{i_5} \\ \hat{j_5} \\ \hat{k_5} \end{array} \right\}$$
$$+ \left\{ \begin{array}{ccc} x(10) & 0 & 0 \end{array} \right\} [T1] \left\{ \begin{array}{c} \hat{i_5} \\ \hat{j_5} \\ \hat{k_5} \end{array} \right\} \quad \text{(B.25)}$$

It is important to note that the angular velocity represented by equation B.25 is in the body fixed coordinate system $(\hat{i_5}, \hat{j_5}, \hat{k_5})$. Thus, the angular velocity of the fifth coordinate system, $\vec{\omega}_{CS}$, is equal to the angular velocity of the outboard body, $\vec{\omega}_2$.

### Angular Acceleration

The angular acceleration of the outboard body is found by differentiating the angular velocity, equation B.25, with respect to time.

$$\vec{\alpha}_2 = \frac{d}{dt}\vec{\omega}_2 \tag{B.26}$$

$$\vec{\alpha}_2 = \dot{\vec{\omega}}_2 + \vec{\omega}_{CS} \times \vec{\omega}_2 \tag{B.27}$$

Since the angular velocity of the coordinate system is equal to the angular velocity of the outboard body the second term of equation 2.31 is zero. The simplified equation for the angular acceleration is given by,

$$\begin{aligned}
\vec{\alpha}_2 = &\left\{ \begin{array}{ccc} 0 & 0 & \dot{x}(6) \end{array} \right\} [T5] \left\{ \begin{array}{c} \hat{i_5} \\ \hat{j_5} \\ \hat{k_5} \end{array} \right\} + \left\{ \begin{array}{ccc} 0 & 0 & x(6) \end{array} \right\} [\dot{T5}] \left\{ \begin{array}{c} \hat{i_5} \\ \hat{j_5} \\ \hat{k_5} \end{array} \right\} \\
&+ \left\{ \begin{array}{ccc} 0 & \dot{x}(7) & 0 \end{array} \right\} [T4] \left\{ \begin{array}{c} \hat{i_5} \\ \hat{j_5} \\ \hat{k_5} \end{array} \right\} + \left\{ \begin{array}{ccc} 0 & x(7) & 0 \end{array} \right\} [\dot{T4}] \left\{ \begin{array}{c} \hat{i_5} \\ \hat{j_5} \\ \hat{k_5} \end{array} \right\} \\
&+ \left\{ \begin{array}{ccc} 0 & 0 & \dot{x}(8) \end{array} \right\} [T3] \left\{ \begin{array}{c} \hat{i_5} \\ \hat{j_5} \\ \hat{k_5} \end{array} \right\} + \left\{ \begin{array}{ccc} 0 & 0 & x(8) \end{array} \right\} [\dot{T3}] \left\{ \begin{array}{c} \hat{i_5} \\ \hat{j_5} \\ \hat{k_5} \end{array} \right\} \\
&+ \left\{ \begin{array}{ccc} 0 & \dot{x}(9) & 0 \end{array} \right\} [T2] \left\{ \begin{array}{c} \hat{i_5} \\ \hat{j_5} \\ \hat{k_5} \end{array} \right\} + \left\{ \begin{array}{ccc} 0 & x(9) & 0 \end{array} \right\} [\dot{T2}] \left\{ \begin{array}{c} \hat{i_5} \\ \hat{j_5} \\ \hat{k_5} \end{array} \right\} \\
&+ \left\{ \begin{array}{ccc} \dot{x}(10) & 0 & 0 \end{array} \right\} [T1] \left\{ \begin{array}{c} \hat{i_5} \\ \hat{j_5} \\ \hat{k_5} \end{array} \right\} + \left\{ \begin{array}{ccc} x(10) & 0 & 0 \end{array} \right\} [\dot{T1}] \left\{ \begin{array}{c} \hat{i_5} \\ \hat{j_5} \\ \hat{k_5} \end{array} \right\}
\end{aligned} \tag{B.28}$$

**Position Vector**

The vector describing the position from the ground fixed origin to the center of mass of the outboard body is given by the following,

$$\vec{P}_{G2} = \vec{R1}^{T} \begin{Bmatrix} \hat{i_0} \\ \hat{j_0} \\ \hat{k_0} \end{Bmatrix} - \vec{R2}^{T} \begin{Bmatrix} \hat{i_5} \\ \hat{j_5} \\ \hat{k_5} \end{Bmatrix} - \vec{B}^{T} \begin{Bmatrix} \hat{i_5} \\ \hat{j_5} \\ \hat{k_5} \end{Bmatrix} \tag{B.29}$$

Since the above expression uses multiple coordinate systems, the component writing in the ground fixed system was transformed to the body fixed system by multiplying by the transformation matrix $[T5]$ derived earlier.

$$\vec{P}_{G2} = \vec{R1}^{T} [T5] \begin{Bmatrix} \hat{i_5} \\ \hat{j_5} \\ \hat{k_5} \end{Bmatrix} - \vec{R2}^{T} \begin{Bmatrix} \hat{i_5} \\ \hat{j_5} \\ \hat{k_5} \end{Bmatrix} - \vec{B}^{T} \begin{Bmatrix} \hat{i_5} \\ \hat{j_5} \\ \hat{k_5} \end{Bmatrix} \tag{B.30}$$

The radius vectors, $\vec{R1}$ and $\vec{R1}$, are both aligned in the $\hat{i_2}$ direction. The vector $\vec{R1}$ is defined in the ground fixed coordinate system to be,

$$\vec{R1} = \begin{Bmatrix} RA\cos x(1)\cos x(2) \\ RA\sin x(1)\cos x(2) \\ -RA\sin x(2) \end{Bmatrix} \tag{B.31}$$

The vector $\vec{R2}$ is defined in the body fixed coordinate system to be,

$$\vec{R2} = \begin{Bmatrix} RB\cos x(3)\cos x(4) \\ RB\cos x(3)\sin x(4)\sin x(5) - RB\sin x(3)\cos x(5) \\ RB\cos x(3)\sin x(4)\cos x(5) + RB\sin x(3)\sin x(5) \end{Bmatrix} \tag{B.32}$$

The vector $\vec{B}$ is defined in the body fixed coordinate system to be,

$$\vec{B} = \begin{Bmatrix} -b \\ 0 \\ 0 \end{Bmatrix} \tag{B.33}$$

It should be noted that $\vec{B}$ remains constant in the body fixed coordinate system for any point in time, while $\vec{R1}$ and $\vec{R2}$ change.

**Absolute Velocity**

The absolute velocity of the center of mass of the outboard body was found by differentiating the position vector with respect to time. In the body fixed coordinate system, the absolute velocity was found to be,

$$\vec{V}_{G2} = \dot{\vec{R}1}^T [T5] \begin{Bmatrix} \hat{i_5} \\ \hat{j_5} \\ \hat{k_5} \end{Bmatrix} - \dot{\vec{R}2}^T \begin{Bmatrix} \hat{i_5} \\ \hat{j_5} \\ \hat{k_5} \end{Bmatrix} + \vec{\omega}_2 \times \left[ -\vec{R2}^T \begin{Bmatrix} \hat{i_5} \\ \hat{j_5} \\ \hat{k_5} \end{Bmatrix} - \vec{B}^T \begin{Bmatrix} \hat{i_5} \\ \hat{j_5} \\ \hat{k_5} \end{Bmatrix} \right] \quad \text{(B.34)}$$

The vector $\dot{\vec{R}1}$ was found by differentiating $\vec{R}1$ with respect to time.

$$\begin{aligned} \dot{\vec{R}1}(1) =& -x(6)RA\sin x(1)\cos x(2) - x(7)RA\cos x(1)\sin x(2) \\ \dot{\vec{R}1}(2) =& x(6)RA\cos x(1)\cos x(2) - x(7)RA\sin x(1)\sin x(2) \\ \dot{\vec{R}1}(3) =& -x(7)RA\cos x(2) \end{aligned} \quad \text{(B.35)}$$

The vector $\dot{\vec{R}2}$ was found by differentiating $\vec{R}2$ with respect to time.

$$\begin{aligned} \dot{\vec{R}2}(1) =& -x(8)RB\sin x(3)\cos x(4) - x(9)RB\cos x(3)\sin x(4) \\ \dot{\vec{R}2}(2) =& -x(8)RB\sin x(3)\sin x(4)\sin x(5) + x(9)RB\cos x(3)\cos x(4)\sin x(5) \\ & + x(10)RB\cos x(3)\sin x(4)\cos x(5) - x(8)RB\cos x(3)\cos x(5) \\ & + x(10)RB\sin x(3)\sin x(5) \\ \dot{\vec{R}2}(3) =& -x(8)RB\sin x(3)\sin x(4)\cos x(5) + x(9)RB\cos x(3)\cos x(4)\cos x(5) \\ & - x(10)RB\cos x(3)\sin x(4)\sin x(5) + x(8)RB\cos x(3)\sin x(5) \\ & + x(10)RB\sin x(3)\cos x(5) \end{aligned} \quad \text{(B.36)}$$

**Absolute Acceleration**

The absolute acceleration vector of the center of mass of the outboard body, in body fixed coordinates, was determined by differentiating the velocity vector, equation B.34, with respect to time.

$$\begin{aligned}\vec{A}_{G2} = \ddot{\vec{R}}1^T\,[T5]\begin{Bmatrix}\hat{i_5}\\ \hat{j_5}\\ \hat{k_5}\end{Bmatrix} - \ddot{\vec{R}}2^T\begin{Bmatrix}\hat{i_5}\\ \hat{j_5}\\ \hat{k_5}\end{Bmatrix}\\ + \vec{\alpha}_2 \times \left[-\vec{R}2^T\begin{Bmatrix}\hat{i_5}\\ \hat{j_5}\\ \hat{k_5}\end{Bmatrix} - \vec{B}^T\begin{Bmatrix}\hat{i_5}\\ \hat{j_5}\\ \hat{k_5}\end{Bmatrix}\right] + 2\vec{\omega}_2 \times \left[-\dot{\vec{R}}2^T\begin{Bmatrix}\hat{i_5}\\ \hat{j_5}\\ \hat{k_5}\end{Bmatrix}\right]\\ + \vec{\omega}_2 \times \left[\vec{\omega}_2 \times \left[-\vec{R}2^T\begin{Bmatrix}\hat{i_5}\\ \hat{j_5}\\ \hat{k_5}\end{Bmatrix} - \vec{B}^T\begin{Bmatrix}\hat{i_5}\\ \hat{j_5}\\ \hat{k_5}\end{Bmatrix}\right]\right]\end{aligned} \tag{B.37}$$

The vector $\ddot{\vec{R}}1$ was found by differentiating $\dot{\vec{R}}1$ with respect to time.

$$\begin{aligned}\ddot{\vec{R}}1(1) =& -\dot{x}(6)RA\sin x(1)\cos x(2) - \dot{x}(7)RA\cos x(1)\sin x(2)\\ & - x(6)^2RA\cos x(1)\cos x(2) + 2x(6)x(7)RA\sin x(1)\sin x(2)\\ & - x(7)^2RA\cos x(1)\cos x(2)\\ \ddot{\vec{R}}1(2) =& \dot{x}(6)RA\cos x(1)\cos x(2) - \dot{x}(7)RA\sin x(1)\sin x(2)\\ & - x(6)^2RA\sin x(1)\cos x(2) - 2x(6)x(7)RA\cos x(1)\sin x(2)\\ & - x(7)^2RA\sin x(1)\cos x(2)\\ \ddot{\vec{R}}1(3) =& -\dot{x}(7)RA\cos x(2) + x(7)^2RA\sin x(2)\end{aligned} \tag{B.38}$$

The vector $\ddot{\vec{R}}2$ was found by differentiating $\dot{\vec{R}}2$ with respect to time.

$$
\begin{aligned}
\ddot{\vec{R}}2(1) =& -\dot{x}(8)RB\sin x(3)\cos x(4) - \dot{x}(9)RB\cos x(3)\sin x(4) - x(8)^2RB\cos x(3)\cos x(4) \\
& 2x(8)x(9)RB\sin x(3)\sin x(4) - x(9)^2RB\cos x(3)\cos x(4) \\
\ddot{\vec{R}}2(2) =& -\dot{x}(8)RB\sin x(3)\sin x(4)\sin x(5) + \dot{x}(9)RB\cos x(3)\cos x(4)\sin x(5) \\
& + \dot{x}(10)RB\cos x(3)\sin x(4)\cos x(5) - \dot{x}(8)RB\cos x(3)\cos x(5) \\
& + \dot{x}(10)RB\sin x(3)\sin x(5) - x(8)^2RB\cos x(3)\sin x(4)\sin x(5) \\
& - x(9)^2RB\cos x(3)\sin x(4)\sin x(5) - x(10)^2RB\cos x(3)\sin x(4)\sin x(5) \\
& + x(8)^2RB\sin x(3)\cos x(5) + x(10)^2RB\sin x(3)\cos x(5) \\
& - 2x(8)x(9)RB\sin x(3)\cos x(4)\sin x(5) - 2x(8)x(10)RB\sin x(3)\sin x(4)\cos x(5) \\
& + 2x(9)x(10)RB\cos x(3)\cos x(4)\cos x(5) + 2x(8)x(10)RB\cos x(3)\sin x(5) \\
\ddot{\vec{R}}2(3) =& -\dot{x}(8)RB\sin x(3)\sin x(4)\cos x(5) + \dot{x}(9)RB\cos x(3)\cos x(4)\cos x(5) \\
& + \dot{x}(10)RB\cos x(3)\sin x(4)\sin x(5) + \dot{x}(8)RB\cos x(3)\sin x(5) \\
& + \dot{x}(10)RB\sin x(3)\cos x(5) - x(8)^2RB\cos x(3)\sin x(4)\cos x(5) \\
& - x(9)^2RB\cos x(3)\sin x(4)\cos x(5) - x(10)^2RB\cos x(3)\sin x(4)\cos x(5) \\
& - x(8)^2RB\sin x(3)\sin x(5) - x(10)^2RB\sin x(3)\sin x(5) \\
& - 2x(8)x(9)RB\sin x(3)\cos x(4)\cos x(5) + 2x(8)x(10)RB\sin x(3)\sin x(4)\sin x(5) \\
& - 2x(9)x(10)RB\cos x(3)\cos x(4)\sin x(5) + 2x(8)x(10)RB\cos x(3)\cos x(5)
\end{aligned}
\tag{B.39}
$$

At this point, the acceleration of the center of mass of the outboard body must be sectioned into $\dot{x}$ and non $\dot{x}$ terms, as in equation 2.61 for the two dimensional model. The first term appearing in equation B.37, $\ddot{\vec{R}}1$, has $\dot{x}(6)$, $\dot{x}(7)$ and non $\dot{x}$ terms so it must be split into three pieces. Taking the partial derivative of $\ddot{\vec{R}}1$ with respect to $\dot{x}(6)$ yields the following,

$$
\begin{aligned}
\ddot{\vec{R}}1_{\dot{x}(6)}(1) =& -RA\sin x(1)\cos x(2) \\
\ddot{\vec{R}}1_{\dot{x}(6)}(2) =& RA\cos x(1)\cos x(2) \\
\ddot{\vec{R}}1_{\dot{x}(6)}(3) =& 0
\end{aligned}
\tag{B.40}
$$

Taking the partial derivative of $\ddot{\vec{R}}1$ with respect to $\dot{x}(7)$ yields the following,

$$\begin{aligned}
\ddot{\vec{R}}1_{\dot{x}(7)}(1) &= -RA\cos x(1)\sin x(2) \\
\ddot{\vec{R}}1_{\dot{x}(7)}(2) &= -RA\sin x(1)\sin x(2) \\
\ddot{\vec{R}}1_{\dot{x}(7)}(3) &= -RA\cos x(2)
\end{aligned} \tag{B.41}$$

The vector of non $\dot{x}$ terms is given by,

$$\begin{aligned}
\ddot{\vec{R}}1_x(1) =& -x(6)^2 RA\cos x(1)\cos x(2) + 2x(6)x(7)RA\sin x(1)\sin x(2) \\
& - x(7)^2 RA\cos x(1)\cos x(2) \\
\ddot{\vec{R}}1_x(2) =& -x(6)^2 RA\sin x(1)\cos x(2) - 2x(6)x(7)RA\cos x(1)\sin x(2) \\
& - x(7)^2 RA\sin x(1)\cos x(2) \\
\ddot{\vec{R}}1_x(3) =& x(7)^2 RA\sin x(2)
\end{aligned} \tag{B.42}$$

The term $\ddot{\vec{R}}1$ can now be written as a combination of equations B.40, B.41 and B.42 as follows,

$$\ddot{\vec{R}}1 = \ddot{\vec{R}}1_{\dot{x}(6)}\left[\dot{x}(6)\right] + \ddot{\vec{R}}1_{\dot{x}(7)}\left[\dot{x}(7)\right] + \ddot{\vec{R}}1_x \tag{B.43}$$

The transformation matrix [T5] does not have any $\dot{x}$ terms; therefore, it does not need to be sectioned.

The next term appearing in equation B.37, $\ddot{\vec{R}}2$, has $\dot{x}(8)$, $\dot{x}(9)$ , $\dot{x}(10)$ , and non $\dot{x}$ terms so it must be split into four pieces. Taking the partial derivative of $\ddot{\vec{R}}2$ with respect to $\dot{x}(8)$ yields the following,

$$\begin{aligned}
\ddot{\vec{R}}2_{\dot{x}(8)}(1) &= -RB\sin x(3)\cos x(4) \\
\ddot{\vec{R}}2_{\dot{x}(8)}(2) &= -RB\sin x(3)\sin x(4)\sin x(5) - RB\cos x(3)\cos x(5) \\
\ddot{\vec{R}}2_{\dot{x}(8)}(3) &= -RB\sin x(3)\sin x(4)\cos x(5) - RB\cos x(3)\sin x(5)
\end{aligned} \tag{B.44}$$

Taking the partial derivative of $\ddot{\vec{R}}2$ with respect to $\dot{x}(9)$ yields the following,

$$\begin{aligned}
\ddot{\vec{R}}2_{\dot{x}(9)}(1) =& - RB\cos x(3)\sin x(4)\\
\ddot{\vec{R}}2_{\dot{x}(9)}(2) =& RB\cos x(3)\cos x(4)\sin x(5)\\
\ddot{\vec{R}}2_{\dot{x}(9)}(3) =& RB\cos x(3)\cos x(4)\cos x(5)
\end{aligned} \tag{B.45}$$

Taking the partial derivative of $\ddot{\vec{R}}2$ with respect to $\dot{x}(10)$ yields the following,

$$\begin{aligned}
\ddot{\vec{R}}2_{\dot{x}(10)}(1) =& 0\\
\ddot{\vec{R}}2_{\dot{x}(10)}(2) =& + RB\cos x(3)\sin x(4)\cos x(5) + RB\sin x(3)\sin x(5)\\
\ddot{\vec{R}}2_{\dot{x}(10)}(3) =& + RB\cos x(3)\sin x(4)\sin x(5) + RB\sin x(3)\cos x(5)
\end{aligned} \tag{B.46}$$

The vector of non $\dot{x}$ terms is given by,

$$\begin{aligned}
\ddot{\vec{R}}2_x(1) =& - x(8)^2 RB\cos x(3)\cos x(4) + 2x(8)x(9)RB\sin x(3)\sin x(4)\\
& - x(9)^2 RB\cos x(3)\cos x(4)\\
\ddot{\vec{R}}2_x(2) =& - x(8)^2 RB\cos x(3)\sin x(4)\sin x(5) - x(9)^2 RB\cos x(3)\sin x(4)\sin x(5)\\
& - x(10)^2 RB\cos x(3)\sin x(4)\sin x(5) + x(8)^2 RB\sin x(3)\cos x(5)\\
& + x(10)^2 RB\sin x(3)\cos x(5) - 2x(8)x(9)RB\sin x(3)\cos x(4)\sin x(5)\\
& - 2x(8)x(10)RB\sin x(3)\sin x(4)\cos x(5) + 2x(9)x(10)RB\cos x(3)\cos x(4)\cos x(5)\\
& + 2x(8)x(10)RB\cos x(3)\sin x(5)\\
\ddot{\vec{R}}2_x(3) =& - x(8)^2 RB\cos x(3)\sin x(4)\cos x(5) - x(9)^2 RB\cos x(3)\sin x(4)\cos x(5)\\
& - x(10)^2 RB\cos x(3)\sin x(4)\cos x(5) - x(8)^2 RB\sin x(3)\sin x(5)\\
& - x(10)^2 RB\sin x(3)\sin x(5) - 2x(8)x(9)RB\sin x(3)\cos x(4)\cos x(5)\\
& + 2x(8)x(10)RB\sin x(3)\sin x(4)\sin x(5) - 2x(9)x(10)RB\cos x(3)\cos x(4)\sin x(5)\\
& + 2x(8)x(10)RB\cos x(3)\cos x(5)
\end{aligned} \tag{B.47}$$

The term $\ddot{\vec{R}}2$ can now be written as a combination of equations B.44, B.45, B.46 and B.47 as follows,

$$\ddot{\vec{R}}2 = \ddot{\vec{R}}2_{\dot{x}(8)}\left[\dot{x}(8)\right] + \ddot{\vec{R}}2_{\dot{x}(9)}\left[\dot{x}(9)\right] + \ddot{\vec{R}}2_{\dot{x}(10)}\left[\dot{x}(10)\right] + \ddot{\vec{R}}2_{x} \tag{B.48}$$

The term $\vec{\alpha}_2$, derived in equation B.28, has $\dot{x}(6)$, $\dot{x}(7)$, $\dot{x}(8)$, $\dot{x}(9)$, $\dot{x}(10)$, and non $\dot{x}$ terms. Taking the partial derivative with respect to $\dot{x}(6)$ gives,

$$\vec{\alpha}_{2_{\dot{x}(6)}} = \left\{ \begin{array}{c} 0 \\ 0 \\ 1 \end{array} \right\} [T5] \tag{B.49}$$

Taking the partial derivative with respect to $\dot{x}(7)$ gives,

$$\vec{\alpha}_{2_{\dot{x}(7)}} = \left\{ \begin{array}{c} 0 \\ 1 \\ 0 \end{array} \right\} [T4] \tag{B.50}$$

Taking the partial derivative with respect to $\dot{x}(8)$ gives,

$$\vec{\alpha}_{2_{\dot{x}(8)}} = \left\{ \begin{array}{c} 0 \\ 0 \\ 1 \end{array} \right\} [T3] \tag{B.51}$$

Taking the partial derivative with respect to $\dot{x}(9)$ gives,

$$\vec{\alpha}_{2_{\dot{x}(9)}} = \left\{ \begin{array}{c} 0 \\ 1 \\ 0 \end{array} \right\} [T2] \tag{B.52}$$

Taking the partial derivative with respect to $\dot{x}(10)$ gives,

$$\vec{\alpha}_{2_{\dot{x}(10)}} = \left\{ \begin{array}{c} 1 \\ 0 \\ 0 \end{array} \right\} [T1] \tag{B.53}$$

The vector of non $\dot{x}$ terms is given by,

$$\vec{\alpha}_2 = \left\{ \begin{array}{ccc} 0 & 0 & x(6) \end{array} \right\} [\dot{T5}] \left\{ \begin{array}{c} \hat{i_5} \\ \hat{j_5} \\ \hat{k_5} \end{array} \right\} + \left\{ \begin{array}{ccc} 0 & x(7) & 0 \end{array} \right\} [\dot{T4}] \left\{ \begin{array}{c} \hat{i_5} \\ \hat{j_5} \\ \hat{k_5} \end{array} \right\}$$
$$+ \left\{ \begin{array}{ccc} 0 & 0 & x(8) \end{array} \right\} [\dot{T3}] \left\{ \begin{array}{c} \hat{i_5} \\ \hat{j_5} \\ \hat{k_5} \end{array} \right\} + \left\{ \begin{array}{ccc} 0 & x(9) & 0 \end{array} \right\} [\dot{T2}] \left\{ \begin{array}{c} \hat{i_5} \\ \hat{j_5} \\ \hat{k_5} \end{array} \right\}$$
$$+ \left\{ \begin{array}{ccc} x(10) & 0 & 0 \end{array} \right\} [\dot{T1}] \left\{ \begin{array}{c} \hat{i_5} \\ \hat{j_5} \\ \hat{k_5} \end{array} \right\} \quad \text{(B.54)}$$

The term $\vec{\alpha}_2$ can now be written as a combination of equations B.49, B.50, B.51, B.52, B.53 and B.54 as follows,

$$\vec{\alpha}_2 = \vec{\alpha}_{2_{\dot{x}(6)}} [\dot{x}(6)] + \vec{\alpha}_{2_{\dot{x}(7)}} [\dot{x}(7)] + \vec{\alpha}_{2_{\dot{x}(8)}} [\dot{x}(8)] + \vec{\alpha}_{2_{\dot{x}(9)}} [\dot{x}(9)] + \vec{\alpha}_{2_{\dot{x}(10)}} [\dot{x}(10)] + \vec{\alpha}_{2_x} \quad \text{(B.55)}$$

The rest of the terms in equation B.37 are non $\dot{x}$ dependent so they do not need to be sectioned. The absolute acceleration of the center of mass of the outboard body can now be written as,

$$\vec{A}_{G2} = \left( \ddot{\vec{R}}1^T_{\dot{x}(6)} [T] \begin{Bmatrix} \hat{i_5} \\ \hat{j_5} \\ \hat{k_5} \end{Bmatrix} + \vec{\alpha}_{2_{\dot{x}(6)}} \times \left[ -\vec{R}2^T \begin{Bmatrix} \hat{i_5} \\ \hat{j_5} \\ \hat{k_5} \end{Bmatrix} - \vec{B}^T \begin{Bmatrix} \hat{i_5} \\ \hat{j_5} \\ \hat{k_5} \end{Bmatrix} \right] \right) \dot{x}(6)$$
$$+ \left( \ddot{\vec{R}}1^T_{\dot{x}(7)} [T] \begin{Bmatrix} \hat{i_5} \\ \hat{j_5} \\ \hat{k_5} \end{Bmatrix} + \vec{\alpha}_{2_{\dot{x}(7)}} \times \left[ -\vec{R}2^T \begin{Bmatrix} \hat{i_5} \\ \hat{j_5} \\ \hat{k_5} \end{Bmatrix} - \vec{B}^T \begin{Bmatrix} \hat{i_5} \\ \hat{j_5} \\ \hat{k_5} \end{Bmatrix} \right] \right) \dot{x}(7)$$
$$+ \left( -\ddot{\vec{R}}2^T_{\dot{x}(8)} \begin{Bmatrix} \hat{i_5} \\ \hat{j_5} \\ \hat{k_5} \end{Bmatrix} + \vec{\alpha}_{2_{\dot{x}(8)}} \times \left[ -\vec{R}2^T \begin{Bmatrix} \hat{i_5} \\ \hat{j_5} \\ \hat{k_5} \end{Bmatrix} - \vec{B}^T \begin{Bmatrix} \hat{i_5} \\ \hat{j_5} \\ \hat{k_5} \end{Bmatrix} \right] \right) \dot{x}(8)$$
$$+ \left( -\ddot{\vec{R}}2^T_{\dot{x}(9)} \begin{Bmatrix} \hat{i_5} \\ \hat{j_5} \\ \hat{k_5} \end{Bmatrix} + \vec{\alpha}_{2_{\dot{x}(9)}} \times \left[ -\vec{R}2^T \begin{Bmatrix} \hat{i_5} \\ \hat{j_5} \\ \hat{k_5} \end{Bmatrix} - \vec{B}^T \begin{Bmatrix} \hat{i_5} \\ \hat{j_5} \\ \hat{k_5} \end{Bmatrix} \right] \right) \dot{x}(9)$$
$$+ \left( -\ddot{\vec{R}}2^T_{\dot{x}(10)} \begin{Bmatrix} \hat{i_5} \\ \hat{j_5} \\ \hat{k_5} \end{Bmatrix} + \vec{\alpha}_{2_{\dot{x}(10)}} \times \left[ -\vec{R}2^T \begin{Bmatrix} \hat{i_5} \\ \hat{j_5} \\ \hat{k_5} \end{Bmatrix} - \vec{B}^T \begin{Bmatrix} \hat{i_5} \\ \hat{j_5} \\ \hat{k_5} \end{Bmatrix} \right] \right) \dot{x}(10)$$
$$+ \ddot{\vec{R}}1_x - \ddot{\vec{R}}2_x + \vec{\alpha}_{2_x} \times \left[ -\vec{R}2^T \begin{Bmatrix} \hat{i_5} \\ \hat{j_5} \\ \hat{k_5} \end{Bmatrix} - \vec{B}^T \begin{Bmatrix} \hat{i_5} \\ \hat{j_5} \\ \hat{k_5} \end{Bmatrix} \right] + 2\vec{\omega}_2 \times \left[ -\dot{\vec{R}}2^T \begin{Bmatrix} \hat{i_5} \\ \hat{j_5} \\ \hat{k_5} \end{Bmatrix} \right]$$
$$+ \vec{\omega}_2 \times \left[ \vec{\omega}_2 \times \left[ -\vec{R}2^T \begin{Bmatrix} \hat{i_5} \\ \hat{j_5} \\ \hat{k_5} \end{Bmatrix} - \vec{B}^T \begin{Bmatrix} \hat{i_5} \\ \hat{j_5} \\ \hat{k_5} \end{Bmatrix} \right] \right] \quad \text{(B.56)}$$

To simplify equation B.56, the group of terms dependent on $\dot{x}(6)$ are expressed as $\vec{A}_{G2_{\dot{x}(6)}}$, the group of terms dependent on $\dot{x}(7)$ are expressed as $\vec{A}_{G2_{\dot{x}(7)}}$, the group of terms dependent on $\dot{x}(8)$ are expressed as $\vec{A}_{G2_{\dot{x}(8)}}$, the group of terms dependent on $\dot{x}(9)$ are expressed as $\vec{A}_{G2_{\dot{x}(9)}}$, the group of terms dependent on $\dot{x}(10)$ are expressed as $\vec{A}_{G2_{\dot{x}(10)}}$, and the rest of the terms are expressed as $\vec{A}_{G2_x}$.

$$\vec{A}_{G2} = \vec{A}_{G2_{\dot{x}(6)}} [\dot{x}(6)] + \vec{A}_{G2_{\dot{x}(7)}} [\dot{x}(7)] + \vec{A}_{G2_{\dot{x}(8)}} [\dot{x}(8)] + \vec{A}_{G2_{\dot{x}(9)}} [\dot{x}(9)] + \vec{A}_{G2_{\dot{x}(10)}} [\dot{x}(10)] + \vec{A}_{G2_x} \quad \text{(B.57)}$$

**Partial Angular Velocity**

As noted in section 2.2, the partial derivative of the angular velocity with respect to each generalized speed is needed to form the equations of motion based on Kane's principles. In the three dimensional case there are five generalized speeds, $x(6)$, $x(7)$ , $x(8)$ , $x(9)$ and $x(10)$, thus the five partial angular velocities are given below.

$$\frac{\partial \vec{\omega}_2}{\partial x(6)} = \left\{ \begin{array}{c} 0 \\ 0 \\ 1 \end{array} \right\} [T5] \tag{B.58}$$

$$\frac{\partial \vec{\omega}_2}{\partial x(7)} = \left\{ \begin{array}{c} 0 \\ 1 \\ 0 \end{array} \right\} [T4] \tag{B.59}$$

$$\frac{\partial \vec{\omega}_2}{\partial x(8)} = \left\{ \begin{array}{c} 0 \\ 0 \\ 1 \end{array} \right\} [T3] \tag{B.60}$$

$$\frac{\partial \vec{\omega}_2}{\partial x(9)} = \left\{ \begin{array}{c} 0 \\ 1 \\ 0 \end{array} \right\} [T2] \tag{B.61}$$

$$\frac{\partial \vec{\omega}_2}{\partial x(10)} = \left\{ \begin{array}{c} 1 \\ 0 \\ 0 \end{array} \right\} [T1] \tag{B.62}$$

**Partial Absolute Velocity**

The partial absolute velocity with respect to each generalized speed is also required to form the equations of motion. The partial absolute velocity with respect to the first generalized speed is found by differentiating equation B.34 with respect to $x(6)$. The transformation matrix [T5], and the vectors $\vec{R}2$ and $\vec{B}$ do not depend on either of the generalized speeds so they remain as a constant in the differentiation.

$$\frac{\partial \vec{V}_{G2}}{\partial x(6)} = \frac{\partial \dot{\vec{R}}1^T}{\partial x(6)}\,[T]\left\{\begin{array}{c}\hat{i_5}\\ \hat{j_5}\\ \hat{k_5}\end{array}\right\} - \frac{\partial \dot{\vec{R}}2^T}{\partial x(6)}\left\{\begin{array}{c}\hat{i_5}\\ \hat{j_5}\\ \hat{k_5}\end{array}\right\} + \frac{\partial \vec{\omega}_2}{\partial x(6)} \times \left[-\vec{R}2^T\left\{\begin{array}{c}\hat{i_5}\\ \hat{j_5}\\ \hat{k_5}\end{array}\right\} - \vec{B}^T\left\{\begin{array}{c}\hat{i_5}\\ \hat{j_5}\\ \hat{k_5}\end{array}\right\}\right] \quad \text{(B.63)}$$

The vector $\dot{\vec{R}}2$, equation B.36, does not contain any $x(6)$ terms so the partial derivative of $\dot{\vec{R}}2$ with respect to $x(6)$ is zero. This simplifies equation B.63 to the following,

$$\frac{\partial \vec{V}_{G2}}{\partial x(6)} = \frac{\partial \dot{\vec{R}}1^T}{\partial x(6)}\,[T]\left\{\begin{array}{c}\hat{i_5}\\ \hat{j_5}\\ \hat{k_5}\end{array}\right\} + \frac{\partial \vec{\omega}_2}{\partial x(6)} \times \left[-\vec{R}2^T\left\{\begin{array}{c}\hat{i_5}\\ \hat{j_5}\\ \hat{k_5}\end{array}\right\} - \vec{B}^T\left\{\begin{array}{c}\hat{i_5}\\ \hat{j_5}\\ \hat{k_5}\end{array}\right\}\right] \quad \text{(B.64)}$$

By differentiating equation B.35 with respect to generalized speed $x(6)$, the following expression was derived for $\frac{\partial \dot{\vec{R}}1}{\partial x(6)}$,

$$\frac{\partial \dot{\vec{R}}1}{\partial x(6)} = \left\{\begin{array}{c}-RA\sin x(1)\cos x(2)\\ RA\cos x(1)\cos x(2)\\ 0\end{array}\right\} \quad \text{(B.65)}$$

The partial absolute velocity with respect to the second generalized speed is found by differentiating equation B.34 with respect to $x(7)$. The transformation matrix [T5], and the vectors $\vec{R}2$ and $\vec{B}$ do not depend on either of the generalized speeds so they remains as a constant in the differentiation.

$$\frac{\partial \vec{V}_{G2}}{\partial x(7)} = \frac{\partial \dot{\vec{R}}1^T}{\partial x(7)}\,[T]\left\{\begin{array}{c}\hat{i_5}\\ \hat{j_5}\\ \hat{k_5}\end{array}\right\} - \frac{\partial \dot{\vec{R}}2^T}{\partial x(7)}\left\{\begin{array}{c}\hat{i_5}\\ \hat{j_5}\\ \hat{k_5}\end{array}\right\} + \frac{\partial \vec{\omega}_2}{\partial x(7)} \times \left[-\vec{R}2^T\left\{\begin{array}{c}\hat{i_5}\\ \hat{j_5}\\ \hat{k_5}\end{array}\right\} - \vec{B}^T\left\{\begin{array}{c}\hat{i_5}\\ \hat{j_5}\\ \hat{k_5}\end{array}\right\}\right] \quad \text{(B.66)}$$

The vector $\dot{\vec{R}}2$, equation B.36, does not contain any $x(7)$ terms so the partial derivative of $\dot{\vec{R}}2$ with respect to $x(7)$ is zero. This simplifies equation B.66 to the following,

$$\frac{\partial \vec{V}_{G2}}{\partial x(7)} = \frac{\partial \dot{\vec{R}}1^T}{\partial x(7)}\,[T]\left\{\begin{array}{c}\hat{i_5}\\ \hat{j_5}\\ \hat{k_5}\end{array}\right\} + \frac{\partial \vec{\omega}_2}{\partial x(7)} \times \left[-\vec{R}2^T\left\{\begin{array}{c}\hat{i_5}\\ \hat{j_5}\\ \hat{k_5}\end{array}\right\} - \vec{B}^T\left\{\begin{array}{c}\hat{i_5}\\ \hat{j_5}\\ \hat{k_5}\end{array}\right\}\right] \quad \text{(B.67)}$$

By differentiating equation B.35 with respect to generalized speed $x(7)$, the following expression was derived for $\frac{\partial \dot{\vec{R}}1}{\partial x(7)}$,

$$\frac{\partial \dot{\vec{R}}1}{\partial x(7)} = \left\{\begin{array}{c} -RA\cos x(1)\sin x(2)\\ -RA\sin x(1)\sin x(2)\\ -RA\cos x(2)\end{array}\right\} \quad \text{(B.68)}$$

The partial absolute velocity with respect to the third generalized speed is found by differentiating equation B.34 with respect to $x(8)$. Again, the transformation matrix [T5], and the vectors $\vec{R}2$ and $\vec{B}$ do not depend on either of the generalized speeds so they remains as a constant in the differentiation.

$$\frac{\partial \vec{V}_{G2}}{\partial x(8)} = \frac{\partial \dot{\vec{R}}1^T}{\partial x(8)}\,[T]\left\{\begin{array}{c}\hat{i_5}\\ \hat{j_5}\\ \hat{k_5}\end{array}\right\} - \frac{\partial \dot{\vec{R}}2^T}{\partial x(8)}\left\{\begin{array}{c}\hat{i_5}\\ \hat{j_5}\\ \hat{k_5}\end{array}\right\} + \frac{\partial \vec{\omega}_2}{\partial x(8)} \times \left[-\vec{R}2^T\left\{\begin{array}{c}\hat{i_5}\\ \hat{j_5}\\ \hat{k_5}\end{array}\right\} - \vec{B}^T\left\{\begin{array}{c}\hat{i_5}\\ \hat{j_5}\\ \hat{k_5}\end{array}\right\}\right] \quad \text{(B.69)}$$

The vector $\dot{\vec{R}}1$, equation B.35, does not contain any $x(8)$ terms so the partial derivative of $\dot{\vec{R}}1$ with respect to $x(8)$ is zero. This simplifies equation B.69 to the following,

$$\frac{\partial \vec{V}_{G2}}{\partial x(8)} = -\frac{\partial \dot{\vec{R}}2^T}{\partial x(8)}\left\{\begin{array}{c}\hat{i_5}\\ \hat{j_5}\\ \hat{k_5}\end{array}\right\} + \frac{\partial \vec{\omega}_2}{\partial x(8)} \times \left[-\vec{R}2^T\left\{\begin{array}{c}\hat{i_5}\\ \hat{j_5}\\ \hat{k_5}\end{array}\right\} - \vec{B}^T\left\{\begin{array}{c}\hat{i_5}\\ \hat{j_5}\\ \hat{k_5}\end{array}\right\}\right] \quad \text{(B.70)}$$

By differentiating equation B.36 with respect to generalized speed $x(8)$, the following expression was derived for $\frac{\partial \dot{\vec{R}}2}{\partial x(8)}$,

$$\frac{\partial \dot{\vec{R}}2}{\partial x(8)} = \left\{\begin{array}{c} -RB\sin x(3)\cos x(4) \\ -RB\sin x(3)\sin x(4)\sin x(5) - RB\cos x(3)\cos x(5) \\ -RB\sin x(3)\sin x(4)\cos x(5) + RB\cos x(3)\sin x(5)\end{array}\right\} \quad \text{(B.71)}$$

The partial absolute velocity with respect to the fourth generalized speed is found by differentiating equation B.34 with respect to $x(9)$. Again, the transformation matrix [T5], and the vectors $\vec{R}2$ and $\vec{B}$ do not depend on either of the generalized speeds so they remains as a constant in the differentiation.

$$\frac{\partial \vec{V}_{G2}}{\partial x(9)} = \frac{\partial \dot{\vec{R}}1^T}{\partial x(9)}\,[T]\left\{\begin{array}{c}\hat{i_5}\\ \hat{j_5}\\ \hat{k_5}\end{array}\right\} - \frac{\partial \dot{\vec{R}}2^T}{\partial x(9)}\left\{\begin{array}{c}\hat{i_5}\\ \hat{j_5}\\ \hat{k_5}\end{array}\right\} + \frac{\partial \vec{\omega}_2}{\partial x(9)} \times \left[-\vec{R}2^T\left\{\begin{array}{c}\hat{i_5}\\ \hat{j_5}\\ \hat{k_5}\end{array}\right\} - \vec{B}^T\left\{\begin{array}{c}\hat{i_5}\\ \hat{j_5}\\ \hat{k_5}\end{array}\right\}\right] \quad \text{(B.72)}$$

The vector $\dot{\vec{R}}1$, equation B.35, does not contain any $x(9)$ terms so the partial derivative of $\dot{\vec{R}}1$ with respect to $x(9)$ is zero. This simplifies equation B.72 to the following,

$$\frac{\partial \vec{V}_{G2}}{\partial x(9)} = -\frac{\partial \dot{\vec{R}}2^T}{\partial x(9)}\left\{\begin{array}{c}\hat{i_5}\\ \hat{j_5}\\ \hat{k_5}\end{array}\right\} + \frac{\partial \vec{\omega}_2}{\partial x(9)} \times \left[-\vec{R}2^T\left\{\begin{array}{c}\hat{i_5}\\ \hat{j_5}\\ \hat{k_5}\end{array}\right\} - \vec{B}^T\left\{\begin{array}{c}\hat{i_5}\\ \hat{j_5}\\ \hat{k_5}\end{array}\right\}\right] \quad \text{(B.73)}$$

By differentiating equation B.36 with respect to generalized speed $x(9)$, the following expression was derived for $\frac{\partial \dot{\vec{R}}2}{\partial x(9)}$,

$$\frac{\partial \dot{\vec{R}}2}{\partial x(9)} = \left\{\begin{array}{c} -RB\cos x(3)\sin x(4) \\ RB\cos x(3)\cos x(4)\sin x(5) \\ RB\cos x(3)\cos x(4)\cos x(5)\end{array}\right\} \quad \text{(B.74)}$$

The partial absolute velocity with respect to the fifth generalized speed is found by differentiating equation B.34 with respect to $x(10)$. Again, the transformation matrix [T5], and the vectors $\vec{R}2$ and $\vec{B}$ do not depend on either of the generalized speeds so they remains as a constant in the differentiation.

$$\frac{\partial \vec{V}_{G2}}{\partial x(10)} = \frac{\partial \dot{\vec{R}}1^T}{\partial x(10)}\,[T] \left\{ \begin{array}{c} \hat{i_5} \\ \hat{j_5} \\ \hat{k_5} \end{array} \right\} - \frac{\partial \dot{\vec{R}}2^T}{\partial x(10)} \left\{ \begin{array}{c} \hat{i_5} \\ \hat{j_5} \\ \hat{k_5} \end{array} \right\} + \frac{\partial \vec{\omega}_2}{\partial x(10)} \times \left[ -\vec{R}2^T \left\{ \begin{array}{c} \hat{i_5} \\ \hat{j_5} \\ \hat{k_5} \end{array} \right\} - \vec{B}^T \left\{ \begin{array}{c} \hat{i_5} \\ \hat{j_5} \\ \hat{k_5} \end{array} \right\} \right] \quad \text{(B.75)}$$

The vector $\dot{\vec{R}}1$, equation B.35, does not contain any $x(10)$ terms so the partial derivative of $\dot{\vec{R}}1$ with respect to $x(10)$ is zero. This simplifies equation B.69 to the following,

$$\frac{\partial \vec{V}_{G2}}{\partial x(10)} = -\frac{\partial \dot{\vec{R}}2^T}{\partial x(10)} \left\{ \begin{array}{c} \hat{i_5} \\ \hat{j_5} \\ \hat{k_5} \end{array} \right\} + \frac{\partial \vec{\omega}_2}{\partial x(10)} \times \left[ -\vec{R}2^T \left\{ \begin{array}{c} \hat{i_5} \\ \hat{j_5} \\ \hat{k_5} \end{array} \right\} - \vec{B}^T \left\{ \begin{array}{c} \hat{i_5} \\ \hat{j_5} \\ \hat{k_5} \end{array} \right\} \right] \quad \text{(B.76)}$$

By differentiating equation B.36 with respect to generalized speed $x(108)$, the following expression was derived for $\frac{\partial \dot{\vec{R}}2}{\partial x(10)}$,

$$\frac{\partial \dot{\vec{R}}2}{\partial x(10)} = \left\{ \begin{array}{c} 0 \\ RB\cos x(3)\sin x(4)\cos x(5) + RB\sin x(3)\sin x(5) \\ -RB\cos x(3)\sin x(4)\sin x(5) + RB\sin x(3)\cos x(5) \end{array} \right\} \quad \text{(B.77)}$$

### B.0.1 Generalized Inertial Forces

The inertial terms of Kane's equations, represented in equation 2.17, can now be assembled for each generalized speed. It is important to note that the mass matrix $[m]$ and the inertia tensor $[I]$ are not changing with respect to time so the terms $[\dot{m}]$ and $[\dot{I}]$ of equation 2.17 are set to zero. For the generalized speed, $x(6)$, equation 2.17 becomes,

$$\vec{Q}^*_{x(6)} = \frac{\partial \vec{V}_{G_2}}{\partial x(6)} \cdot \left\{ -[m]\,\vec{A}_{G_2} \right\} + \frac{\partial \vec{\omega}_2}{\partial x(6)} \cdot \{-[I]\,\vec{\alpha}_2\} \quad \text{(B.78)}$$

For generalized speed, $x(7)$, equation 2.17 becomes,

$$\vec{Q}^*_{x(7)} = \frac{\partial \vec{V}_{G_2}}{\partial x(7)} \cdot \left\{ - [m]\, \vec{A}_{G_2} \right\} + \frac{\partial \vec{\omega}_2}{\partial x(7)} \cdot \{ - [I]\, \vec{\alpha}_2 \} \tag{B.79}$$

For the generalized speed, $x(8)$, equation 2.17 becomes,

$$\vec{Q}^*_{x(8)} = \frac{\partial \vec{V}_{G_2}}{\partial x(8)} \cdot \left\{ - [m]\, \vec{A}_{G_2} \right\} + \frac{\partial \vec{\omega}_2}{\partial x(8)} \cdot \{ - [I]\, \vec{\alpha}_2 \} \tag{B.80}$$

For generalized speed, $x(9)$, equation 2.17 becomes,

$$\vec{Q}^*_{x(9)} = \frac{\partial \vec{V}_{G_2}}{\partial x(9)} \cdot \left\{ - [m]\, \vec{A}_{G_2} \right\} + \frac{\partial \vec{\omega}_2}{\partial x(9)} \cdot \{ - [I]\, \vec{\alpha}_2 \} \tag{B.81}$$

For the generalized speed, $x(10)$, equation 2.17 becomes,

$$\vec{Q}^*_{x(10)} = \frac{\partial \vec{V}_{G_2}}{\partial x(10)} \cdot \left\{ - [m]\, \vec{A}_{G_2} \right\} + \frac{\partial \vec{\omega}_2}{\partial x(10)} \cdot \{ - [I]\, \vec{\alpha}_2 \} \tag{B.82}$$

These equations needs to be divided into into a matrix of partial derivatives with respect to each $\dot{x}$ term and a vector of non $\dot{x}$ terms. Using equations B.57 and B.55, equation B.78 can be sectioned into $\dot{x}(6)$, $\dot{x}(7)$, $\dot{x}(8)$, $\dot{x}(9)$, $\dot{x}(10)$,and non $\dot{x}$ components. The group of terms dependent on $\dot{x}(6)$ can be represented by the following,

$$QQ^*_{66} = \frac{\partial \vec{V}_{G_2}}{\partial x(6)} \cdot \left\{ - [m]\, \vec{A}_{G_{2_{\dot{x}(6)}}} \right\} + \frac{\partial \vec{\omega}_2}{\partial x(6)} \cdot \left\{ - [I]\, \vec{\alpha}_{2_{(\dot{x})(6)}} \right\} \tag{B.83}$$

The group of terms dependent on $\dot{x}(7)$ can be represented by the following,

$$QQ^*_{67} = \frac{\partial \vec{V}_{G_2}}{\partial x(6)} \cdot \left\{ - [m]\, \vec{A}_{G_{2_{\dot{x}(7)}}} \right\} + \frac{\partial \vec{\omega}_2}{\partial x(6)} \cdot \left\{ - [I]\, \vec{\alpha}_{2_{(\dot{x})(7)}} \right\} \tag{B.84}$$

The group of terms dependent on $\dot{x}(8)$ can be represented by the following,

$$QQ^*_{68} = \frac{\partial \vec{V}_{G_2}}{\partial x(6)} \cdot \left\{ - [m]\, \vec{A}_{G_{2_{\dot{x}(8)}}} \right\} + \frac{\partial \vec{\omega}_2}{\partial x(6)} \cdot \left\{ - [I]\, \vec{\alpha}_{2_{(\dot{x})(8)}} \right\} \tag{B.85}$$

The group of terms dependent on $\dot{x}(9)$ can be represented by the following,

$$QQ^*_{69} = \frac{\partial \vec{V}_{G_2}}{\partial x(6)} \cdot \left\{ - [m] \vec{A}_{G_{2_{\dot{x}(9)}}} \right\} + \frac{\partial \vec{\omega}_2}{\partial x(6)} \cdot \left\{ - [I] \vec{\alpha}_{2_{\dot{(x)}(9)}} \right\} \tag{B.86}$$

The group of terms dependent on $\dot{x}(10)$ can be represented by the following,

$$QQ^*_{610} = \frac{\partial \vec{V}_{G_2}}{\partial x(6)} \cdot \left\{ - [m] \vec{A}_{G_{2_{\dot{x}(10)}}} \right\} + \frac{\partial \vec{\omega}_2}{\partial x(6)} \cdot \left\{ - [I] \vec{\alpha}_{2_{\dot{(x)}(10)}} \right\} \tag{B.87}$$

The group of non $\dot{x}$ dependent terms can be represented by the following,

$$Q^*_6 = \frac{\partial \vec{V}_{G_2}}{\partial x(6)} \cdot \left\{ - [m] \vec{A}_{G_{2_x}} \right\} + \frac{\partial \vec{\omega}_2}{\partial x(6)} \cdot \{ - [I] \vec{\alpha}_{2_x} \} \tag{B.88}$$

Using equations B.57 and B.55, equation B.79 can be sectioned into $\dot{x}(6)$, $\dot{x}(7)$, $\dot{x}(8)$, $\dot{x}(9)$, $\dot{x}(10)$,and non $\dot{x}$ components. The group of terms dependent on $\dot{x}(6)$ can be represented by the following,

$$QQ^*_{76} = \frac{\partial \vec{V}_{G_2}}{\partial x(7)} \cdot \left\{ - [m] \vec{A}_{G_{2_{\dot{x}(6)}}} \right\} + \frac{\partial \vec{\omega}_2}{\partial x(7)} \cdot \left\{ - [I] \vec{\alpha}_{2_{\dot{(x)}(6)}} \right\} \tag{B.89}$$

The group of terms dependent on $\dot{x}(7)$ can be represented by the following,

$$QQ^*_{77} = \frac{\partial \vec{V}_{G_2}}{\partial x(7)} \cdot \left\{ - [m] \vec{A}_{G_{2_{\dot{x}(7)}}} \right\} + \frac{\partial \vec{\omega}_2}{\partial x(7)} \cdot \left\{ - [I] \vec{\alpha}_{2_{\dot{(x)}(7)}} \right\} \tag{B.90}$$

The group of terms dependent on $\dot{x}(8)$ can be represented by the following,

$$QQ^*_{78} = \frac{\partial \vec{V}_{G_2}}{\partial x(7)} \cdot \left\{ - [m] \vec{A}_{G_{2_{\dot{x}(8)}}} \right\} + \frac{\partial \vec{\omega}_2}{\partial x(7)} \cdot \left\{ - [I] \vec{\alpha}_{2_{\dot{(x)}(8)}} \right\} \tag{B.91}$$

The group of terms dependent on $\dot{x}(9)$ can be represented by the following,

$$QQ^*_{79} = \frac{\partial \vec{V}_{G_2}}{\partial x(7)} \cdot \left\{ - [m] \vec{A}_{G_{2_{\dot{x}(9)}}} \right\} + \frac{\partial \vec{\omega}_2}{\partial x(7)} \cdot \left\{ - [I] \vec{\alpha}_{2_{\dot{(x)}(9)}} \right\} \tag{B.92}$$

The group of terms dependent on $\dot{x}(10)$ can be represented by the following,

$$QQ^*_{710} = \frac{\partial \vec{V}_{G_2}}{\partial x(7)} \cdot \left\{ - [m] \vec{A}_{G_{2_{\dot{x}(10)}}} \right\} + \frac{\partial \vec{\omega}_2}{\partial x(7)} \cdot \left\{ - [I] \vec{\alpha}_{2_{\dot{(x)}(10)}} \right\} \tag{B.93}$$

The group of non $\dot{x}$ dependent terms can be represented by the following,

$$Q_7^* = \frac{\partial \vec{V}_{G_2}}{\partial x(7)} \cdot \left\{ - [m] \, \vec{A}_{G_{2_x}} \right\} + \frac{\partial \vec{\omega}_2}{\partial x(7)} \cdot \{ - [I] \, \vec{\alpha}_{2_x} \} \tag{B.94}$$

Using equations B.57 and B.55, equation B.80 can be sectioned into $\dot{x}(6)$, $\dot{x}(7)$, $\dot{x}(8)$, $\dot{x}(9)$, $\dot{x}(10)$,and non $\dot{x}$ components. The group of terms dependent on $\dot{x}(6)$ can be represented by the following,

$$QQ_{86}^* = \frac{\partial \vec{V}_{G_2}}{\partial x(8)} \cdot \left\{ - [m] \, \vec{A}_{G_{2_{\dot{x}(6)}}} \right\} + \frac{\partial \vec{\omega}_2}{\partial x(8)} \cdot \left\{ - [I] \, \vec{\alpha}_{2_{\dot{(x)}(6)}} \right\} \tag{B.95}$$

The group of terms dependent on $\dot{x}(7)$ can be represented by the following,

$$QQ_{87}^* = \frac{\partial \vec{V}_{G_2}}{\partial x(8)} \cdot \left\{ - [m] \, \vec{A}_{G_{2_{\dot{x}(7)}}} \right\} + \frac{\partial \vec{\omega}_2}{\partial x(8)} \cdot \left\{ - [I] \, \vec{\alpha}_{2_{\dot{(x)}(7)}} \right\} \tag{B.96}$$

The group of terms dependent on $\dot{x}(8)$ can be represented by the following,

$$QQ_{88}^* = \frac{\partial \vec{V}_{G_2}}{\partial x(8)} \cdot \left\{ - [m] \, \vec{A}_{G_{2_{\dot{x}(8)}}} \right\} + \frac{\partial \vec{\omega}_2}{\partial x(8)} \cdot \left\{ - [I] \, \vec{\alpha}_{2_{\dot{(x)}(8)}} \right\} \tag{B.97}$$

The group of terms dependent on $\dot{x}(9)$ can be represented by the following,

$$QQ_{89}^* = \frac{\partial \vec{V}_{G_2}}{\partial x(8)} \cdot \left\{ - [m] \, \vec{A}_{G_{2_{\dot{x}(9)}}} \right\} + \frac{\partial \vec{\omega}_2}{\partial x(8)} \cdot \left\{ - [I] \, \vec{\alpha}_{2_{\dot{(x)}(9)}} \right\} \tag{B.98}$$

The group of terms dependent on $\dot{x}(10)$ can be represented by the following,

$$QQ_{810}^* = \frac{\partial \vec{V}_{G_2}}{\partial x(8)} \cdot \left\{ - [m] \, \vec{A}_{G_{2_{\dot{x}(10)}}} \right\} + \frac{\partial \vec{\omega}_2}{\partial x(8)} \cdot \left\{ - [I] \, \vec{\alpha}_{2_{\dot{(x)}(10)}} \right\} \tag{B.99}$$

The group of non $\dot{x}$ dependent terms can be represented by the following,

$$Q_8^* = \frac{\partial \vec{V}_{G_2}}{\partial x(8)} \cdot \left\{ - [m] \, \vec{A}_{G_{2_x}} \right\} + \frac{\partial \vec{\omega}_2}{\partial x(8)} \cdot \{ - [I] \, \vec{\alpha}_{2_x} \} \tag{B.100}$$

Using equations B.57 and B.55, equation B.81 can be sectioned into $\dot{x}(6)$, $\dot{x}(7)$, $\dot{x}(8)$, $\dot{x}(9)$, $\dot{x}(10)$,and non $\dot{x}$ components. The group of terms dependent on $\dot{x}(6)$ can be represented by the following,

$$QQ_{96}^* = \frac{\partial \vec{V}_{G_2}}{\partial x(9)} \cdot \left\{ - [m] \, \vec{A}_{G_{2_{\dot{x}(6)}}} \right\} + \frac{\partial \vec{\omega}_2}{\partial x(9)} \cdot \left\{ - [I] \, \vec{\alpha}_{2_{\dot{(x)}(6)}} \right\} \tag{B.101}$$

The group of terms dependent on $\dot{x}(7)$ can be represented by the following,

$$QQ^*_{97} = \frac{\partial \vec{V}_{G_2}}{\partial x(9)} \cdot \left\{ - [m] \, \vec{A}_{G_{2_{\dot{x}(7)}}} \right\} + \frac{\partial \vec{\omega}_2}{\partial x(9)} \cdot \left\{ - [I] \, \vec{\alpha}_{2_{\dot{(x)}(7)}} \right\} \tag{B.102}$$

The group of terms dependent on $\dot{x}(8)$ can be represented by the following,

$$QQ^*_{98} = \frac{\partial \vec{V}_{G_2}}{\partial x(9)} \cdot \left\{ - [m] \, \vec{A}_{G_{2_{\dot{x}(8)}}} \right\} + \frac{\partial \vec{\omega}_2}{\partial x(9)} \cdot \left\{ - [I] \, \vec{\alpha}_{2_{\dot{(x)}(8)}} \right\} \tag{B.103}$$

The group of terms dependent on $\dot{x}(9)$ can be represented by the following,

$$QQ^*_{99} = \frac{\partial \vec{V}_{G_2}}{\partial x(9)} \cdot \left\{ - [m] \, \vec{A}_{G_{2_{\dot{x}(9)}}} \right\} + \frac{\partial \vec{\omega}_2}{\partial x(9)} \cdot \left\{ - [I] \, \vec{\alpha}_{2_{\dot{(x)}(9)}} \right\} \tag{B.104}$$

The group of terms dependent on $\dot{x}(10)$ can be represented by the following,

$$QQ^*_{910} = \frac{\partial \vec{V}_{G_2}}{\partial x(9)} \cdot \left\{ - [m] \, \vec{A}_{G_{2_{\dot{x}(10)}}} \right\} + \frac{\partial \vec{\omega}_2}{\partial x(9)} \cdot \left\{ - [I] \, \vec{\alpha}_{2_{\dot{(x)}(10)}} \right\} \tag{B.105}$$

The group of non $\dot{x}$ dependent terms can be represented by the following,

$$Q^*_9 = \frac{\partial \vec{V}_{G_2}}{\partial x(9)} \cdot \left\{ - [m] \, \vec{A}_{G_{2_x}} \right\} + \frac{\partial \vec{\omega}_2}{\partial x(9)} \cdot \{ - [I] \, \vec{\alpha}_{2_x} \} \tag{B.106}$$

Using equations B.57 and B.55, equation B.82 can be sectioned into $\dot{x}(6)$, $\dot{x}(7)$, $\dot{x}(8)$, $\dot{x}(9)$, $\dot{x}(10)$,and non $\dot{x}$ components. The group of terms dependent on $\dot{x}(6)$ can be represented by the following,

$$QQ^*_{106} = \frac{\partial \vec{V}_{G_2}}{\partial x(10)} \cdot \left\{ - [m] \, \vec{A}_{G_{2_{\dot{x}(6)}}} \right\} + \frac{\partial \vec{\omega}_2}{\partial x(10)} \cdot \left\{ - [I] \, \vec{\alpha}_{2_{\dot{(x)}(6)}} \right\} \tag{B.107}$$

The group of terms dependent on $\dot{x}(7)$ can be represented by the following,

$$QQ^*_{107} = \frac{\partial \vec{V}_{G_2}}{\partial x(10)} \cdot \left\{ - [m] \, \vec{A}_{G_{2_{\dot{x}(7)}}} \right\} + \frac{\partial \vec{\omega}_2}{\partial x(10)} \cdot \left\{ - [I] \, \vec{\alpha}_{2_{\dot{(x)}(7)}} \right\} \tag{B.108}$$

The group of terms dependent on $\dot{x}(8)$ can be represented by the following,

$$QQ^*_{108} = \frac{\partial \vec{V}_{G_2}}{\partial x(10)} \cdot \left\{ - [m] \, \vec{A}_{G_{2_{\dot{x}(8)}}} \right\} + \frac{\partial \vec{\omega}_2}{\partial x(10)} \cdot \left\{ - [I] \, \vec{\alpha}_{2_{\dot{(x)}(8)}} \right\} \tag{B.109}$$

The group of terms dependent on $\dot{x}(9)$ can be represented by the following,

$$QQ^*_{109} = \frac{\partial \vec{V}_{G_2}}{\partial x(10)} \cdot \left\{ - [m] \, \vec{A}_{G_{2_{\dot{x}(9)}}} \right\} + \frac{\partial \vec{\omega}_2}{\partial x(10)} \cdot \left\{ - [I] \, \vec{\alpha}_{2_{(\dot{x})(9)}} \right\} \tag{B.110}$$

The group of terms dependent on $\dot{x}(10)$ can be represented by the following,

$$QQ^*_{1010} = \frac{\partial \vec{V}_{G_2}}{\partial x(10)} \cdot \left\{ - [m] \, \vec{A}_{G_{2_{\dot{x}(10)}}} \right\} + \frac{\partial \vec{\omega}_2}{\partial x(10)} \cdot \left\{ - [I] \, \vec{\alpha}_{2_{(\dot{x})(10)}} \right\} \tag{B.111}$$

The group of non $\dot{x}$ dependent terms can be represented by the following,

$$Q^*_{10} = \frac{\partial \vec{V}_{G_2}}{\partial x(10)} \cdot \left\{ - [m] \, \vec{A}_{G_{2_x}} \right\} + \frac{\partial \vec{\omega}_2}{\partial x(10)} \cdot \{ - [I] \, \vec{\alpha}_{2_x} \} \tag{B.112}$$

The partial derivative matrix of $\dot{(x)}$ terms and vector of non $\dot{x}$ terms can now be assembled.

$$\begin{Bmatrix} Q^*_{x(6)} \\ Q^*_{x(7)} \\ Q^*_{x(8)} \\ Q^*_{x(9)} \\ Q^*_{x(10)} \end{Bmatrix} = \begin{bmatrix} QQ^*_{66} & QQ^*_{67} & Q^*_{68} & QQ^*_{69} & QQ^*_{610} \\ QQ^*_{76} & QQ^*_{77} & Q^*_{78} & QQ^*_{79} & QQ^*_{710} \\ QQ^*_{86} & QQ^*_{87} & Q^*_{88} & QQ^*_{89} & QQ^*_{810} \\ QQ^*_{96} & QQ^*_{97} & Q^*_{98} & QQ^*_{99} & QQ^*_{910} \\ QQ^*_{106} & QQ^*_{107} & Q^*_{108} & QQ^*_{109} & QQ^*_{1010} \end{bmatrix} \begin{Bmatrix} \dot{x}(6) \\ \dot{x}(7) \\ \dot{x}(8) \\ \dot{x}(9) \\ \dot{x}(10) \end{Bmatrix} + \begin{Bmatrix} Q^*_6 \\ Q^*_7 \\ Q^*_8 \\ Q^*_9 \\ Q^*_{10} \end{Bmatrix} \tag{B.113}$$

### B.0.2 Generalized Active Forces

The following external forces are exerted on the outboard body of the system: the force due to gravity and the force of the systems springs. The external forces were first compiled in the ground fixed coordinate system and then transformed to the body fixed coordinate system using transformation matrix $[T]$. The force due to gravity, in ground fixed coordinates, is given by the following,

$$\vec{F}_{grav} = \left\{ \begin{array}{c} mg \\ 0 \\ 0 \end{array} \right\} \tag{B.114}$$

The force of the systems springs was more complex to calculate. The force in each of the springs was calculated separately in the ground fixed coordinate system and then transformed to the body fixed coordinate system. The ground fixed spring end locations ($\vec{LE}$, $\vec{LF}$, and $\vec{LG}$), the body fixed spring end locations ($\vec{D}1$, $\vec{D}2$, and $\vec{D}3$ ), the spring equilibrium length ($ED$, $EF$, and $EG$), and the spring constants ($K_E$, $K_F$, $K_G$), were all input into the simulation as constants. Each of these quantities is described in detail in Appendix F.

The first step in calculating the spring forces is to determine the length of the spring. A position vector is defined from each of the ground fixed spring attachment points to the body fixed spring attachment point as follows. For the first spring (E) the position vector is described as follows,

$$\vec{P}_{ED} = -\vec{LE}^T \left\{ \begin{array}{c} \hat{i}_0 \\ \hat{j}_0 \\ \hat{k}_0 \end{array} \right\} + \vec{R1}^T \left\{ \begin{array}{c} \hat{i}_0 \\ \hat{j}_0 \\ \hat{k}_0 \end{array} \right\} - \vec{R2}^T \left\{ \begin{array}{c} \hat{i}_5 \\ \hat{j}_5 \\ \hat{k}_5 \end{array} \right\} + \vec{D1}^T \left\{ \begin{array}{c} \hat{i}_5 \\ \hat{j}_5 \\ \hat{k}_5 \end{array} \right\} \tag{B.115}$$

It is required that all terms be in the ground fixed coordinate system, so the transformation matrix $[TT5]$ was used to convert vectors from the body fixed coordinate system. After transformation, the position vector of equation B.115 becomes,

$$\vec{P}_{ED} = -\vec{LE}^T \left\{ \begin{array}{c} \hat{i}_0 \\ \hat{j}_0 \\ \hat{k}_0 \end{array} \right\} + \vec{R1}^T \left\{ \begin{array}{c} \hat{i}_0 \\ \hat{j}_0 \\ \hat{k}_0 \end{array} \right\} - \vec{R2}^T [TT5] \left\{ \begin{array}{c} \hat{i}_0 \\ \hat{j}_0 \\ \hat{k}_0 \end{array} \right\} + \vec{D}^T [TT5] \left\{ \begin{array}{c} \hat{i}_0 \\ \hat{j}_0 \\ \hat{k}_0 \end{array} \right\} \tag{B.116}$$

The length of spring E can now be found by calculating the magnitude of the position vector $\vec{P}_{ED}$. This quantity is denoted $|\vec{P}_{ED}|$.

Similar expressions can be derived for the five other springs.

$$\vec{P}_{FD} = -\vec{LF}^T \begin{Bmatrix} \hat{i_0} \\ \hat{j_0} \\ \hat{k_0} \end{Bmatrix} + \vec{R1}^T \begin{Bmatrix} \hat{i_0} \\ \hat{j_0} \\ \hat{k_0} \end{Bmatrix} - \vec{R2}^T [TT5] \begin{Bmatrix} \hat{i_0} \\ \hat{j_0} \\ \hat{k_0} \end{Bmatrix} + \vec{D2}^T [TT5] \begin{Bmatrix} \hat{i_0} \\ \hat{j_0} \\ \hat{k_0} \end{Bmatrix} \tag{B.117}$$

The length of spring F can now be found by calculating the magnitude of the position vector $\vec{P}_{FD}$. This quantity is denoted $|\vec{P}_{FD}|$.

$$\vec{P}_{GD} = -\vec{LG}^T \begin{Bmatrix} \hat{i_0} \\ \hat{j_0} \\ \hat{k_0} \end{Bmatrix} + \vec{R1}^T \begin{Bmatrix} \hat{i_0} \\ \hat{j_0} \\ \hat{k_0} \end{Bmatrix} - \vec{R2}^T [TT5] \begin{Bmatrix} \hat{i_0} \\ \hat{j_0} \\ \hat{k_0} \end{Bmatrix} + \vec{D3}^T [TT5] \begin{Bmatrix} \hat{i_0} \\ \hat{j_0} \\ \hat{k_0} \end{Bmatrix} \tag{B.118}$$

The length of spring G can now be found by calculating the magnitude of the position vector $\vec{P}_{GD}$. This quantity is denoted $|\vec{P}_{GD}|$.

$$\vec{P}_{HD} = -\vec{LH}^T \begin{Bmatrix} \hat{i_0} \\ \hat{j_0} \\ \hat{k_0} \end{Bmatrix} + \vec{R1}^T \begin{Bmatrix} \hat{i_0} \\ \hat{j_0} \\ \hat{k_0} \end{Bmatrix} - \vec{R2}^T [TT5] \begin{Bmatrix} \hat{i_0} \\ \hat{j_0} \\ \hat{k_0} \end{Bmatrix} + \vec{D3}^T [TT5] \begin{Bmatrix} \hat{i_0} \\ \hat{j_0} \\ \hat{k_0} \end{Bmatrix} \tag{B.119}$$

The length of spring H can now be found by calculating the magnitude of the position vector $\vec{P}_{HD}$. This quantity is denoted $|\vec{P}_{HD}|$.

$$\vec{P}_{ID} = -\vec{LI}^T \begin{Bmatrix} \hat{i_0} \\ \hat{j_0} \\ \hat{k_0} \end{Bmatrix} + \vec{R1}^T \begin{Bmatrix} \hat{i_0} \\ \hat{j_0} \\ \hat{k_0} \end{Bmatrix} - \vec{R2}^T [TT5] \begin{Bmatrix} \hat{i_0} \\ \hat{j_0} \\ \hat{k_0} \end{Bmatrix} + \vec{D3}^T [TT5] \begin{Bmatrix} \hat{i_0} \\ \hat{j_0} \\ \hat{k_0} \end{Bmatrix} \tag{B.120}$$

The length of spring G can now be found by calculating the magnitude of the position vector $\vec{P}_{ID}$. This quantity is denoted $|\vec{P}_{ID}|$.

$$\vec{P}_{JD} = -\vec{LJ}^T \begin{Bmatrix} \hat{i_0} \\ \hat{j_0} \\ \hat{k_0} \end{Bmatrix} + \vec{R1}^T \begin{Bmatrix} \hat{i_0} \\ \hat{j_0} \\ \hat{k_0} \end{Bmatrix} - \vec{R2}^T [TT5] \begin{Bmatrix} \hat{i_0} \\ \hat{j_0} \\ \hat{k_0} \end{Bmatrix} + \vec{D3}^T [TT5] \begin{Bmatrix} \hat{i_0} \\ \hat{j_0} \\ \hat{k_0} \end{Bmatrix} \tag{B.121}$$

The length of spring G can now be found by calculating the magnitude of the position vector $\vec{P}_{JD}$. This quantity is denoted $|\vec{P}_{JD}|$.

The next step is to calculate the total stretch from equilibrium for each spring. This is accomplished by subtracting the zero force spring length from the spring length as follows,

$$\delta_E = |\vec{P}_{ED}| - ED \tag{B.122}$$

$$\delta_F = |\vec{P}_{FD}| - FD \tag{B.123}$$

$$\delta_G = |\vec{P}_{GD}| - GD \tag{B.124}$$

$$\delta_H = |\vec{P}_{HD}| - HD \tag{B.125}$$

$$\delta_I = |\vec{P}_{ID}| - ID \tag{B.126}$$

$$\delta_J = |\vec{P}_{JD}| - JD \tag{B.127}$$

The spring force acts in the opposite direction of the spring length position vector. A unit vector in the direction of the applied force for spring E is given by,

$$\vec{D}ir_E = -\frac{\vec{P}_{ED}}{|\vec{P}_{ED}|} \tag{B.128}$$

Similarly, unit vectors in the direction of the applied force for the 5 additional springs are given by,

$$\vec{D}ir_F = -\frac{\vec{P}_{FD}}{|\vec{P}_{FD}|} \tag{B.129}$$

$$\vec{D}ir_G = -\frac{\vec{P}_{GD}}{|\vec{P}_{GD}|} \tag{B.130}$$

$$\vec{D}ir_H = -\frac{\vec{P}_{HD}}{|\vec{P}_{HD}|} \tag{B.131}$$

$$\vec{D}ir_I = -\frac{\vec{P}_{ID}}{|\vec{P}_{ID}|} \tag{B.132}$$

$$\vec{D}ir_J = -\frac{\vec{P}_{JD}}{|\vec{P}_{JD}|} \tag{B.133}$$

The force in each spring can now be calculated.

$$\vec{F}_E = K_E\ \delta_E\ \vec{D}ir_E \tag{B.134}$$

$$\vec{F}_F = K_F\ \delta_F\ \vec{D}ir_F \tag{B.135}$$

$$\vec{F}_G = K_G\ \delta_G\ \vec{D}ir_G \tag{B.136}$$

$$\vec{F}_H = K_H\ \delta_H\ \vec{D}ir_H \tag{B.137}$$

$$\vec{F}_I = K_I\ \delta_I\ \vec{D}ir_I \tag{B.138}$$

$$\vec{F}_J = K_J \; \delta_J \; \vec{D}ir_J \tag{B.139}$$

The external forces are now transformed to the body fixed coordinate system by multiplying by the transformation matrix $[T]$ as follows,

$$\vec{F}_{grav_2} = \vec{F}^T_{grav} \, [T5] \left\{ \begin{array}{c} \hat{i_5} \\ \hat{j_5} \\ \hat{k_5} \end{array} \right\} \tag{B.140}$$

$$\vec{F}_{E_2} = \vec{F}^T_E \, [T5] \left\{ \begin{array}{c} \hat{i_5} \\ \hat{j_5} \\ \hat{k_5} \end{array} \right\} \tag{B.141}$$

$$\vec{F}_{F_2} = \vec{F}^T_F \, [T5] \left\{ \begin{array}{c} \hat{i_5} \\ \hat{j_5} \\ \hat{k_5} \end{array} \right\} \tag{B.142}$$

$$\vec{F}_{G_2} = \vec{F}^T_G \, [T5] \left\{ \begin{array}{c} \hat{i_5} \\ \hat{j_5} \\ \hat{k_5} \end{array} \right\} \tag{B.143}$$

$$\vec{F}_{H_2} = \vec{F}^T_H \, [T5] \left\{ \begin{array}{c} \hat{i_5} \\ \hat{j_5} \\ \hat{k_5} \end{array} \right\} \tag{B.144}$$

$$\vec{F}_{I_2} = \vec{F}^T_I \, [T5] \left\{ \begin{array}{c} \hat{i_5} \\ \hat{j_5} \\ \hat{k_5} \end{array} \right\} \tag{B.145}$$

$$\vec{F}_{J_2} = \vec{F}^T_J \, [T5] \left\{ \begin{array}{c} \hat{i_5} \\ \hat{j_5} \\ \hat{k_5} \end{array} \right\} \tag{B.146}$$

The sum of the forces on the outboard body in the body fixed coordinate system is given by,

$$\sum \vec{F} = \vec{F}_{grav_2} + \vec{F}_{E_2} + \vec{F}_{F_2} + \vec{F}_{G_2} + \vec{F}_{H_2} + \vec{F}_{I_2} + \vec{F}_{J_2} \tag{B.147}$$

The sum of the moments on the outboard body, about the center of mass, G, is found by taking the cross product of the position from the center of mass to the point of force application and the applied force. Since the gravitation force acts at the center of mass, the resultant moment contribution from this force is zero. The springs forces, for springs E, F, and G, are located at a distance $(\vec{D1} - \vec{B})$, $(\vec{D2} - \vec{B})$, and $(\vec{D3} - \vec{B})$ away from the center of mass, respectively, so the sum of the moments on the outboard body about the center of mass, G is given by,

$$\begin{aligned}\sum \vec{M}_{G_2} = \left(\vec{D1} - \vec{B}\right) \times \sum \left(\vec{F}_{E_2}\right) + \left(\vec{D2} - \vec{B}\right) \times \sum \left(\vec{F}_{F_2}\right) + \left(\vec{D3} - \vec{B}\right) \times \sum \left(\vec{F}_{G_2}\right) \\ + \left(\vec{D4} - \vec{B}\right) \times \sum \left(\vec{F}_{H_2}\right) + \left(\vec{D5} - \vec{B}\right) \times \sum \left(\vec{F}_{I_2}\right) + \left(\vec{D6} - \vec{B}\right) \times \sum \left(\vec{F}_{J_2}\right)\end{aligned} \tag{B.148}$$

The generalized active forces can now be assembled using equation 2.18 for each generalized speed. For the generalized speed $x(6)$, the active force is found to be,

$$\vec{Q}_{x(6)} = \frac{\partial \vec{V}_{G_2}}{\partial x(6)} \cdot \sum \vec{F} + \frac{\partial \vec{\omega}_2}{\partial x(6)} \cdot \sum M_{G_2} \tag{B.149}$$

For the generalized speed $x(7)$, the active force is found to be,

$$\vec{Q}_{x(7)} = \frac{\partial \vec{V}_{G_2}}{\partial x(7)} \cdot \sum \vec{F} + \frac{\partial \vec{\omega}_2}{\partial x(7)} \cdot \sum M_{G_2} \tag{B.150}$$

For the generalized speed $x(8)$, the active force is found to be,

$$\vec{Q}_{x(8)} = \frac{\partial \vec{V}_{G_2}}{\partial x(8)} \cdot \sum \vec{F} + \frac{\partial \vec{\omega}_2}{\partial x(8)} \cdot \sum M_{G_2} \tag{B.151}$$

For the generalized speed $x(9)$, the active force is found to be,

$$\vec{Q}_{x(9)} = \frac{\partial \vec{V}_{G_2}}{\partial x(9)} \cdot \sum \vec{F} + \frac{\partial \vec{\omega}_2}{\partial x(9)} \cdot \sum M_{G_2} \tag{B.152}$$

For the generalized speed $x(10)$, the active force is found to be,

$$\vec{Q}_{x(10)} = \frac{\partial \vec{V}_{G_2}}{\partial x(10)} \cdot \sum \vec{F} + \frac{\partial \vec{\omega}_2}{\partial x(10)} \cdot \sum M_{G_2} \tag{B.153}$$

The generalized active forces can be represented by the following column vector,

$$\begin{Bmatrix} Q_{x(6)} \\ Q_{x(7)} \\ Q_{x(8)} \\ Q_{x(9)} \\ Q_{x(10)} \end{Bmatrix} = \begin{Bmatrix} Q_6 \\ Q_7 \\ Q_8 \\ Q_9 \\ Q_{10} \end{Bmatrix} \tag{B.154}$$

### B.0.3 Assembling Kane's Equations

Using the quantities derived in equation B.113 and B.154, Kane's equation's can be assemble as per equation 2.19.

$$\begin{bmatrix} QQ^*_{66} & QQ^*_{67} & QQ^*_{68} & QQ^*_{69} & QQ^*_{610} \\ QQ^*_{76} & QQ^*_{77} & QQ^*_{78} & QQ^*_{79} & QQ^*_{710} \\ QQ^*_{86} & QQ^*_{87} & QQ^*_{88} & QQ^*_{89} & QQ^*_{810} \\ QQ^*_{96} & QQ^*_{97} & QQ^*_{98} & QQ^*_{99} & QQ^*_{910} \\ QQ^*_{106} & QQ^*_{107} & QQ^*_{108} & QQ^*_{109} & QQ^*_{1010} \end{bmatrix} \begin{Bmatrix} \dot{x}(6) \\ \dot{x}(7) \\ \dot{x}(8) \\ \dot{x}(9) \\ \dot{x}(10) \end{Bmatrix} + \begin{Bmatrix} Q^*_6 \\ Q^*_7 \\ Q^*_8 \\ Q^*_9 \\ Q^*_{10} \end{Bmatrix} + \begin{Bmatrix} Q_6 \\ Q_7 \\ Q_8 \\ Q_9 \\ Q_{10} \end{Bmatrix} = \begin{Bmatrix} 0 \\ 0 \\ 0 \\ 0 \\ 0 \end{Bmatrix} \tag{B.155}$$

The vector of first derivative of generalized speeds can be determined by grouping the non $\dot{x}$ terms on the right hand side of equation 2.101 and by multiplying both sides of the equation by the inverse of the $QQ$ matrix.

$$\begin{Bmatrix} \dot{x}(6) \\ \dot{x}(7) \\ \dot{x}(8) \\ \dot{x}(9) \\ \dot{x}(10) \end{Bmatrix} = [QQ]^{-1} \left\{ - \begin{Bmatrix} Q^*_6 \\ Q^*_7 \\ Q^*_8 \\ Q^*_9 \\ Q^*_{10} \end{Bmatrix} - \begin{Bmatrix} Q_6 \\ Q_7 \\ Q_8 \\ Q_9 \\ Q_{10} \end{Bmatrix} \right\} \tag{B.156}$$

# Appendix C

# Coordinate System Definitions

In order to convert the data collected during the experimental testing into useful information, two coordinate systems were defined for the physical model using the reference bodies described in Chapter 3. The following is a complete description of the creation of the unit vectors using the camera position of the markers on the reference bodies. The diagram below shows the marker location for the ground fixed reference body.

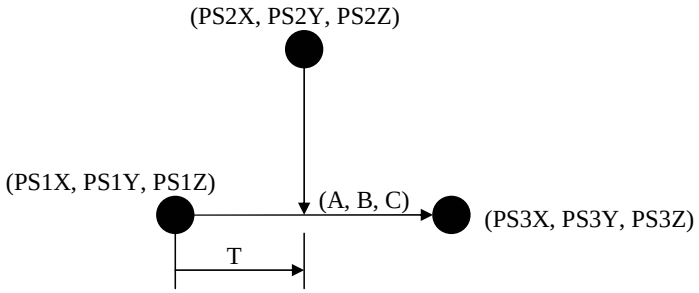


Figure C.1: Marker Definition

The $\vec{j}_0$ direction is defined in camera coordinates $(\vec{i}_C, \vec{j}_C, \vec{k}_C)$, by the following expression,

$$\vec{j}_0 = \frac{\left(P\vec{S}3 - P\vec{S}1\right)}{\left|P\vec{S}3 - P\vec{S}1\right|} \tag{C.1}$$

Since the sensor positions are given in camera coordinates, the vector $\vec{j_0}$ is comprised of $(\vec{i_C}, \vec{j_C}, \vec{k_C})$ components as follows,

$$\vec{j_0} = j_x\vec{i_C} + j_y\vec{j_C} + j_z\vec{k_C} \tag{C.2}$$

The line through the the points PS2 and the point along the line defined by the $\vec{j_0}$ direction that yield the minimum distance to point PS2, shown as (A,B,C) in Figure C.1, gives the $\vec{i_0}$ direction. The location of point (A,B,C) is given by,

$$(A, B, C) = T\vec{j_0} + P\vec{S}1 \tag{C.3}$$

The distance between point PS2 and (A,B,C) is given by,

$$d = \sqrt{(PS2X - A)^2 + (PS2Y - B)^2 + (PS2Z - C)^2} \tag{C.4}$$

The minimum distance, $d_{min}$, is found by substituting the expression for (A,B,C) found in equation C.3 into equation C.4 and taking the derivative with respect to T. The $\vec{i_0}$ direction is then defined by the following,

$$\vec{i_0} = \frac{\left(P\vec{S}1 + T\vec{j_0} - P\vec{S}2\right)}{\left|P\vec{S}1 + T\vec{j_0} - P\vec{S}2\right|} \tag{C.5}$$

Similarly to $\vec{j_0}$, the vector $\vec{i_0}$ is composed of $(\vec{i_C}\vec{j_C}, \vec{k_C})$ components as follows,

$$\vec{i_0} = i_x\vec{i_C} + i_y\vec{j_C} + i_z\vec{k_C} \tag{C.6}$$

Finally, the $\vec{k_0}$ direction is found by taking the cross product of the $\vec{i_0}$ direction and the $\vec{j_0}$ direction as follows,

$$\vec{k_0} = \vec{i_0} \times \vec{j_0} \tag{C.7}$$

The vector $\vec{k_0}$ is also composed of $(\vec{i_C}\vec{j_C}, \vec{k_C})$ components as follows,

$$\vec{k}_0 = k_x\vec{i}_C + k_y\vec{j}_C + k_z\vec{k}_C \tag{C.8}$$

The transformation from ground fixed coordinates to camera coordinates is defined by the following,

$$[T_{GF}] = \begin{bmatrix} i_x & i_y & i_z \\ j_x & j_y & j_z \\ k_x & k_y & k_z \end{bmatrix} \tag{C.9}$$

An identical formulation was produced for the body fixed coordinate system, except the $\vec{j}_0$ direction was defined to be in the opposite direction.

In order to transform the digitizing pointer data into camera coordinates for the tip of the pointer, the following method was used. First, the rigid body file for the pointer, containing the body fixed distances between the markers and the tip, was obtained from the Northern digital directory. Alternatively, this information could be obtained using the 6D Architect (Northern Digital) software. At a single point in time, a pointer fixed coordinate system was created by subtracting two horizontal sensors positions to create the $j_p$ direction, subtracting two vertical sensors to create the $k_p$ direction, and by finding the cross product of $j_p$ and $k_p$ to obtain $i_p$. Next, the pointer fixed coordinate system was used to transform the vectors from the tip of the pointer to each marker in rigid body file data into the camera coordinate system. This transformed vector was subtracted from the camera coordinates for each of the six marker at this specific point in time, to yield six estimates for the tip location in camera coordinates. This routine was implemented for each time step in the trial, and an average for the trial was calculated for each marker. Finally, the estimates for the tip from each marker were averaged to yield a single estimate for the tip location.

# Appendix D

# Viscous Damping Approximation

In order to estimate the viscous damping in the experimental data, the following procedure was followed. Two peaks were picked off the plot. Peaks after the 2 $s$ mark were selected to avoid considering Coulomb damping. The peaks, $X_1 = -17.6\ mm$ at time $t_1 = 2.2\ s$, $X_2 = -25.0\ mm$ at time $t_2 = 3.1\ s$, were selected. Next the amplitudes of the peaks, $x_1$ and $x_2$, were determined by subtracting the known y direction equilibrium position for marker number 1 of 38.3 $mm$. The amplitudes were found to be $x_1 = 20.7\ mm$ and $x_2 = 13.3\ mm$. If linear viscous damping is assumed, the following equation can be written [27],

$$\zeta = \sqrt{\frac{1}{1 + \frac{\omega_d(t_2 - t_1)}{\ln \frac{x1\cos(\omega_d t_1)}{x2\cos(\omega_d t_2)}}}} \tag{D.1}$$

Using equation D.1, the damping ratio was determined to be $\zeta = 0.22$.

# Appendix E

# Spring Stiffness Plots

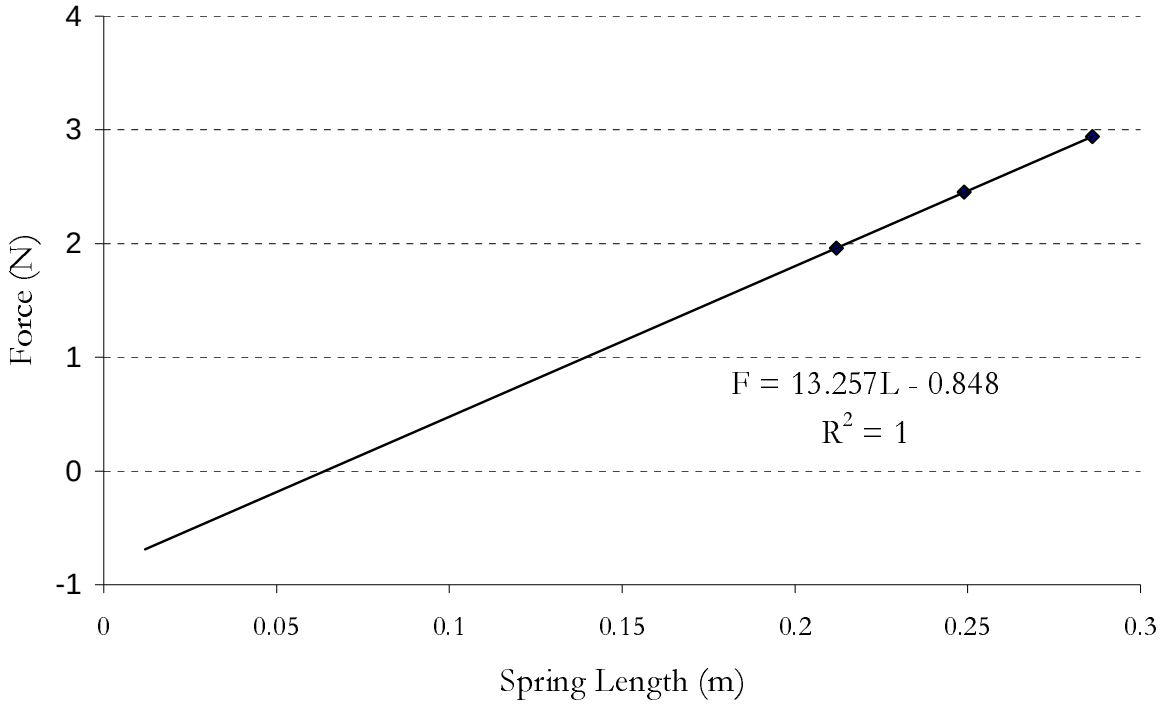


Figure E.1: Force versus Spring E Length

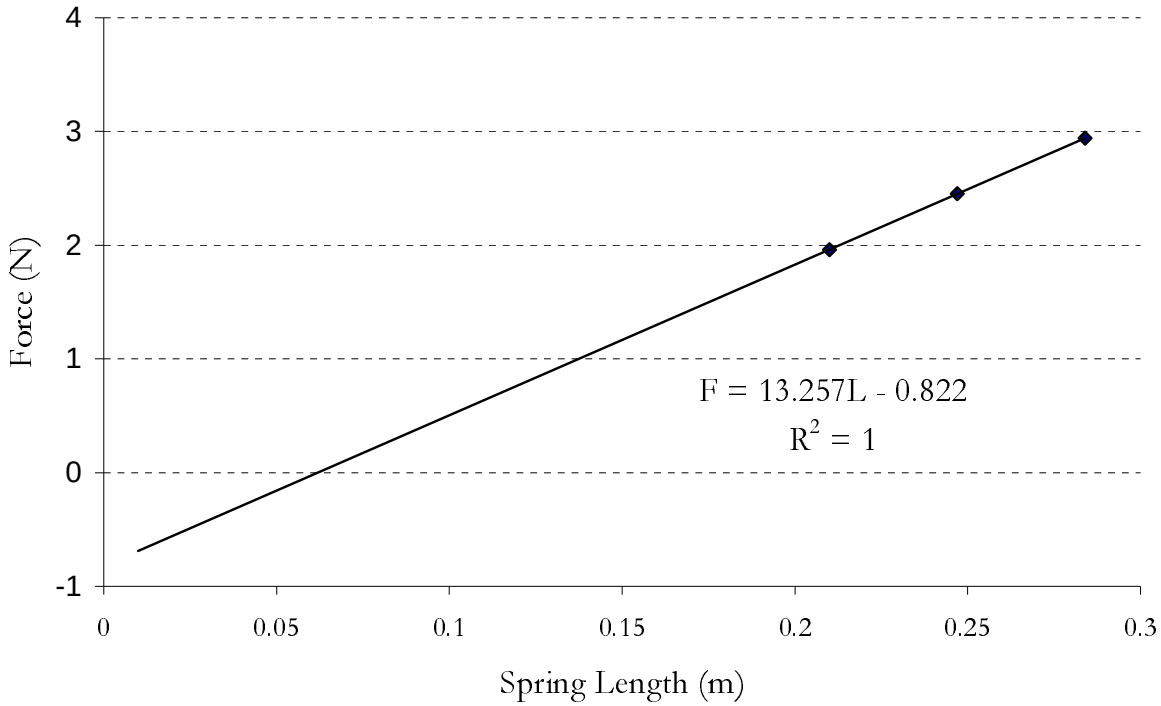


Figure E.2: Force versus Spring F Length

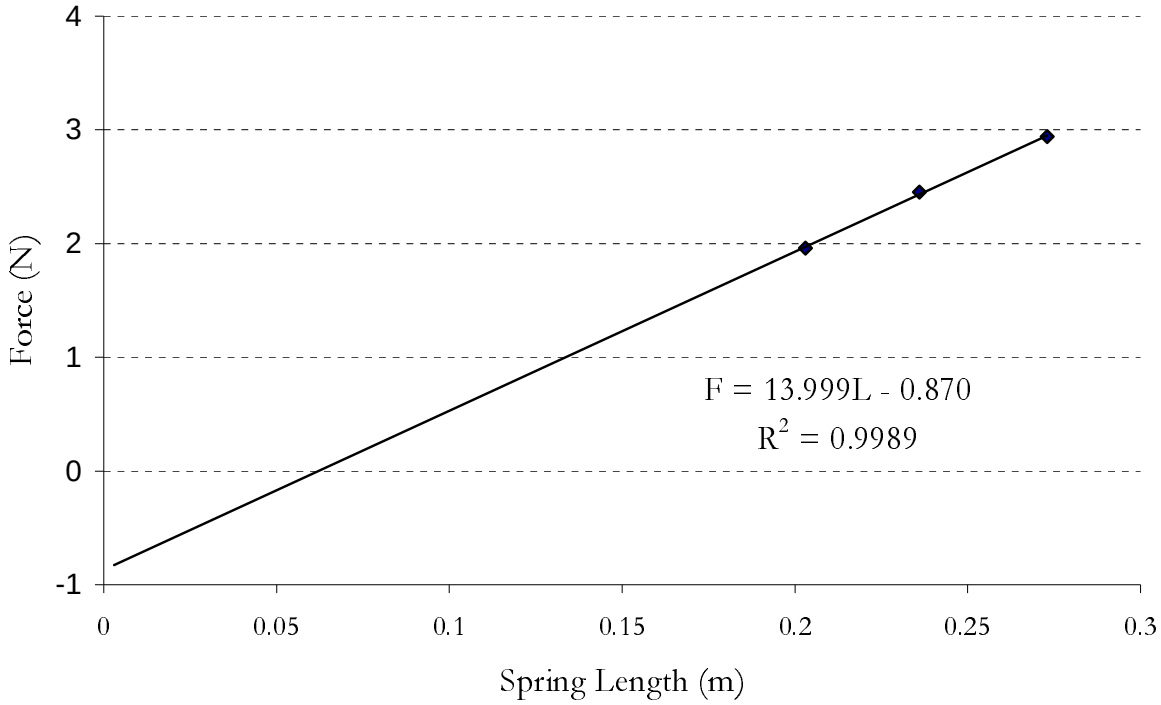


Figure E.3: Force versus Spring G Length

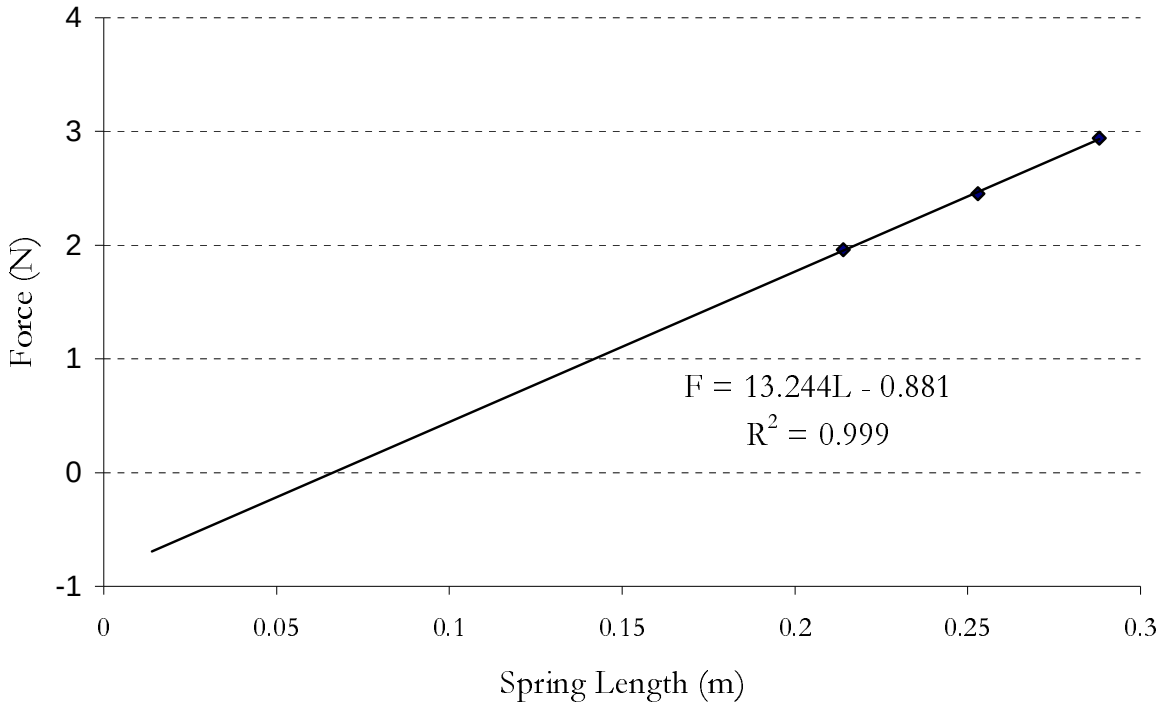


Figure E.4: Force versus Spring H Length

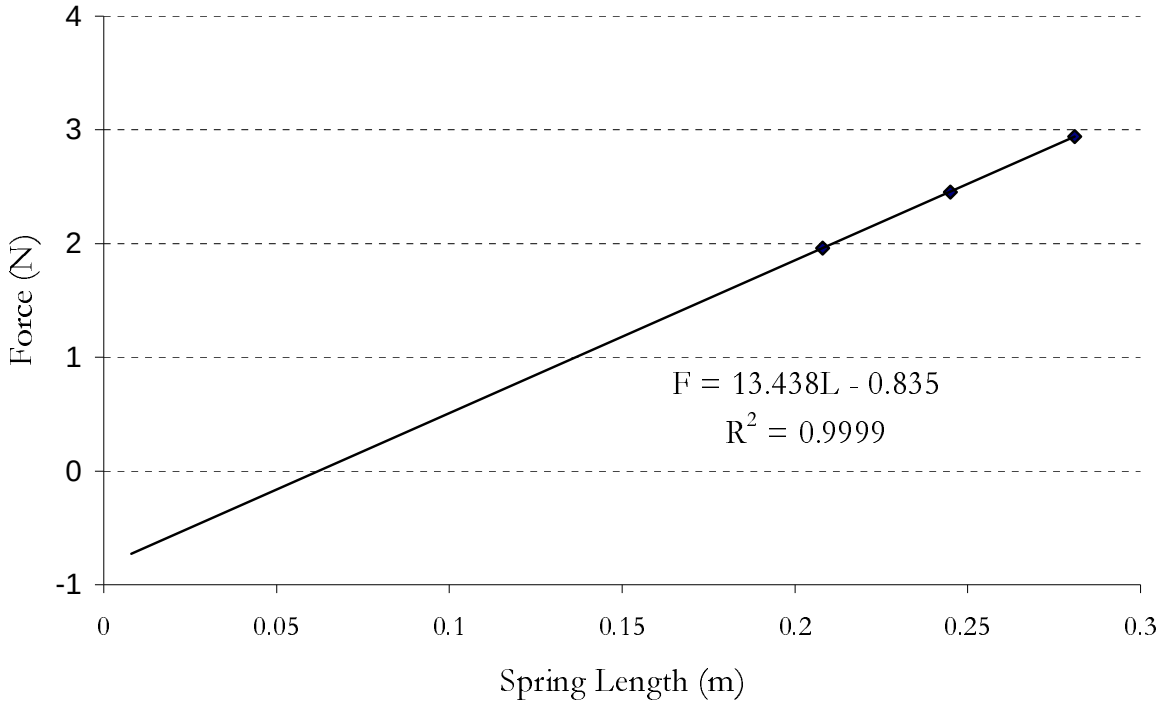


Figure E.5: Force versus Spring I Length

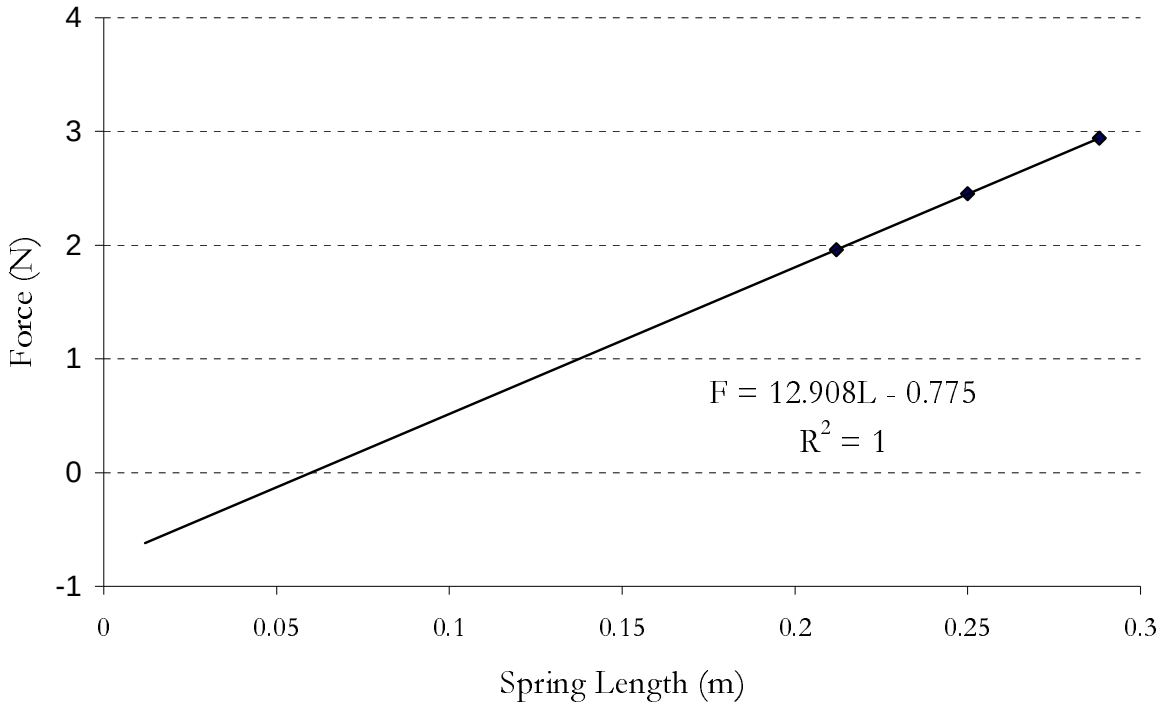


Figure E.6: Force versus Spring J Length

# Appendix F

# Constant Input File

| CONSTANT | VALUE | DEFINITION | UNITS |
|---|---|---|---|
| $RA$ | 0.0381 | inboard body radius | $m$ |
| $RB$ | 0.00635 | Ouboard radius | $m$ |
| $B(1)$<br>$B(2)$<br>$B(3)$ | $-0.1539$<br>$-0.0011$<br>$-0.0053$ | Vector from COM of outboard<br>to center of small sphere<br>in (i5,j5,k5) coordinates | $m$ |
| $D1(1)$<br>$D1(2)$<br>$D1(3)$ | 0.0905<br>0.0480<br>0.0265 | Vector from center of small sphere<br>to spring E body fixed attachment<br>point in (i5,j5,k5) coordinates | $m$ |
| $D2(1)$<br>$D2(2)$<br>$D2(3)$ | 0.0917<br>0.0029<br>$-0.0543$ | Vector from center of small sphere<br>to spring F body fixed attachment<br>point in (i5,j5,k5) coordinates | $m$ |
| $D3(1)$<br>$D3(2)$<br>$D3(3)$ | 0.0898<br>$-0.0437$<br>0.0234 | Vector from center of small sphere<br>to spring G body fixed attachment<br>point in (i5,j5,k5) coordinates | $m$ |
| $D4(1)$<br>$D4(2)$<br>$D4(3)$ | 0.1286<br>0.0466<br>0.0249 | Vector from center of small sphere<br>to spring H body fixed attachment<br>point in (i5,j5,k5) coordinates | $m$ |
| $D5(1)$<br>$D5(2)$<br>$D5(3)$ | 0.1303<br>0.0028<br>$-0.0521$ | Center of small sphere<br>to spring I body fixed attachment<br>point in (i5,j5,k5) coordinates | $m$ |
| $D6(1)$<br>$D6(2)$<br>$D6(3)$ | 0.1299<br>$-0.0436$<br>0.0243 | Center of small sphere<br>to spring J body fixed attachment<br>point in (i5,j5,k5) coordinates | $m$ |
| $MASS$ | .1755 | Mass of outboard body | $kg$ |
| $MOI(1,1)$ | 0.000071 | Ixx | $kg \cdot m^2$ |
| $MOI(1,2)$ | $-0.00000019$ | Ixy | $kg \cdot m^2$ |
| $MOI(1,3)$ | 0.000023 | Ixz | $kg \cdot m^2$ |
| $MOI(2,1)$ | $-0.00000019$ | Ixy | $kg \cdot m^2$ |
| $MOI(2,2)$ | 0.0014 | Iyy | $kg \cdot m^2$ |
| $MOI(2,3)$ | 0.0000028 | Iyz | $kg \cdot m^2$ |
| $MOI(3,1)$ | 0.000023 | Ixz | $kg \cdot m^2$ |
| $MOI(3,2)$ | 0.0000028 | Iyz | $kg \cdot m^2$ |
| $MOI(3,3)$ | 0.0014 | Izz | $kg \cdot m^2$ |
| $LE(1)$<br>$LE(2)$<br>$LE(3)$ | $-0.0754$<br>$-0.2767$<br>0.1616 | Center of inboard body to<br>spring E ground attachment<br>point in (i0,j0,k0) coordinates | $m$ |
| $LF(1)$<br>$LF(2)$<br>$LF(3)$ | $-0.0710$<br>$-0.0088$<br>$-0.3042$ | Center of inboard body to<br>spring F ground attachment<br>point in (i0,j0,k0) coordinates | $m$ |

| CONSTANT | VALUE | DEFINITION | UNITS |
|---|---|---|---|
| $LG(1)$ | $-0.0800$ | Center of inboard body to | |
| $LG(2)$ | 0.2790 | spring G ground fixed attachment | $m$ |
| $LG(3)$ | 0.1471 | point in (i0,j0,k0) coordinates | |
| $LH(1)$ | $-0.1200$ | Center of inboard body to | |
| $LH(2)$ | $-0.2761$ | spring H ground fixed attachment | $m$ |
| $LH(3)$ | 0.1625 | points in (i0,j0,k0) coordinates | |
| $LI(1)$ | $-0.1152$ | Center of inboard body to | |
| $LI(2)$ | $-0.0080$ | spring I ground attachment | $m$ |
| $LI(3)$ | $-0.3043$ | point in (i0,j0,k0) coordinates | |
| $LJ(1)$ | $-0.1249$ | Center of inboard body to | |
| $LJ(2)$ | 0.2782 | spring J ground attachment | $m$ |
| $LJ(3)$ | 0.1481 | point in (i0,j0,k0) coordinates | |
| $ED$ | 0.064 | Spring E zero force length | $m$ |
| $FD$ | 0.062 | Spring F zero force length | $m$ |
| $GD$ | 0.062 | Spring G zero force length | $m$ |
| $HD$ | 0.067 | Spring H zero force length | $m$ |
| $ID$ | 0.062 | Spring I zero force length | $m$ |
| $JD$ | 0.060 | Spring J zero force length | $m$ |
| $KE$ | 13.257 | Spring E spring constant | $N/m$ |
| $KF$ | 13.257 | Spring F spring constant | $N/m$ |
| $KG$ | 13.999 | Spring G spring constant | $N/m$ |
| $KH$ | 13.244 | Spring H spring constant | $N/m$ |
| $KI$ | 13.438 | Spring I spring constant | $N/m$ |
| $KJ$ | 12.908 | Spring J spring constant | $N/m$ |
| $SCS1(1)$ | 0.3082 | Vector from center of small | |
| $SCS1(2)$ | 0.0394 | sphere to 1st body fixed marker | $m$ |
| $SCS1(3)$ | 0.0072 | in (i5,j5,k5) coordinates | |
| $SCS2(1)$ | 0.3441 | Vector from center of small | |
| $SCS2(2)$ | 0.0015 | sphere to 2st body fixed marker | $m$ |
| $SCS2(3)$ | 0.0072 | in (i5,j5,k5) coordinates | |
| $SCS3(1)$ | 0.3082 | Vector from center of small | |
| $SCS3(2)$ | $-0.0367$ | sphere to 3rd body fixed marker | $m$ |
| $SCS3(3)$ | 0.0072 | in (i5,j5,k5) coordinates | |
| $SCS4(1)$ | 0.3281 | Vector from center of small | |
| $SCS4(2)$ | 0.0015 | sphere to 4th body fixed marker | $m$ |
| $SCS4(3)$ | 0.0273 | in (i5,j5,k5) coordinates | |
| $DT$ | 0.01 | Time increment | $s$ |
| $TMAX$ | 5.0 | Simulation length | $s$ |

Table F.1: Model Constant Input File.